VOLCANO SEISMICITY IN ALASKA

By

Helena Buurman

RECOMMENDED:

Dr. Jeffrey Freymueller

Dr. Stephanie Prejean

Dr. Glenn Thompson

Dr. Michael West
Advisory Committee Chair

Dr. Michael Whalen
Chair, Department of Geology and Geophysics

APPROVED:

Dr. Paul Layer
Dean, College of Natural Science and Mathematics

Dr. John Eichelberger
Dean of the Graduate School

29 April 2013
Date

VOLCANO SEISMICITY IN ALASKA

A

THESIS

Presented to the faculty

of the University of Alaska Fairbanks

in Partial Fulfillment of the Requirements

for the degree of

DOCTOR OF PHILOSOPHY

By

Helena Buurman

Fairbanks, Alaska

May 2013

Abstract

I examine the many facets of volcano seismicity in Alaska: from the short-lived eruption seismicity that is limited to only the few weeks during which a volcano is active, to the seismicity that occurs in the months following an eruption, and finally to the long-term volcano seismicity that occurs in the years in which volcanoes are dormant.

I use the rich seismic dataset that was recorded during the 2009 eruption of Redoubt Volcano to examine eruptive volcano seismicity. I show that the progression of magma through the conduit system at Redoubt could be readily tracked by the seismicity. Many of my interpretations benefited greatly from the numerous other datasets collected during the eruption. Rarely was there volcanic activity that did not manifest itself in some way seismically, however, resulting in a remarkably complete chronology within the seismic record of the 2009 eruption.

I also use the Redoubt seismic dataset to study post-eruptive seismicity. During the year following the eruption there were a number of unexplained bursts of shallow seismicity that did not culminate in eruptive activity despite closely mirroring seismic signals that had preceded explosions less than a year prior. I show that these episodes of shallow seismicity were in fact related to volcanic processes much deeper in the volcanic edifice by demonstrating that earthquakes that were related to magmatic activity during the eruption were also present during the renewed shallow unrest. These results show that magmatic processes can continue for many months after eruptions end, suggesting that volcanoes can stay active for much longer than previously thought.

In the final chapter I characterize volcanic earthquakes on a much broader scale by analyzing a decade of continuous seismic data across 46 volcanoes in the Aleutian arc to search for regional-scale trends in volcano seismicity. I find that volcanic earthquakes below 20 km depth are much more common in the central region of the arc than they are in the eastern and western regions. I tie these observations to trends in magma

geochemistry and regional tectonic features, and present two hypotheses to explain what could control volcanism in the Aleutian arc.

Table of Contents

Page

List of Figures

Page

Page

List of Tables

Page

List of Appendices

Acknowledgements

Thank you Mike, for 7 years of mentoring, for Monday morning tea, for letting me soar around the wildest and most remote craters and calderas this country has to offer, for finding me opportunities on other continents to do much the same there, for all your considerable patience, for the encouragement to pursue (often fruitless but almost always interesting) side projects with AVO monitoring data, for looking the other way while I chased after adventure on my bike, for being a good listener, for TTODAYs, for prodding me in the right direction but still letting me find dead ends … all the support and guidance I could have asked for. Thank you Cyrus, for teaching me the field stuff, for blue-bird days on the sides of bulging volcanoes about to explode, for that time you found the way down through the fog around the glaciers and past the bears during that less-than-ideal descent off Spurr, and for your unwavering support all these years. Thank you Paskie, for making me part of the team, for keeping me on my toes and for sending me out to what felt like the very edge of the world. Thank you Kate, Janet and Dz, for bringing me along to breathtaking places I wouldn't have otherwise made it to, and helping me earn my geology, water sampling and GPS badges. Thank you Seth, for sending me down this road in the first place. Thank you dear friends (you know who you are), for Tuesday rehearsals, for epic games of hockey, for Sunday brunches, for late night saunas and for all manner of adventuring – you have been my family away from home. And thank you Bennie, Mum and Erica, for your unconditional admiration and encouragement to pursue my dreams, however far-flung they may be.

Introduction

Volcanoes have captured my imagination for as long as I can remember. As a child, they were one of the few things that truly frightened me. Now I find their unpredictability and their destructive power simultaneously fascinating and humbling. Despite putting people on the moon, manipulating human genes and splitting the atom, we are still unable to satisfactorily explain how and why volcanoes erupt the way they do. And with the destructive global effects of major eruptions—not to mention the direct impact they have on the millions of people that live on the slopes of volcanoes around the world—it is of utmost importance that we gain a thorough understanding of how volcanic systems work. This is what draws me to the study of volcanoes.

The biggest challenge in understanding how volcanoes work stems from our inability to see below the surface of the Earth. Once lava erupts at the surface numerous direct measurements can be made that can tell us about its composition, viscosity and temperature, which allow us to model how it will behave. Prior to eruption, however, we are left to guess at how magma travels through the crust. Numerous methods have been developed to image the subsurface beneath volcanoes, such as satellite-based remote sensing techniques, gas measurements and high pressure experiments that attempt to simulate the conditions at many kilometers depth. But none have been nearly as successful in gaining insight into volcanic processes as studying the small earthquakes that occur in great numbers beneath volcanoes.

People have associated earthquakes with volcanoes for thousands of years. The first detailed account of a volcanic eruption, recorded by Pliny the Younger who witnessed the 79 A.D. eruption of Mount Vesuvius, describes the escalation in earthquake activity which preceded the infamous eruption that devastated the cities of Pompeii and Herculaneum. Modern seismic monitoring of volcanoes dates back over 150 years to when the first seismometer to record volcanic earthquakes was installed on the

slopes of Mount Vesuvius in 1862 (Zobin, 2012). But it was not until 1910, when Fusakichi Omori started to study earthquakes generated during eruptions at a number of Japanese volcanoes, that earthquake monitoring became the primary method with which to forecast and monitor volcanic eruptions. What Omori was the first to appreciate was that volcanoes produce a large variety of seismic signals, both during eruptive activity and at times where they otherwise appear to lie dormant (Omori, 1912). Since the shape of an earthquake waveform is controlled by the type of earthquake source, the location where it occurs beneath the surface, and the material that the seismic waves travel through, seismic signals at volcanoes provide a snapshot into processes occurring within the crust below volcanoes. The challenge for volcano seismologists lies with interpreting exactly how these signals relate to volcanic processes.

Our understanding of volcano-seismic signals has increased dramatically in the past 30 years thanks to technological advances that have improved our ability to record and analyze seismic data. Seismometers are now small and robust enough that they can be deployed close to or even within volcanic craters where they are able to record and transmit continuous data in real-time. Much of the seismicity recorded by these instruments consists of subtle volcano-seismic signals that the early seismometers were not capable of detecting. Increases in computing power and speed have also enabled us to mathematically simulate volcanic earthquakes, improving our understanding of how the signals are generated and how they travel through volcanic rock. By comparing simulated earthquakes with recorded seismic data and then appealing to other datasets such as visual observations, gas emission data and satellite imagery, we have been able to piece together what processes generate volcanic earthquakes. We now know, for example, that one process that can generate earthquakes rich in low frequency energy (< 5 Hz) is the movement of fluids (such as magma or gas) through a constriction in a narrow conduit (Chouet, 1988), that growing lava domes can be associated with small (M_L<0) repeating earthquakes that have identical waveforms (e.g., Iverson et al., 2006) and that signals that result from rockfalls emerge gradually from the background noise whereas signals from

explosions have much more abrupt, impulsive onsets (e.g., Deroin and McNutt, 2012; Chouet and Matoza, 2013). Armed with these observations and interpretations, we are able to monitor volcanoes in unprecedented detail.

Yet despite these tremendous advances, many volcano-seismic signals remain poorly understood. We are often not able to determine whether an increase in earthquake activity at a volcano is due to ascending magma that is about to erupt at the surface, or merely due to tectonically-driven stress changes in the crust, changes to the hydrothermal system or ice and debris avalanches on the steeper portions of volcanic edifices. Appealing to deformation or satellite data can often assist with the interpretation, but more often than not there is no other corroborating information that can help to elucidate these puzzling earthquake sources. Volcanoes also continue to surprise us with "new" seismic signals that have never previously been observed, such as the gliding tremor observed during the 2009 Redoubt eruption (Hotovec et al., 2012). These signals often force us to rethink our original hypotheses of certain seismogenic sources, but ultimately they also help advance our understanding of how many volcano-seismic signals are generated.

The motivation for my dissertation is straightforward: I wish to further our understanding of how volcanic processes generate volcano-seismic signals in order to improve our ability to monitor volcanoes and forecast volcanic eruptions. Thanks to the close collaboration between the University of Alaska Fairbanks and the U.S. Geological Survey, I have spent the majority of my graduate school career seismically monitoring volcanoes in Alaska and responding to volcanic crises. In addition to working closely with the seismic data, I have spent a significant amount of time working as a field technician installing and doing maintenance work at many of the seismic networks on Alaskan volcanoes. Both the fieldwork and the monitoring duties that I have participated in have shaped the way I think about volcanic systems, and have given me unusual perspective on the limits to our understanding of volcano-seismic signals.

In the first chapter I examine volcano seismicity generated during eruptive activity by presenting a seismic chronology of the 2009 Redoubt eruption. I use our current understanding of volcano-seismic signals to identify volcanic activity such as lahars, explosions and lava dome growth. I also examine aspects of the seismic record that are less well understood, such as the many weeks of sustained tremor prior to the onset of the eruption, and place them in context with other geophysical observations in order to relate them to volcanic processes. This study provides a crucial reference point for future studies of the 2009 Redoubt eruption, which will undoubtedly involve much more detailed and focused investigations of specific seismic signals.

In the second chapter I examine the seismicity that occurred in the year following the end of the 2009 Redoubt eruption. During this period there were a number of unexplained bursts of shallow seismicity that did not culminate in eruptive activity despite being similar in character to some of the signals that were recorded at the height of the eruptive activity less than a year prior. I examine the seismic record over 5 years and show that these episodes of shallow seismicity were in fact related to volcanic processes much deeper in the volcanic edifice, shedding new light on how long volcanic systems remain active following the end of eruptive activity.

In the final chapter I take a much broader look at volcano seismicity and examine the past 10 years of seismic monitoring data recorded at 46 volcanoes located along the Aleutian arc. I search for regional-scale variations in volcano seismicity generated at volcanoes while they lie dormant, and compare these to geochemical variations at the volcanoes across the arc. I then tie these observations to regional-scale tectonic stresses and hypothesize that the variations in earthquake depth and geochemistry are a manifestation of the ease at which magma ascends through the crust. These results suggest that the regional stress regime could be a major control of certain characteristics of the volcano seismicity and, ultimately, the behavior of the volcanic systems as a whole

.

Chapter 1 The seismicity of the 2009 Redoubt eruption[1]

1.1 Abstract

Redoubt Volcano erupted in March 2009 following 6 months of precursory seismic activity. The 4.5-month-long eruptive sequence was accompanied by phreatic and magmatic explosions, periods of steady dome growth, lahars, seismic swarms, extended episodes of volcanic tremor and changes in the background seismicity rate. This study presents a seismic chronology of the eruption and places it in context with the variety of other geological and geophysical data that were recorded during the eruptive period. We highlight 6 notable seismic swarms, 3 of which preceded large explosions. The swarms varied from an hour to several days in duration, and contained tens to over 7000 earthquakes. Many of the swarms were dominated by low frequency type earthquakes that contained families of repeating events. Seismic tremor varied considerably in frequency, amplitude and duration during the eruption with distinct characteristics accompanying different types of volcanic activity. The explosion signals during March 23-24 were the most energetic, and the explosions on March 26-29 contained proportionally more low frequency energy (0.033-0.3 Hz). Two seismic stations were particularly well-suited to recording lahars that flowed down the Drift River valley. Data from these stations showed that lahars were generated by the majority of the explosion events, as well as during the continuous eruptive activity on March 29 when no large explosions occurred. We also examine the seismicity which occurred outside of the explosion and swarm episodes, and find several families of repeating VT earthquakes which begin shortly before the April 4 explosion and that continue through May 2009, locating between 3 and 6 km below sea level.

[1] Buurman, H., West, M.E., Thompson, G., 2012, The Seismicity of the 2009 Redoubt eruption: Journal of Volcanology and Geothermal Research, doi: 10.1016/j.jvolgeores.2012.04.024.

1.2 Introduction

Redoubt Volcano is a 3108 m high stratovolcano in the Cook Inlet region of south-central Alaska that has erupted three times since the mid 1960s (Schaefer, 2012; Bull and Buurman, 2012). Given its recent eruptive history, its location near communities, oil platforms, an oil storage facility, and its potential impact to air traffic routes, Redoubt Volcano was closely monitored when unrest began in summer 2008. The seismic network at that time consisted of 5 single-component and 2 3-component L-4 and L-22 model telemetered short-period seismometers within 25 km of the vent, operated by the Alaska Volcano Observatory (AVO) (Fig. 1.1). As the level of unrest increased the network was augmented: two additional telemetered broadband Guralp 6TD instruments and a telemetered single-component short-period L-4 seismometer were installed in late February 2009 and 4 campaign-style broadband Guralp 6TD seismometers with on-site recording were deployed in the 2 days prior to the magmatic explosions that occurred in late March 2009.

In this paper we present an overview of the seismic activity that was associated with the 2009 eruption of Redoubt Volcano. There are many aspects to the seismicity both prior to and during the eruptive episode, including swarm activity, tremor episodes, seismicity from explosion signals and lahars and variations in the background hourly earthquake rates. When referring to explosion events, we follow the numbering scheme used by Schaefer (2012) who numbers them 0-19. Our objective is to place each set of seismic patterns in the context of other geological and geophysical observations. As a result, this paper encompasses a wide variety of seismic signals that were generated by a range of volcanic processes. For organisational simplicity we include brief discussion and speculation of the seismic sources within the individual sections instead of in a lengthy discussion section at the end, and close with a brief eruption summary that encompasses the major conclusions drawn from the seismic record. We begin with a short eruption overview to provide context for our seismological interpretations.

1.3 Eruption overview

Retrospective analysis of continuous GPS data indicates that inflation began as early as May 2008 (Grapenthin et al., 2012), but the earliest signs of unrest at Redoubt Volcano recognised by AVO were reports by field geologists working on the edifice of H_2S odors from fumaroles near the ice-covered 1990 lava dome in July 2008. Brief bursts of tremor in the 2-6 Hz range were recorded in September 2008 coincident with reports from local part-time residents of explosion-type noises in the vicinity of the summit, and in late September crevasses began to expand in the upper Drift Glacier (Bleick et al., 2012; Schaefer, 2012). Continued enlargement of these ice fractures, combined with increased and anomalous gas emissions (Werner et al., 2012) prompted AVO to increase the Volcano Alert Level and Aviation Color Code to advisory/yellow on November 5, 2008 (Schaefer, 2012). Deep long-period earthquakes began in December 2008 at depths between 28 and 32 km below the edifice (Power et al., 2012). The onset of high amplitude, broadband tremor in late January 2009 marked a further increase in seismicity at Redoubt Volcano. This tremor was accompanied by increased gas emissions, the appearance of collapse holes in the glacier and reports of mudflows emerging from various locations along the Drift glacier (Bleick et al., 2012; Werner et al., 2012; Schaefer, 2012). The tremor became sustained in early February, ending abruptly with the first seismic swarm on February 26, 2009 (Table 1).

The first explosion of the eruption sequence (event 0) occurred on March 15, accompanied by weak tremor (Table 2). This explosion formed a hole in the crater glacier and deposited a small amount of ash that lacked juvenile material at the summit (Bleick et al., 2012; Wallace et al., 2012). The second seismic swarm began 5 days later, marking the build-up to the first magmatic explosion (event 1; see Table 1). The swarm lasted 66 hours and was dominated by repeating earthquakes comparable to those observed during the previous eruption of Redoubt Volcano in 1989 (Power et al., 2012; Power et al., 1994). Towards the end of the swarm a small lava dome was observed in the hole formed by event 0. During the final hours of the swarm volcanic tremor increased significantly

before culminating in a nine-hour sequence of six magmatic explosions (events 1-6) that destroyed the small lava dome and produced ash plumes up to 18 km ASL (Schaefer, 2012; Bull and Buurman, 2012; Schneider and Hoblitt, 2012). The explosions produced pyroclastic density currents and tephra fall, as well as lahars which travelled down the Drift River valley, reaching the coast (Table 3; Bull and Buurman, 2012; Waythomas et al., 2012; Wallace et al., 2012). Sustained, high amplitude tremor continued for 9 hours following this initial explosion sequence.

Two more explosions occurred on March 26 (events 7-8), the second of which produced the highest ash cloud of the eruption to 18.9 km ASL (Schaefer, 2012; Schneider and Hoblitt, 2012; Table 2). Fall deposits from these explosions suggest that a second lava dome may have effused in the pause between events 6 and 7 (Wallace et al., 2012), but no satellite observations were available to confirm the dome's presence. Events 7 and 8 were followed by an 8-hour-long vigorous seismic swarm that merged into tremor immediately before the next explosion (event 9) on March 27. This event marked the first in a sequence of powerful explosions (events 9-18) that produced finer-grained ash deposits than the March 23-24 sequence (Wallace et al., 2012). These later explosions produced many lahars and were preceded by distinctive episodes of tremor that exhibited steady, exponential increases in dominant frequency up to nearly 30 Hz (Hotovec et al., 2012). The fourth seismic swarm on March 29 marked the end of this explosion sequence, and was followed by a high amplitude spasmodic tremor episode lasting 20 hours accompanied by continuous, low-level ash emissions (Schneider and Hoblitt, 2012). Effusion of a third lava dome was observed in the days following the seismic swarm before it was destroyed by the explosions on April 4. The final explosion of the eruption (event 19) occurred on April 4 and was preceded by a 43-hour swarm of low amplitude repeating earthquakes. Retrospective analyses of satellite images, the seismic and infrasound records and the fall deposits from event 19 suggest that failure of the lava dome played a part in the onset of the explosive activity (Bull and Buurman, 2012). Event 19 also produced the longest sustained ash emissions and the largest and

most water-rich lahars, inundating the Drift River valley to the coast (Waythomas et al., 2012).

Lava effusion followed these explosions for the remainder of the eruption. A new lava dome was observed on April 5 and continued to grow throughout May and into mid-June, after which time the growth rate slowed considerably (Bull et al., 2012; Diefenbach et al., 2012). Several clusters of high-frequency repeating earthquakes located at depths of 3-6 km below sea level accompanied the dome growth and continued through the end of May. The final and longest-lived seismic swarm began on May 2 and lasted through May 7, producing over 7000 low-amplitude, repeating earthquakes. This seismic swarm coincided with a change in the vesicularity and texture of the extruding lava dome, which continued to grow until July 2009, when the eruption was declared over (Bull et al., 2012; Diefenbach, et al., 2012).

1.4 Data

We combine earthquake information from multiple catalogs to get the best qualities from each. Discussions that rely on hypocenter location are based on an analyst-reviewed catalog (Dixon et al., 2010). This catalog provides the highest quality depths and locations and has a magnitude of completeness of 0.4. Most of the earthquake analyses in this paper are based on bulk processing of hundreds to thousands of events. For these analyses we prefer the temporal completeness of an algorithm-based (i.e. automated) catalog with a lower threshold for inclusion. Though the errors of the hypocenter solutions are much larger in the automated catalog, the algorithm-based approach identifies 37,000 earthquakes between January and May 2009 compared to the 3766 analyst-reviewed solutions during the same period.

The automated catalog is based on traditional single channel earthquake detections using short- to long-term signal ratios. These detections are compared across nearby stations and associated into events when they are consistent with P phase travel times from a pre-computed grid of trial locations. The short- to long-term signal ratios are

computed in two frequency bands (0.8-5 Hz and 3-25 Hz) to detect both low frequency and volcano-tectonic earthquakes. We require events to register P-wave arrivals at 4 stations for inclusion in the catalog. A thorough description of the methodology can be found in Thompson and West (2010). The eruption caused significant outages at RSO—a station critical to both earthquake catalogs. When RSO was not operational, most notably from March 23 to April 16, the smallest earthquakes registered only on 3 stations and as a result did not meet the criteria for inclusion in the catalog. At all times, however, there is sufficient station coverage that events of magnitude -0.9 are generally included in our analyses.

Our analyses include classifying earthquakes as 'repeating events'. We assess this using cross correlation-based clustering techniques applied to waveforms from one representative data channel. For each event we segment a 7 second seismogram beginning 1 second before the P-wave and filtered using a 4-pole Butterworth filter between 0.5-25 Hz. Each event is then cross correlated against all other events. We use hierarchical clustering to group the cross correlations into event families. Within each family all events have an average cross correlation value with all other events of 0.75 or greater. This method is described further in Buurman and West (2010). Because of the large number of earthquakes, we cross-correlate the catalog in groups of 500 consecutive events. If an event is part of a family of four or more members we consider it a 'repeating event', in line with other studies (Buurman and West, 2010; Thelen et al., 2010).

1.5 Swarms

Methods

In this section we analyse earthquakes using methods that allow direct comparison between the different swarms. Earthquake swarms are defined as increases in earthquake rates within a given volume over a relatively concentrated period of time without a single outstanding shock (Mogi, 1963). We quantify this rather loose definition using our own criteria, identifying swarms as episodes during which the hourly rate of

earthquakes exceeds 50, or when the hourly rate of repeating earthquakes exceeds 20 (Fig. 1.2). Swarm onsets are identified as the time when the hourly rate of earthquakes exceeds the previous six-hour average, and swarms are considered over when the hourly rate returns to the stable mean background rate for the following 6 hours. We find that a six-hour average accounts for natural fluctuations in seismicity. Six swarms are identified using these criteria. We refer to each of the six swarms by the UTC date when the activity began. For analyses that rely on waveform characteristics, we use data from short-period station REF unless otherwise noted. This is one of the closest stations to the vent and it operated throughout the entire period of unrest. Because of its close proximity to the vent, this station recorded lower amplitude activity in the summit region but was susceptible to clipping during the most energetic seismicity. Most of the analyses that follow do not require unclipped data, although where data are clipped we refer to broadband station RDWB.

February 26 swarm

The first swarm began on February 26, 2009, 25 days before the first magmatic explosion. The onset was sudden and occurred just 6 hours following the end of a 3-week long tremor episode. Initial earthquake activity peaked at 91 events per hour but this high rate quickly diminished and the activity continued to fluctuate around 30 events per hour for the remainder of the swarm, which lasted 29 hours in total. The activity ended abruptly on February 27; however, the background rate of earthquakes that followed remained higher than it had been through most of January (Fig. 1.2). This elevated rate was sustained until the onset of the next swarm on March 20.

The majority of earthquakes during the February 26 swarm are small ($<M_L$ 1), although there is some scatter in size particularly early in the swarm and again during the last 12 hours evident in Figure 1.3A. Most of the events are dissimilar, and only 6% meet our criteria for repeating events (described in section 3) (Fig. 1.4A). The waveforms vary greatly in shape, with some events exhibiting P- and S-wave arrivals and others showing

more emergent onsets. For all events, however, the majority of energy in the spectrum occurs between 1 and 7 Hz at station REF. These waveform characteristics are not typical for volcano-tectonic earthquakes, which usually have impulsive P-wave arrivals and are dominated by frequencies between 5-15 Hz (Lahr et al., 1994). While volcano-tectonic earthquakes are regularly recorded at Redoubt Volcano, they rarely occur as swarms; waveforms with lower dominant frequencies and more emergent P-wave arrivals such as those recorded during the February 26 swarm are historically more typical (Lahr et al., 1994).

The February 26 swarm marked the transition from 3 weeks of seismicity dominated by tremor to a further 3 weeks of seismicity dominated by a higher rate of detected earthquakes, suggesting that a large-scale change had occurred below or within the edifice. Our interpretation for this change is that the gas movement that had been generating the tremor became blocked, leading to higher pressures and gas-driven cracking. The closed volcanic system then produced a higher rate of background seismicity as the fluids continued to enter the system but could not reach the surface. Werner et al. (2012) reported the lowest measurements of SO_2 emissions during the precursory build-up to the eruption on February 27. Although these data lack the temporal resolution to confirm the closing of the gas system, their results support this model.

March 20 swarm

The second swarm began on March 20 and culminated in a series of magmatic explosions (events 1-6). The swarm lasted 66 hours and had two pulses: a first smaller pulse that peaked at 45 events per hour between March 20 and 21; and a second pulse beginning late on March 21 which peaked at 82 events per hour. The first pulse increased gradually over 10 hours, while the second pulse had a rapid onset (Fig. 1.3B) that prompted AVO to increase the Volcano Alert Level and Aviation Color Code to

watch/orange. Volcanic tremor occurred towards the end of the second pulse, increasing in amplitude until it dominated the seismic record shortly before the magmatic explosions.

The majority of earthquakes during both pulses are small ($M_L < 0.8$), repeating earthquakes that cluster into three main families (Fig. 1.3B, 1.4B). The smallest of these families occurs exclusively during the first pulse of activity, and is characterised by waveforms with peak frequencies around 5 Hz, broad spectral content and visible P- and S-wave arrivals (Fig. 1.3B). The second and largest family has low rates during the first pulse but later increases significantly to dominate the second pulse of seismicity, dying out with the onset of the last family. One of the most striking features of this second family is the waveform evolution that occurs over its duration, where the waveforms gradually change shape, dropping from a peak frequency of around 5.1 Hz to 4.4 Hz. The third family differs considerably, exhibiting peak frequencies around 2.5 Hz with no clear S-wave arrivals (Fig. 1.3B). This type of earthquake is often referred to as a long-period or 'LP' event, and is characteristic of the seismic swarms during the 1989-90 eruption (Power et al., 2012; Chouet et al. 1994; Stephens and Chouet 2001). The magnitudes of these events are also distinct: where the maximum amplitudes varies widely within the first two families, the amplitudes in the last family are tightly clustered, growing steadily until they become dwarfed by the volcanic tremor in the final hours before the eruption onset (Fig. 1.3B).

The presence of different earthquake families during the swarm indicates that several different processes were occurring within the edifice in the final hours before the eruption. The clear P- and S-wave arrivals present in the first two families indicate that they were generated by brittle failure within the edifice, and their repetitive nature suggests that they originated in approximately the same location. Given the timing of these earthquakes prior to the eruption onset, it is likely that they were generated from the incremental opening of cracks ahead of the rising magma body. When a crack opens

slowly the shift in hypocenter location (i.e. the migration of the crack tip) is small and will not necessarily be obvious in the earthquake locations. The waveforms in the last earthquake family are much lower in frequency and were generated by a very different source. The timing of this family coincided with the growth of the first lava dome: the family emerged around 1700 UTC and the dome was observed in satellite images at 2000 UTC on March 22 (Bull et al., 2012). It is therefore likely that a process related to dome growth generated this family of earthquakes, and that the onset of the family occurred once the conduit had been widened enough to allow the magma to move through the shallow edifice. We speculate that as the earthquakes increased in amplitude, the rate of extrusion increased which in turn generated tremor through rapid degassing. Once the extrusion rate became rapid enough that the magma could not equilibrate through degassing, the explosive phase of the eruption began.

March 27 swarm

The third swarm of the eruptive sequence lasted only 8.5 hours and occurred prior to the 9th explosion of the sequence on March 27 (Schaefer 2012), less than six hours after the previous explosion on March 26. Activity increased suddenly within the hour shortly before 00:00 UTC on March 27 and the event rate remained around 50 events per hour for the majority of the swarm, reaching a peak of 92 events per hour in the 2 hours before the explosion.

This sequence represents the most powerful swarm of the 2009 eruption. The majority of earthquakes have local magnitudes of 1.5, and the largest event of the sequence is a M_L 2.6 earthquake that occurred late in the swarm. Although almost all the events in the sequence clipped at the summit stations, the events remained on scale at broadband station RDWB, 10 km to the west of the vent (Fig. 1.1). The swarm was dominated by a single event family characterised by an impulsive P-wave arrival and a definitive S-wave arrival (Fig. 1.3C; 1.4C). Event amplitudes steadily increased over the first 6 hours of the swarm from M_L 0.7 - 1.6, before rapidly decreasing in magnitude. As

the event size decreased, so did the time between events until they merged into tremor. During the final minutes before the explosion the frequency of the tremor glided exponentially as a function of time from less than 1 Hz to 10 Hz. Hotovec et al. (2012) model these gliding tremor episodes as regularly repeating stick-slip earthquakes that are tightly clustered in time and space.

The episode of gliding tremor that followed the swarm was the first of several instances of this phenomenon that occurred during the explosive activity on March 27-29 (events 9-18; Hotovec et al., 2012). Fee et al. (2012) noted a difference in the infrasonic explosion signal characteristics during this same period and attributed it to a change in eruptive style, from the subplinian-type activity observed during the early phase of the eruption to vulcanian activity. Wallace et al. (2012) also observed a change in the tephra componentry, finding much finer grainsizes indicative of more explosive activity following the March 27 swarm. These observations each support a change in the eruptive behaviour around March 27, and the timing of the March 27 swarm strongly suggests that it heralded the shift in activity. Hotovec et al. (2012) examined the March 27 swarm closely and concluded that the location and focal mechanism solution for the repeating events indicated stick-slip behaviour along the conduit walls. A change in the viscosity of the ascending magma could explain why this type of activity was not observed earlier in the eruption, and could also account for the differences observed in the explosion characteristics compared to the earlier sequence on March 23-24. However this cannot be corroborated with other evidence.

March 29 swarm

This hour-long swarm occurred just hours after event 18 on March 29 and preceded an episode of high amplitude tremor and continuous but weak eruptive activity (Schneider and Hoblitt, 2012). In addition to the 37 events of sufficient size for the automated catalog, there are a few hundred smaller events that can be observed on

summit stations (Power et al., 2012). The events are generally small, lack clear S arrivals (Fig. 1.3D), and have a high degree of waveform similarity (correlation > 0.9, Fig. 1.4D). Satellite data indicate that the third lava dome emerged on March 29 (Bull et al., 2012). Our interpretation for this swarm is similar to our interpretation for the 3rd main family of waveforms in the March 20 swarm: directly related to dome growth. As a fresh plug of magma ascended, it is possible that friction in the conduit created stick-slip earthquakes. The decreasing amplitude of the earthquakes suggest that once the conduit was widened, the shear mechanism weakened as dome growth became continuous and, eventually, aseismic. Although the waveforms between the March 23 events and the March 29 swarm are dissimilar, the 18 large explosions that separated these two episodes may have changed the conduit geometry enough that the same process occurred in a different location, resulting in the dissimilarity between the two swarms.

April 2 swarm

This swarm preceded the April 4 explosions that produced the highest ash column of the eruption (Schaefer 2012). The swarm had a rapid onset (<2 hours) and lasted 43 hours. The peak of 107 events per hour occurred in the middle of the swarm and declined over the next day before the explosion (Fig. 1.3E). This decreasing event rate contributed to a decision by AVO staff to downgrade the Volcano Alert Level and Aviation Color Code to warning/orange on April 3. 77% of the events were repeating, dominated by a family of emergent low amplitude waveforms that evolved considerably over the course of the swarm (Fig. 1.4E). During the swarm the dominant spectral peak at 2.7 Hz became gradually stronger while energy above 7 Hz became weaker. Although the swarm contained nearly 2000 earthquakes, none of the events were of sufficient size to be located in the analyst-reviewed catalog.

Visual observations indicate that dome growth stalled during the swarm (Bull et al., 2012, Diefenbach et al., 2012). The change in magma effusion rate could have been

caused by a change in the magma supply rate, an increase in viscosity or an equilibration of the pressure in the conduit. This transition is seen in the steady evolution of seismic waveforms. In light of the stalled dome growth, the evolving seismic signature probably reflects changing material properties near the source of the earthquakes, though we also cannot rule out a changing source location or a change in the bulk properties of the edifice.

May 2 swarm

The final swarm was the longest-lived (five days), and occurred well after the explosive activity had ceased during a period of continuous dome growth. Earthquake amplitudes are markedly smaller than the other magmatic swarms, with 7400 events of sufficient size for the automated catalog (Fig. 1.3F). Power et al. (2012) examine the larger population of events too small to be recorded beyond the summit stations. Though the earthquakes are generally small, they occur at higher rates (up to 191 events per hour) than any of the other swarms (Table 1). Waveforms throughout this swarm are highly repetitive and emergent with dominant frequencies near 3.5 Hz (Fig. 1.4F). Early on May 6, two additional waveform families were detected, concurrent with the increase in event rate and amplitude of the main repeating family. The families all share waveform characteristics, and likely originate in the same region.

Several measures point to a change in the volcanic system in conjunction with the May 2 seismic swarm. Gas measurements show an increase in SO_2 and CO_2 around May 4 (Lopez et al., 2012; Werner et al., 2012). Lava dome samples show a change in vesicularity and texture (Bull et al, 2012), and the effusion rate increased following the May 2 swarm (Diefenbach et al, 2012). These factors together suggest that there may have been an influx of a different batch of magma. The earthquakes could have been the result of failure around the edges of the extruding lava dome as new magma entered the system below, similar to the model proposed by Iverson et al. (2006) during the Mount St Helens eruption in 2004-2008. Alternatively they may have been generated in response to

the influx of different magma into the upper conduit. The different lava textures observed in the samples indicate that the new material may have had different properties that caused it to move differently through the conduit. The swarm may have reflected slip-stick at the edges of the magma plug as the dome adjusted to the new extrusion rate. There is insufficient data with which to be able to distinguish between these models, however, and we instead leave them both as possible sources for the May 2 swarm.

1.6 Volcanic tremor

The first episode of tremor associated with the 2009 eruption occurred in late September 2008, when several bursts were recorded at the summit stations. These events had durations less than 2 minutes, and were dominated by frequencies between 1 and 4 Hz. Aside from these brief events in September, no more tremor was detected until January 2009.

Beginning in late January, tremor featured regularly in the seismic record. In lieu of a lengthy chronology, we examine the notable styles of tremor that occurred during the eruption of Redoubt Volcano. Our waveform analyses are based on station REF for its high fidelity and continuity of operation (Fig. 1.1).

Tremor amplitudes are reported using surface-wave reduced displacement denoted as D_{RS} (Fehler, 1983). Each D_{RS} value is the root-mean-square displacement of a one-minute window measured on the vertical component of station REF, then corrected for geometrical spreading (assuming surface waves, and a wavelength of 1 km). No corrections for attenuation or site effects are made. Note that in Figure 1.2 we plot a downsampled version of this 1-minute D_{RS} timeseries: we plot the median value for each hour. We do this because, in the figure, we wish to emphasize the (continuous) tremor amplitude and filter out transient signals including earthquakes and noise spikes. As a result, any tremor bursts which lasted less than 30 minutes cannot be seen in Figure 1.2.

Also note that McNutt et al. (2012) use a different D_{RS} methodology more suited to the (transient) explosion signals.

Late January high amplitude precursory tremor

Tremor activity began in earnest at 1810 UTC on January 24, 2009 as a 4-minute burst of broadband tremor (energy up to 10 Hz) with an amplitude of 16 cm^2. At 1000 UTC on January 25 there was a gradual onset of tremor, which increased from 0.4 cm^2 to > 2 cm^2 at 1047 UTC. Amplitudes of 2-5 cm^2 were sustained until around 1500 UTC and prompted AVO staff to increase the Volcano Alert Level and Aviation Color Code from advisory/yellow to watch/orange (Schaefer, 2012). The January 25 tremor (Fig. 1.5A) was dominated by frequencies between 2.5 and 6 Hz, although there was some energy as high as 18 Hz. Examination of the continuous data at the summit stations showed that this tremor consisted of closely spaced low frequency earthquakes which contained some higher frequency energy (Fig. 1.5A). At stations further from the edifice these individual events were not discernable from continuous tremor, suggesting that they originated at shallow depths in the edifice. After 1500 UTC low amplitude tremor (D_{RS} of 0.5-1.0 cm^2) lasted a further 24 hours.

There were several more bursts of tremor over the following days. The most significant were 3 bursts between 1930 and 2200 UTC on January 30 exceeding 5 cm^2. This episode was strong enough to be recorded at the seismic networks on the nearby Iliamna (54 km) and Spurr (94 km) volcanoes. The final burst was followed by continuous tremor with amplitude 1-3 cm^2 lasting 3 hours.

Shallow volcano-tectonic earthquakes began suddenly on January 25 coincident with the tremor episodes. Werner et al. (2012) also report an increase in SO_2 flux during late January and early February. We interpret these notable changes in seismicity and gas flux as evidence for magma intrusion into the shallow crust. Inflation beginning in May 2008 indicates that a small volume of magma moved into the mid crust between 5 and 13

km below sea level (Grapenthin et al., 2012). This ascent appears to have been aseismic, since there were no changes in the seismic record at that time. The uptick in activity in January can be interpreted as the 'renewed' ascent of magma from the mid crust to shallower depths between 3-6 km. This model accounts for the rapid onset of seismicity in January by the arrival of magma in the shallow crust. The earthquakes are generated by the fracturing of rock below the edifice in response to the intruding magma and the tremor is a result of the increased degassing of the shallow magma body.

February 2-March 20: sustained tremor

A new tremor sequence beginning on February 5 had a very different character. The spectrum was dominated by frequencies between 2.5 and 5 Hz with a peak at 2.9 Hz, representing a much narrower spectrum than the tremor in late January (Fig. 1.5B). The February tremor varied from a steady, low amplitude-type tremor with D_{RS} 0.2 cm^2 to 12 hour periods of slightly more broadband (frequencies of 1-5 Hz), higher amplitude activity peaked between 3 and 4 Hz with D_{RS} up to 1 cm^2. This style of tremor continued for 20 days (Fig. 1.2) and ended abruptly on February 26 with a vigorous (10 cm^2) 5 minute burst of broadband tremor containing energy above 10 Hz.

We interpret the source of the sustained tremor as hydrothermal. Leet (1988) showed that low-amplitude (<5 cm^2) tremor can be generated by steam bubble growth in water as a result from heat transfer from the surrounding rock. McNutt (1992) showed that the amplitude of volcanic tremor scales with eruption intensity, and that the lowest tremor amplitudes (between 0.05-5 cm^2) can be attributed to hydrothermal activity. Given that no magma had arrived at the surface, and that the values of reduced displacement (0.2-1 cm^2) are relatively low compared to other volcanic settings (volcanic tremor can reach extreme amplitudes of 100,000 cm^2 according to McNutt, 1992), it is likely that the sustained precursory tremor was generated by boiling in the shallow hydrothermal system. Although the January tremor was much higher in amplitude and contained higher

frequencies than the February tremor, the episodes shared similar spectral peaks at 2.9 and more weakly at 1.9 Hz.

At 2100 UTC on March 15 there was a 3 hour episode of low amplitude (0.3 cm^2) tremor that coincided with the first phreatic explosion of the eruptive sequence at 2123 UTC (D_{RS} ~ 3 cm^2).

Explosion Tremor

The magmatic explosions of late March and early April were accompanied by high amplitude tremor that remained sustained for periods of hours to days. The explosion tremor was more broadband than the sustained precursory tremor, with energy spread across the spectrum up to 15 Hz during the vigorous episodes (Fig. 1.5C), and up to 9 Hz during quieter periods. The high amplitude explosion tremor had a broad spectrum with the majority of energy concentrated between 1.5 and 7 Hz, and had two main peaks at 1.8 and 2.8 Hz.

The first and most vigorous episode of explosion tremor followed the closely spaced explosion events 4 and 5 on March 23. This episode produced sustained D_{RS} of 2-5 cm^2 for a period of 9 hours, after which the activity became more spasmodic in character. The spasmodic tremor continued for 5 hours before ceasing abruptly prior to event 6. This explosion tremor followed explosive eruptions, suggesting that the tremor was generated by the vigorous degassing that also followed the explosions. If this is true, then this tremor was a direct manifestation of the degassing of the magma which remained in the conduit after the explosions. Similar models have been proposed by Neuberg et al. (2000) who examined tremor associated with explosions at Soufriere Hills Volcano.

Pseudo-Explosion Tremor

The final episode of high amplitude tremor followed the March 29 swarm. We label this tremor as 'pseudo-explosion tremor' because it occurred within the explosive episode of the eruption but did not follow explosive activity. More spasmodic in character, this tremor was similar in amplitude and frequency content to the March 23 explosion tremor (Fig. 1.5D). It generated D_{RS} in the range 0.5-6 cm^2 and lasted for 20 hours, before changing in character to short-lived bursts lasting less than 30 seconds at much lower amplitudes for a further 48 hours before the onset of the April 2 swarm. The pseudo-explosion tremor spectrum was much more sharply peaked than the explosion tremor spectrum. It also shared several peaks with the late January tremor.

Based on the other available data during this period, it is unclear if there was any ongoing volcanic activity that might have generated the pseudo-explosion tremor. SO_2 emission was relatively low (Lopez et al., 2012) and there was no identifiable infrasound signal (D. Fee, personal communication). However, 2 of the 3 lahars that did not follow explosive activity were observed during this episode of tremor, indicating that there was enough activity occurring at the vent to generate a debris flow. It is also notable that growth of the 3rd lava dome was first recorded during this period (Bull et al., 2012), and the emergence of the new lava dome may have melted ice from the crater glacier that triggered the lahar events. Lightning was detected on two occasions around the time that the lahars were generated, suggesting low-level ash emission was occurring (Behnke et al., 2012). These observations suggest that magma and/or gas were actively venting at this time, and that pseudo-explosion tremor is probably a manifestation of that process.

Swarm Tremor

The March 20 swarm: increase in continuous background tremor

Tremor was associated with 2 of the 6 seismic swarms during the 2009 unrest period, but had a very different character during each episode. The first occurrence of

'swarm tremor' occurred near the end of the March 20 swarm (Fig. 1.5E). As the swarm progressed there was a gradual increase in continuous background tremor as well as occasional bursts of higher amplitude tremor that lasted several minutes. The tremor progressively increased and became continuous 1.5 hours before the eruption, producing a maximum D_{RS} of 2.8 cm^2. The spectrum was relatively broad, spanning from 1.5 up to 7 Hz at some summit stations, similar to the explosion and pseudo-explosion tremor spectra. The fact that the earthquakes continued more or less unchanged while the tremor increased indicates that the two processes were likely not directly related to each other. The earthquakes are thought to be associated with the growth of the first lava dome (see section 4.3). It is possible that the concurrent tremor was caused by vibrations from column of magma ascending from the magma reservoir to the surface, in a model similar to that proposed by Jellinek and Bercovici (2011).

The March 27 swarm: earthquakes merging into tremor

The March 27 swarm produced a different type of swarm tremor. Instead of a gradual increase in background tremor, the volcano-tectonic earthquakes in the swarm became progressively closer in time, merging into a continuous signal (Fig. 1.5F). The tremor spectrum for this episode is broad (like the earthquakes that comprise it), contains energy between 1.5 and 9 Hz and is characterised by sharp peaks of similar amplitude, many of which were shared with the different episodes of tremor examined in this section. After 10 minutes of this steady tremor, the dominant frequencies rose exponentially with time to 10 Hz before abruptly stopping. A minute-long pause followed the end of the tremor before explosion event 9 occurred. This marked the first of several periods of 'gliding tremor' prior to explosive eruptions between events 9 and 18. Hotovec et al. (2012) examine these sequences of events in detail, modelling them as accelerating failure at the edges of an ascending magma plug in the shallow conduit.

Comparing tremor with explosion signals

Figure 1.5G shows the explosion on April 4 for comparison with the different types of tremor. Explosion signals are distinguished from tremor signals primarily through their high amplitude and broad frequency content. Energy between 1 and 9 Hz dominates the spectra although significant energy continues above 20 Hz. These signals are generated during continuous ash emission. It is likely that the variations in the signal strength reflect variations in the rate of sustained emission (McNutt and Nishimura, 2008), although we do not observe this directly. McNutt et al. (2012) and Schneider and Hoblitt (2012) compare the explosion signals to plume height, infrasound and lightning in order to examine different aspects of the eruptive activity. We include an example here to illustrate the differences between tremor and explosion signals.

1.7 Explosion Seismicity

Several authors have addressed details of the explosive eruptions at Redoubt Volcano (Fee et al., 2012; Haney and Chouet, 2012; McNutt et al., 2012). The seismic signals associated with these explosions vary greatly. Our objective here is to distil the explosions to simple parameters that can be put in context with the swarms, tremor and lahars. To accomplish this we use total seismic energy, seismic energy in high and low frequency bands, peak amplitude from reduced displacement, and duration.

Energy is estimated from the broadband three-component records of station RDWB (Fig. 1.1). We calculate a relative measure of seismic energy from the trace of the covariance matrix of the three component displacement waveforms in a moving time window (see Montalbetti and Kanasewich (1970) and Ereditato and Luongo (1994) for examples). We sum this measure over the duration of the explosion to get total seismic energy. Energy in high and low frequency bands is calculated with the same technique using waveforms filtered on 0.3-25 Hz and 0.033-0.3 Hz, respectively. Separating the energies at 0.33 Hz segregates earthquakes and most tremor into the higher band. The ratio of low to high frequency energy shows the relative contributions of each to the total seismic energy (Table 2). The duration of the explosion is measured at station SPU on

Mount Spurr, located 85 km northeast of Mount Redoubt (see Power et al., 2012). We also consider the maximum ash cloud height (Schneider and Hoblitt, 2012).

The first explosion occurred on March 15 (Event 0) and is the smallest explosion in several respects: it has the least seismic energy, the lowest plume height and it did not register at station SPU. This event was phreatic in nature as it contained no juvenile material and deposited only a small amount of ash at the vent (Wallace et al., 2012). This, as well as its timing shortly before the onset of the magmatic activity, suggests that this event was an explosion of gas that had sufficient pressure to break a narrow pathway to the surface but was not accompanied by magma.

On March 23 six magmatic explosions occurred over 22 hours (explosions 1-6 in Table 2). The first three were closely spaced in time and had progressively longer durations. Explosions 4-6 had the greatest seismic energy of the 2009 eruption, some of the longest durations and had two ash plumes exceeding 18 km ASL. With the exception of number 6, these explosions contained a smaller fraction of low frequency energy.

The next sequence of explosions (events 7-18) occurred between March 26 and March 29. The majority of these events produced large ash plumes that exceeded heights of 12 km ASL. They also had shorter durations than events 1-6, and many were preceded by gliding tremor (Hotovec et al., 2012). Beginning on March 28, the explosions had a much greater fraction of low frequency energy than the first explosion sequence. Haney and Chouet (2012) take advantage of this low frequency energy to derive a volumetric source depth of 1.9 km below the crater floor for event 12. Fee et al. (2012) note that the infrasonic pulses associated with these later events were more impulsive and shorter in duration than earlier events. The nature of the deposits was also different during this period, exhibiting much finer grain-sizes than deposits from the March 23-24 explosion sequence, although the chemical composition remained unchanged (Wallace et al., 2012). These observations indicate that the style of the eruptive activity changed during the

March 26-29 sequence. It is possible that the viscosity of the magma increased, resulting in a greater build-up of pressure and material behind the magma plug in the conduit producing the more explosive events with correspondingly larger low frequency components.

After a period of lava effusion and dome growth, the final large explosion of the eruption occurred on April 4 (event 19) after a 5-day earthquake swarm (See section 4.6). This explosion was the longest in duration, producing an ash cloud above 15 km ASL and destroying the lava dome that had been growing since March 29. However, it was of modest energy and contained relatively little low frequency energy. The explosion contained two main pulses and several smaller pulses that are examined in detail by Fee et al. (2012) and Schneider and Hoblitt (2012). The proximal deposits from this sequence contained a large amount of material that was derived from the lava dome, suggesting that dome collapse may have played a role in generating the explosion sequence (Bull et al., 2012, Wallace et al., 2012). We speculate that the longer duration, more gradual onset and relative lack of low frequency energy of this explosion were all due to the influence of the collapsing lava dome. The presence of the dome may have inhibited the final ascent of magma in the shallow conduit, causing the initial phase of the explosion to be weaker. Once enough of the dome had collapsed and/or the explosion had removed enough of the dome to clear the vent area, the explosion was able to progress in the fashion typical of the earlier explosion events.

1.8 Lahars

The steep sided, heavily glaciated edifice of Redoubt Volcano makes it an ideal setting for pyroclastic flows, debris avalanches and lahars. The latter is of particular relevance due to the Drift River Marine Terminal at the mouth of the Drift River (Fig. 1.1)—a well-documented hazard prior to the 2009 eruption. During the 1989-90 eruption the larger lahars reached the oil terminal, prompting operations at the terminal to be suspended.

Seismic records from lahars share similar frequency content and duration to pyroclastic flows and can be difficult to distinguish with out additional information (e.g. Marcial et al., 1994; Nye et al., 1995; Huang et al., 2007). Visual observations exist from time-lapse cameras in the Drift River Valley, but the photos rely on daylight and good weather and are therefore sporadic (Bull et al., 2012; Waythomas et al., 2012). Given the location of the seismic stations along the main lahar channel, their more distal locations from the edifice, and the long durations of these seismic signals following the explosions, it is likely that the majority of flow-type seismic signals were due to lahars. Without visual confirmation, however, we cannot conclusively discriminate between pyroclastic flow and lahar signals, and instead we refer to these signals as 'flow events'.

Quantifying the lahar seismic record

Flow signals were identified by visually scanning the data for sustained seismic activity on stations RDE and DFR, which were located on either side of the Drift River valley. Most of the flow events followed explosions and shared some common signal characteristics to the explosions, including durations greater than 10 minutes and energy up to 25 Hz. However, the majority of the energy in the explosion signals was concentrated below 5 Hz, whereas the energy in the flow signals was more broadly distributed in frequency. Figure 1.6 compares the frequency spectra between station NCT, DFR, RDE and RDN. Located close to the vent, the seismic record at station RDN was dominated by the explosion. Stations NCT, DFR and RDE are located at similar distances from the vent and recorded the explosion signals, however only stations DFR and RDE were located near Drift River valley and recorded flow signals. While the explosion and flow signals appeared as discrete events at station DFR, the transition between explosion signal and flow signal at RDE was less clear. Also of note in Figure 1.6 is an apparent discrepancy in the concentration of energy from 8 to 10 Hz between stations RDE and DFR. Regardless of whether this is a site response or sensor noise, it appears consistent throughout the eruption.

We filter waveform data between 5 and 10 Hz to emphasize flow signals over explosion signals. The timing of the flow events is determined from the signal to noise ratio (SNR) of the filtered waveforms at stations RDE and DFR (Fig. 1.6B, D, F, H). We define the noise for each flow event by averaging the signal over a 2 minute window prior to the onset of the activity at the vent. The SNRs of these events were typically double peaked, with the first peak due to the explosion signal and the second peak due to the flow passing close to the station. We define the flow onsets at the SNR minimum between the explosion and lahar peaks. Flow event end times are defined as the time when the SNR drops below 2. Although subjective, these definitions enable a quantitative comparison of the flow seismic records. Errors within the onset times are estimated visually, and range between 1 and 10 minutes largely because of variations in the explosion signals that preceded them. Errors in the end times are based on the transition from SNR 2 to SNR 1.

To estimate the relative location and properties of each flow we examine the seismic amplitude at stations RDE and DFR on opposite sides of the Drift River Valley. We calculate the maximum amplitude of the flow by taking the mean amplitude of the filtered signal in a two-minute window around the peak SNR. The mean amplitude ensures that high amplitude spikes from earthquakes did not contaminate the data.

Lahar comparisons

A total of 20 events are identified, 19 of which are recorded at station RDE and 17 at DFR (Table 3). All but three of the flow events followed the major explosions listed in Table 2. The three remaining flows followed significant summit seismic events. These seismic events may have been very small explosions or gravitational collapses of loose material. The time delay between summit events and the onset of the seismic signal at stations DFR and RDE varied between 4 and 26 minutes. This time difference is influenced by the flow path, the volume of the flow, and the duration of the explosion signal that masks the calculated onset time.

The majority of the flow signals recorded during the March 23-24 explosions had larger seismic amplitudes on both RDE and DFR than those recorded later in the sequence. There were 2 exceptions (Table 3): 1) the first weak flow event (flow event 1) recorded on March 23 was notably smaller than the flows that followed, and 2) the flow following event 19 on April 4 had larger amplitudes than the flows earlier in the sequence. With the exception of the April 4 flow, only the March 23-24 flow events reached the Drift River Marine Terminal (Schaefer, 2012; Waythomas et al., 2012). This suggests that the earlier flows were volumetrically larger than most of the later flows, and that the seismic amplitudes are proportionate to the flow volume.

Most flow events had the highest amplitudes at station RDE, which is closer to the Drift River valley both in distance and elevation making it more sensitive to flows in the main channel. Field observations confirm that the majority of flows, particularly early in the eruption, flowed predominantly down the south side of the river valley close to RDE (Waythomas et al., 2012). Comparison of the maximum amplitudes at RDE and DFR shows some variation between flows. The ratios of the maximum amplitudes on each station are shown in Table 3 and vary in general between 1 and 2. Flows that migrated further north in the valley have higher maximum amplitude ratios. The maximum amplitude ratio is a useful metric from a monitoring perspective, as it indicates a relative location of the flow within the complex channel system.

Higher amplitudes correspond to longer durations in all but one case (flow event 11), where heavy tephra fall was recorded in the Drift River valley and no change in Drift River discharge was observed from the Dumbell Hills camera (Bull and Buurman, 2012), suggesting that this event may have been a pyroclastic flow rather than a lahar. The lower seismic amplitude of flow event 11 may reflect weaker coupling between the pyroclastic flow and the ground, or that the pyroclastic flows are less energetic than the lahars at those distances. Most events had earlier onsets at station DFR, located up-valley of RDE, although 4 events appeared earlier at station RDE. Those events that were seen at RDE

first had lower maximum amplitudes at DFR, suggesting the flow was mostly restricted to the southern part of the valley and lacked the energy needed for the early part of the flow to appear at station DFR.

1.9 Background Seismicity

In this section we examine the seismic event detection rate (EDR) of the automated catalog outside of the swarms identified using the criteria described in section 4. This "background" seismicity includes signals generated by rockfalls and glacial quakes (glaciers cover 80% of the upper volcanic edifice), as well as high- and low-frequency volcanogenic earthquakes. Because the event detection rate is sensitive to many types of seismic activity it is a good qualitative metric of overall unrest. Many volcanoes have increased rates of small earthquakes prior to eruption. Rockfalls demonstrate instability in the upper portions of the edifice that has been shown to be precursory at times (Deroin and McNutt, 2012), and glacier ice is highly sensitive to temperature and deformation near the vent. In the absence of tremor the EDR can, at times, be the primary seismic metric by which to assess unrest. We examine the EDR chronologically, dividing it into 3 sections: 1) prior to the onset of explosive activity, from January 1 through March 20; 2) during the explosive activity, from March 23 through April 2; and 3) following the explosive activity during steady dome growth from April 4 through May 31.

Precursory EDR: January 1-March 20

The first major increase in EDR occurred on January 27, two days after the first significant tremor. This followed a spike in EDR on the January 25 that was coincident with the first episode of high amplitude precursory tremor. Previous to the onset of tremor, the EDR fluctuated mostly between 2 and 6 events per hour (Fig. 1.2). This activity represented the true background seismicity at Redoubt Volcano outside of any eruptive activity, and it was largely dominated by small amplitude events originating from the heavily glaciated edifice. Following the onset of tremor the EDR increased to rates of 3-10 events per hour. Both volcano-tectonic and low-frequency earthquakes were located in the analyst-reviewed catalog, and while the volcano-tectonic activity was

confined to the summit region, earthquakes with lower frequencies exhibited scatter below the edifice down to depths of 4 km. This elevated EDR dropped on February 6 concurrent with the increase in tremor (likely due to the decrease in detection capabilities due to the tremor signal), and remained low until the February 26 swarm. Once the February 26 swarm ended, the seismicity rates returned to the same elevated levels that had persisted during late January and early February.

The onset of tremor indicated an increase in fluid movement in the shallow portions of the magmatic system below Redoubt Volcano. The seismicity that followed was likely also generated by the reactivated shallow hydrothermal system. During the tremor episodes the background noise level at the summit stations was higher which decreased the signal to noise ratio of the earthquake activity and resulted in fewer earthquake detections. This was also the reason for the apparent delay in the increase in the EDR following the first burst of tremor on January 25.

EDR during explosive activity: March 23 – April 2

The seismic record in late March was dominated by explosive activity, episodes of tremor and several seismic swarms—all of which masked the EDR for significant periods of time. In addition, the summit station RSO was destroyed during an explosion on March 23 which reduced the number of smaller earthquake detections.

Following the explosion sequence on March 23-24, the EDR was slightly lower than it had been prior to the March 20 swarm, and was comparable to the background prior to late January (Fig. 1.2). Rates remained low through the second explosion sequence on March 27-29, and picked up again following the March 29 swarm. The increase in EDR following the March 29 swarm coincided with renewed dome growth which was observed during March 29 and April 2 (Bull et al., 2012). However dome growth was also observed between March 24 and March 27 during a period of lower EDR, which suggests that dome growth was not the only source of seismicity during this period.

EDR during steady dome growth: April 4 - May 31

The EDR was highest between the April 2 and May 2 swarms. Immediately following the April 02 swarm the EDR was greater than prior to the swarm, and increased further on April 17 when summit station RSO was repaired (Fig. 1.2). Rates remained fairly steady until the onset of the May 2 swarm. We attribute the high EDR during April and May to the growing lava dome. Dome growth at other volcanoes is often characterised by high rates of low-frequency seismicity and rockfall signals (e.g. Soufriere Hills Volcano (Luckett et al., 2008); Augustine Volcano (Power and Lalla, 2010).The EDR declined slightly after the May 2 swarm, when changes in the dome facies and extrusion rate were observed (Bull et al., 2012). It is likely that the lava dome extruded then had a different seismic character, producing fewer events as the dome grew and cooled.

A notable feature of the background seismicity during this period was the presence of several families of repeating earthquakes which began towards the end of the April 2 swarm and persisted through April and May. These earthquake families were dominated by high frequencies around 10 Hz, had impulsive P- and S-wave arrivals and showed S-P times of 1 second at summit station REF. The fact that these earthquakes were dominated by such high frequencies further increased the significance of their high cross correlation values (>0.75), since high frequency earthquakes recorded at volcanoes are not commonly found to repeat due to their destructive brittle failure source mechanisms. Some of the earthquakes from this repeating family were large enough to be included in the analyst-reviewed catalog, where their locations are scattered around 4km below sea level. Given that they first appeared immediately prior to the last and most voluminous explosion on April 4, it is likely that these events were generated from the stress adjustment around the magma reservoir. This was observed during the 1989 eruption of Redoubt Volcano (Power et al., 1994), as well as at other volcanoes including Mount St Helens in 1980 (Moran, 1994), Augustine in 2006 (Power and Lalla, 2010) and Pinatubo (Mori et al., 1996). This type of seismicity was seen much earlier on during the

1989 eruption than was observed during the 2009 eruption (Power et al., 2012). We speculate that, until the April 4 explosions, not enough material had been removed from the deeper (greater than 4 km depth) magma reservoirs to allow for any stress adjustment. In addition the last explosion on April 4 may have had the effect of finally establishing an open conduit system that was able to support prolonged and stable dome growth that lasted through the end of the eruptive period. These repeating earthquake families were then produced by the relaxation of the conduit system behind the last of the ascending magma, which continued to erupt as a stable lava dome.

1.10 Summary

The progression of magma through the conduit system during the 2009 unrest at Redoubt Volcano can be readily tracked by the seismicity. The deep LP earthquakes in December gave the first indications that magma was moving at depth. By late January it had ascended to depths where gas and heat could easily escape to the surface, generating the precursory tremor and swarm episodes. The first pulse of magma to reach the surface produced a lava dome on March 23 and was preceded by a seismic swarm, which was generated as the shallow conduit system was opened. Dome effusion lasted only 10 hours before a series of magmatic explosions occurred which produced high amplitude tremor that continued for several hours on March 24. The explosions melted much of the ice that formed the upper Drift glacier, generating voluminous lahars that were recorded seismically as they flowed down the Drift River valley to the coast. The next pulse of magma erupted on March 26-30 as a series of powerful explosions, many of which were preceded by tremor that was composed of closely spaced earthquakes. This batch of magma had slightly different properties, producing finer-grained deposits and more impulsive explosion signals. The explosions were followed by a short-lived swarm that accompanied the onset of renewed lava dome growth that continued steadily for several days before stalling, concurrent with a 43-hour seismic swarm. During the final hours of the swarm a family of deeper repeating earthquakes began and persisted through the end of May, reflecting relaxation around the mid-crustal magma storage area in response to the evacuation of the magma. The final and longest-lasting explosion of the eruption

followed the seismic swarm on April 4, generating a large lahar which reached the coast. Lava continued to erupt following the explosive activity and the steady dome growth lasted through June, accompanied by high rates of summit seismicity which was likely generated by the extrusion of the lava dome. A change in the lava properties in early May was accompanied by a long-lived but low amplitude swarm of repeating earthquakes, but no explosive activity followed and the dome continued to grow, largely uninterrupted.

The variety of signals present in the seismic data reflect the variety of volcanic processes which generated them. These processes are often closely linked, as is evident from the interplay between the tremor and swarm sequences, the lahar and explosion signals and the EDR with different types of eruptive activity. Our interpretations of these signals benefited greatly from the numerous other datasets collected during the eruption. Rarely was there volcanic activity that did not manifest itself in some way seismically, however, resulting in a remarkably complete eruption chronology within the seismic record of the 2009 eruption.

It is clear from our preliminary overview that much work remains to be done with the seismic dataset from the 2009 eruption. Many areas within the seismic dataset remain poorly understood, including the sources of the various tremor episodes, the relationship of the seismic signals from the lahars to the physical properties of the flows, and the cause of the waveform evolution observed during several of the swarm episodes. As with the 1989 Redoubt eruption, we expect to see studies emerging from the seismic record for years to come.

1.11 Acknowledgements

Reviews from Phil Dawson, Wendy McCausland and an anonymous reviewer substantially improved this manuscript. We also thank John Power for an early review and additional valuable insights. We were fortunate to draw on the experience and insights from many different people. Useful discussions with Kate Bull, David Fee, Taryn Lopez and John Power greatly assisted many of our interpretations. We thank

Alicia Hotovec for discussions regarding tremor and swarms, David Fee for input on explosion and tremor data and Julie Griswold, Chris Waythomas and Kate Bull for insights into lahars. The map in Figure 1.1 was modified from Ronni Grapenthin. John Paskievitch, Cyrus Read, Max Kaufman, Ed Clark and Ryan Bierma provided technical support in the field, and Cyrus Read provided additional site information that greatly assisted our interpretations. The Alaska Volcano Observatory is a partnership between the U.S. Geological Survey, the Geophysical Institute at the University of Alaska Fairbanks, and the Alaska Division of Geological and Geophysical Surveys.

1.12 References

Behnke, S. A., Thomas, R. J., McNutt, S. R., Krehbiel, P. R., Rison, W. Edens, H. E., 2012. Observations of Volcanic Lightning During the 2009 Eruption of Redoubt Volcano. Journal of Volcanology and Geothermal Research, doi:10.1016/j.jvolgeores.2011.12.010 .

Bleick, H. A., Coombs, M. L., Bull, K., Wessels, R., 2012. Volcano-ice interactions during the precursory phase of unrest preceding the 2009 eruption of Redoubt Volcano. Journal of Volcanology and Geothermal Research,doi: 10.1016/j.jvolgeores.2012.10.008

Bull, K.F and H. Buurman (2012), An overview of the 2009 eruption of Redoubt Volcano, Alaska, J. Volcanol. Geotherm. Res., doi:10.1016/j.jvolgeores.2012.06.024.

Bull, K., Anderson, S. W., Diefenbach, A., Wessels, R. L., Henton, S. M., 2012. Emplacement of the final lava dome of the 2009 eruption of Redoubt volcano. Journal of Volcanology and Geothermal Research,doi: 10.1016/j.jvolgeores.2012.06.014

Buurman, H. West, M.E., 2010. Seismic precursors to volcanic explosions during the 2006 eruption of Augustine Volcano. In: Power, J.A., Coombs, M.L. and Freymueller, J.T. (Eds.), The 2006 eruption of Augustine Volcano. U.S. Geological Survey Professional Paper 1769, Menlo Park, CA, 41-57.

Chouet, B.A., Page, R.A., Stephens, C.D., Lahr, J.C. Power, J.A., 1994. Precursory swarms of long-period events at Redoubt Volcano (1989-1990), Alaska – Their origin and use as a forecasting tool. In: T. P. and Chouet, B. A., (eds.), The 1989-1990 eruptions of Redoubt Volcano, Alaska. Journal of Volcanology and Geothermal Research 62, 95-135.

Deroin, N., McNutt, S., 2012. Rockfalls at Augustine Volcano, Alaska: The influence of eruption precursors and seasonal factors on occurrence patterns 1997–2009. Journal of Volcanology and Geothermal Research, 211, 61-75.

Diefenbach, A.K., Bull, K. F., Wessels, R. L., McGimsey, R., 2012. Photogrammetric monitoring of lava dome growth during the 2009 eruption of Redoubt Volcano. Journal of Volcanology and Geothermal Research, doi:10.1016/j.jvolgeores.2011.12.009.

Dixon, J.P., Stihler, S.D., Power, J.A., Searcy, C., 2010. Catalog of earthquake hypocenters at Alaskan volcanoes: January 1 through December 31, 2009. U.S. Geological Survey Data Series 531, 84 pp.

Ereditato, D., Luongo, G., 1994. Volcanic tremor wave field during quiescent and eruptive activity at Mt. Etna (Sicily). Journal of Volcanology and Geothermal Research 61, 239–25.

Fee, D., McNutt, S., Arnoult, K., Szuberla, C., Olson, J., Lopez, T., 2012. Combining Local and Remote Infrasound Recordings from the 2009 Redoubt Volcano Eruption. Journal of Volcanology and Geothermal Research, doi: 10.1016/j.jvolgeores.2011.09.012

Fehler, M., 1983. Observations of Volcanic Tremor at Mount St. Helens Volcano. Journal of Geophysical Research 88 (B4), 3476-3484.

Grapenthin, R., Freymueller, J. T., Cervelli, P., 2012. Geodetic Observations during the 2009 eruption of Redoubt Volcano: Alaska. Journal of Volcanology and Geothermal Research, doi: 10.1016/j.jvolgeores.2012.11.012.

Haney, M. M., Chouet, B. A., Dawson, P. B., Power, J. A., 2012. Source characteristics of an explosion during the 2009 eruption of Redoubt Volcano, Alaska, from very-long-period seismic waves. Journal of Volcanology and Geothermal Research, doi:10.1016/j.jvolgeores.2012.04.018.

Hotovec, A., Prejean, S., Vidale, J., Gomberg, J., 2012. Strongly Gliding Harmonic Tremor During the 2009 Eruption of Redoubt Volcano:. Journal of Volcanology and Geothermal Research, doi:10.1016/j.jvolgeores.2012.01.001

Huang, C., Yin, H., Chen, C., Yeh, C., Wang, C., 2007. Ground vibrations produced by rock motions and debris flows: Journal of Geophysical Research 112 (F02014). doi:10.1029/2005JF000437.

Iverson, R.M., Dzurisin, D., Gardner C.A., Gerlach, T.M., LaHusen, R.G., Lisowski, M., Major, J.J., Malone, S.D., Messerich, J.A., Moran, S.C., Pallister, J.S., Qamar, A.I., Schilling S.P., Vallance, J.W., 2006. Dynamics of seismogenic volcanic extrusion at Mount St. Helens in 2004-2005, Nature 444, 439-443.

Jellinek, AM, Bercovici, D., 2011. Seismic tremors and magma wagging during explosive volcanism, Nature 470 (7335), 522-525.

Lahr, J., Chouet, B.A., Stephens, C.D., Power, J.A., Page, R.A., 1994. Earthquake classification, location and error analysis in a volcanic environment: implications for the magmatic system at Redoubt Volcano, Alaska. Journal of Volcanology and Geothermal Research 62, 137-151.

Leet, R., 1988. Saturated and Subcooled Hydrothermal Boiling in Groundwater Flow Channels as a Source of Harmonic Tremor. Journal of Geophysical Research 93 (B5), 4835-4849.

Lopez, T., Carn, S., Werner, C., Kelly, P., Doukas, M., Fee, D., Webley, P. W., Cahill, C., Schneider, D., 2012. Ozone Monitoring Instrument (OMI) measurements of sulfur dioxide during the 2009 eruption of Redoubt volcano. Journal of Volcanology and Geothermal Research, doi:10.1016/j.jvolgeores.2012.03.002.

Luckett, R., Loughlin, S., De Angelis, S., Ryan, G., 2008. Volcanic seismicity at Montserrat, a comparison between the 2005 dome growth episode and earlier dome growth. *Journal of Volcanology and Geothermal Research* 177 (4). doi:10.1029/2010GL042547.

Marcial, M., Melosantos, A.A., Hadley, K.C., LaHusen, R.G., Marso, J.N., 1994. Instrumental Lahar Monitoring at Mount Pinatubo. Newhall C. G. and Punongbayan R. S. (Eds.), Fire and Mud: Eruptions and Lahars of Mount Pinatubo, Philippines. PHIVOLCS and University of Washington, Seattle, 1015-1022.

McNutt, S.R., 1992. Volcanic Tremor. Encyclopedia of Earth System Science. Academic Press, San Diego, CA, 417-425.

McNutt, S.R., Nishimura, T., 2008 Volcanic Tremor During Eruptions: Temporal Characteristics, Scaling and Estimates of Vent Radius. Journal of Volcanology and Geothermal Research 178, 10-18.

McNutt, S. R., Thompson, G., West, M.E., Fee, D., Stihler, S., Clark , E., 2012. Local seismic and infrasound observations of the 2009 explosive eruptions of Redoubt Volcano, Alaska. Journal of Volcanology and Geothermal Research.

Mogi, K., 1963. Some discussions on aftershocks, foreshocks and earthquake swarms, the fracture of a semi-infinite body caused by an inner stress origin and its relation to the earthquake phenomena. Bulletin of the Earthquake Research Institute-University of Tokyo 41, 615-658.

Montalbetti, J.F., Kanasewich, E.R., 1970. Enhancement of Teleseismic Body Phases with a Polarization Filter. Geophysical Journal of the Royal Astronomical Society 21, 119–129.

Moran, S.C., 1994, Seismicity at Mount St. Helens, 1987-1992: Evidence for repressurization of an active magmatic system. Journal of Geophysical Research, 99 (B3), 4341-4354.

Mori, J., White, R.A., Harlow, D.H., Okubo, P., Power, J.A., Hoblitt, R.P., Laguerta, E.P., Lanuza, A., Bautista B.C., 1996. Volcanic Earthquakes following the 1991 Climactic Eruption of Mount Pinatubo: Strong Seismicity during a Waning Eruption. Newhall C. G. and Punongbayan R. S. (Eds.), Fire and Mud: Eruptions and Lahars of Mount Pinatubo, Philippines. PHIVOLCS and University of Washington, Seattle, 339-350.

Neuberg, J., Luckett, R., Baptie, B., Olsen, K., 2000. Models of tremor and low-frequency earthquake swarms on Montserrat. Journal of Volcanology and Geothermal Research 101, 83-104.

Nye, C.J., Hammond, W.R., Tytgat, G.C., Dorava, J.M., 1995. June 29,1993, Outburst Flood from Kidazgeni Glacier, Mount Spurr Volcano, Alaska. T. Keith (Ed.), The 1992 Eruptions of Crater Peak Vent, Mount Spurr Volcano, Alaska. USGS Survey Bulletin 2139, 199-204.

Power, J.A., Lalla, D.J., 2010. Seismic observations of Augustine Volcano, 1970-2007. Power, J.A., Coombs, M.L. and Freymueller, J.T. (Eds.), The 2006 eruption of Augustine Volcano. U.S. Geological Survey Professional Paper 1769, Menlo Park, CA, 3-40.

Power, J.A., Lahr, J. C., Page, R.A., Chouet, B. A., Stephens, C.D., Harlow, D.H., Murray, T.L., Davies, J.N., 1994. Seismic evolution of the 1989-1990 eruption sequence of Redoubt Volcano, Alaska. Miller. T. P. and Chouet, B. A., (eds.), The 1989-1990 eruptions of Redoubt Volcano, Alaska. Journal of Volcanology and Geothermal Research 62 (1), 69-94.

Power. J.A., Stihler, S., Chouet, B.A., Haney, M.M., Ketner, D.M., 2012. Seismic observations of Redoubt Volcano, Alaska — 1989–2010 and a conceptual model of the Redoubt magmatic. Journal of Volcanology and Geothermal Research, doi: 10.1016/j.jvolgeores.2012.09.014

Schaefer, J. G., 2012. The eruption of Redoubt Volcano, Alaska. Alaska Division of Geological and Geophysical Surveys Report of Investigations 2011-5, 45 pp.

Schneider, D., Hoblitt, R., 2012. Doppler weather radar observations of the 2009 eruption of Redoubt Volcano. Journal of Volcanology and Geothermal Research, doi: 10.1016/j.jvolgeores.2012.11.004

Stephens, C.D. and Chouet, B.A., 2001. Evolution of the December 14, 1989 precursory long-period event swarm at Redoubt Volcano, Alaska. Journal of Volcanology and Geothermal Research 109, 133-148.

Thelen, W., West, M.E., Senyukov, S., 2010. Seismic Characterization of the Fall 2007 Eruptive Sequence at Bezymianny Volcano, Russia. Journal of Volcanology and Geothermal Research 194, 201-213.

Thompson, G., West., M.E., 2010. Real-time Detection of Earthquake Swarms at Redoubt Volcano, 2009. Seismological Research Letters, 81 (3), 505-513.

Wallace, K., Schaefer, J., Coombs, M., 2012. Character, mass, distribution, and origin of tephra-fall deposits from the 2009 eruption of Redoubt Volcano, Alaska. Journal of Volcanology and Geothermal Research, doi: 10.1016/j.jvolgeores.2012.09.015.

Waythomas, C.F., Pierson, T.C., Major, J.J., Scott, W.E., 2012. Voluminous Ice- and Water-Rich Lahars Generated During the 2009 Eruption of Redoubt Volcano, Alaska. Journal of Volcanology and Geothermal Research, doi:10.1016/j.jvolgeores.2012.05.012.

Werner, C., Kelly, P.J., Doukas,M., Lopez, T., Pfeffer,M., McGimsey, R.G., Neal,C.A., 2012. Degassing associated with the 2009 Eruption of Redoubt Volcano, Alaska. Journal of Volcanology and Geothermal Research, doi:10.1016/j.jvolgeores.2012.04.012.

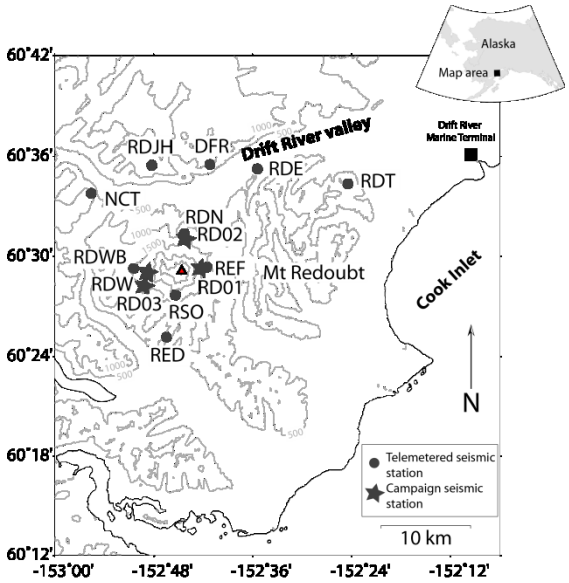

Figure 1.1 Map of the Redoubt seismic network that was operational during the 2009 eruption. The inset shows the location relative to Alaska. Stars indicate campaign-style seismometers with on site recording, and circles indicate the telemetered seismic stations used for monitoring during the eruption.

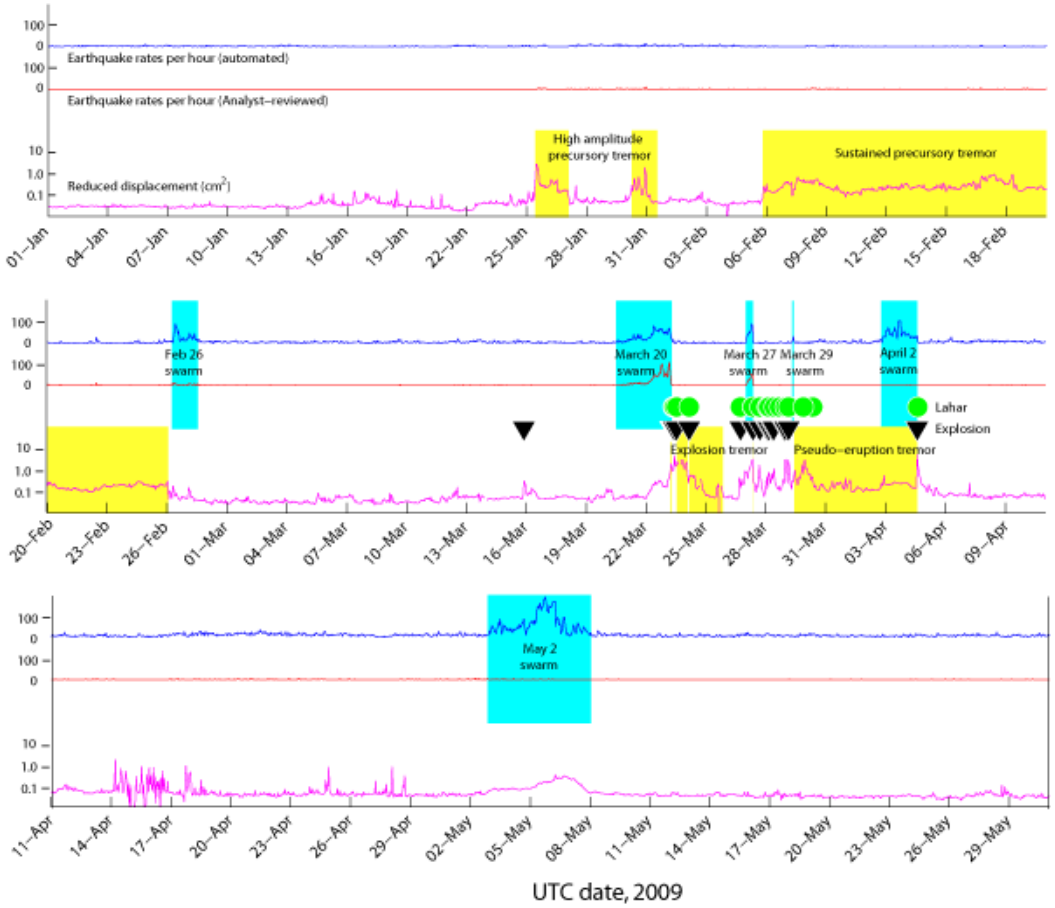

Figure 1.2. Seismicity of the Redoubt eruption, spanning January 1, 2009 through June 1, 2009. Earthquake rates per hour from the automated catalog are shown at the top (blue). The middle time series (red) shows earthquake rates per hour derived from the analyst-reviewed earthquake catalog. Superimposed on these time series are the six swarm episodes (light blue shaded area). The bottom time series shows the log of the surface wave reduced displacement in cm^2 (red), with significant tremor episodes superimposed (yellow shaded area). Explosions are indicated by black triangles and lahars by green circles.

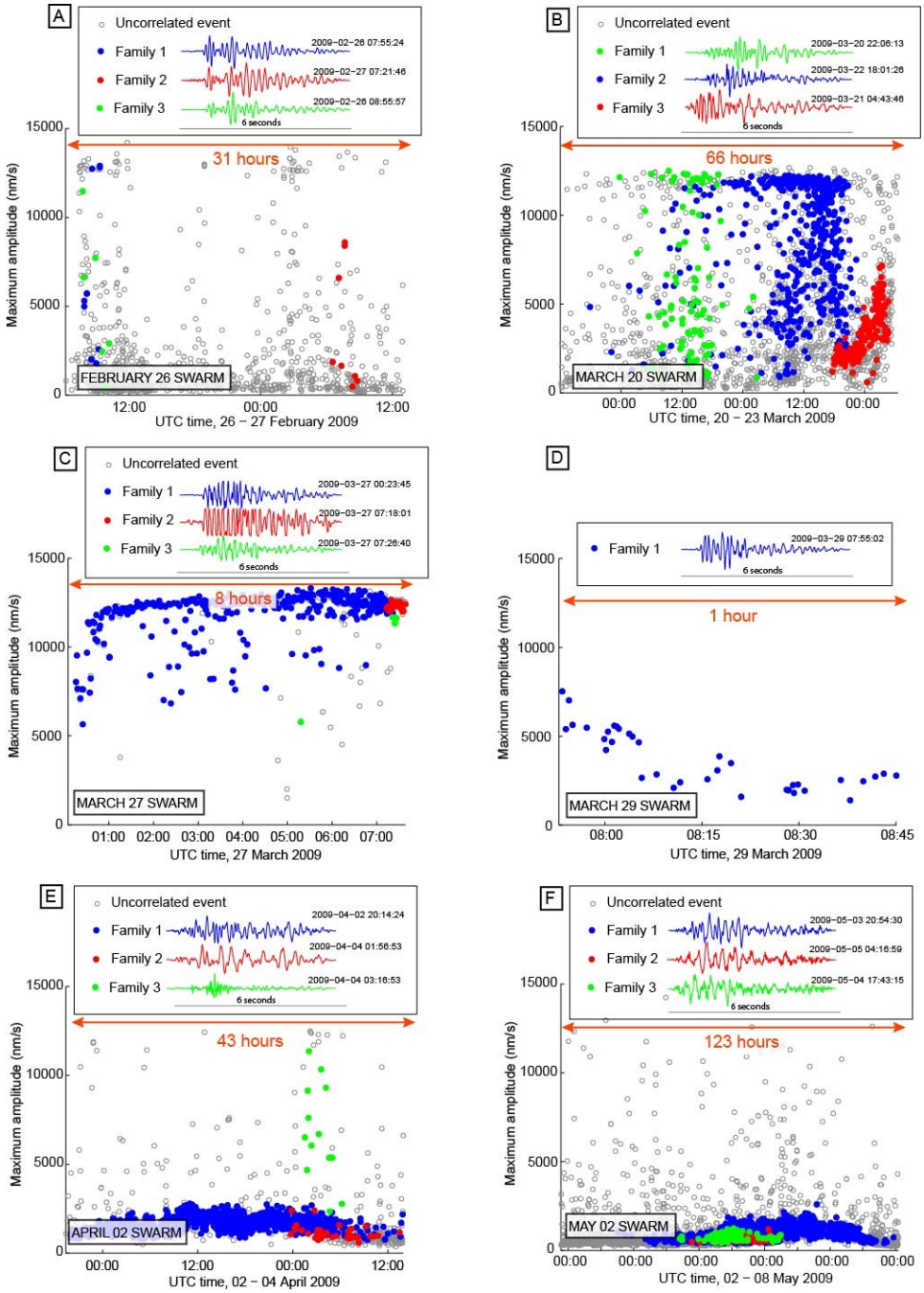

Figure 1.3 Maximum waveform amplitudes (in nm/s) plotted as a function of time for the 6 seismic swarms.

Events belonging to the three largest waveform families within each swarm are coloured, while all other events are plotted as empty circles. Representative waveforms from the 3 largest event families are shown above each plot. A) February 26 swarm, B) March 20 swarm, C) March 27 swarm, D) March 29 swarm, which only contained 1 family of events, E) April 2 swarm, F) May 2 swarm. All waveforms shown were recorded at station REF; note the clipping in panel C.

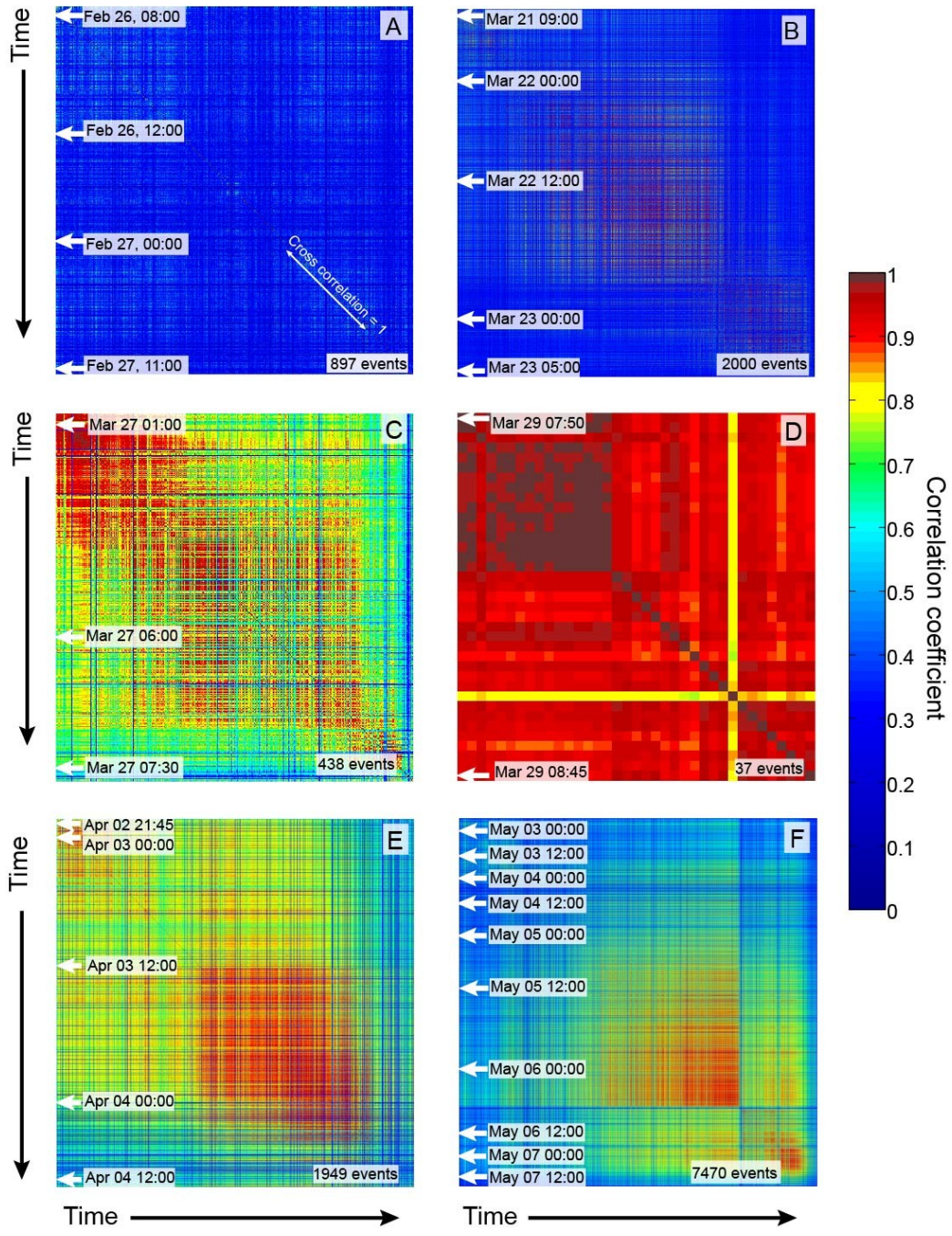

Figure 1.4 Cross correlation plots for the 6 Redoubt swarms.
Each pixel represents a cross correlation pair, where the colour represents the maximum cross correlation value between the two events. Time progresses top to bottom and left to right in each panel, and in each plot the diagonal is equal to 1 (the auto-correlation, highlighted in A). A) February 26 swarm, B) March 21 swarm with the 3 largest families circled, C) March 27 swarm, D), March 29 swarm, E) April 2 swarm, F) May 2 swarm.

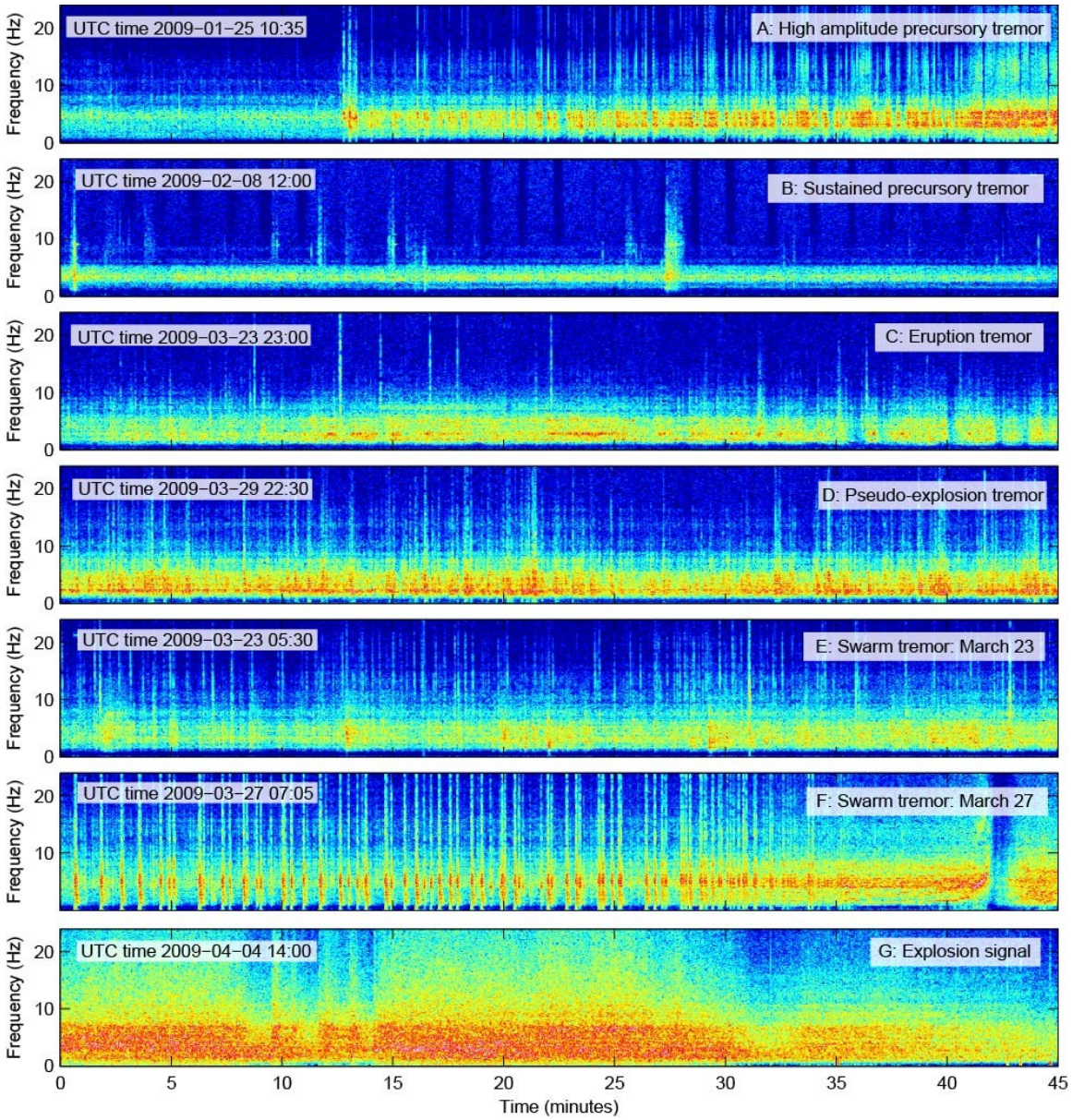

Figure 1.5 Spectrogram examples of the different types of tremor recorded at station REF during the eruption.
The location of REF is shown in Fig. 1.1.

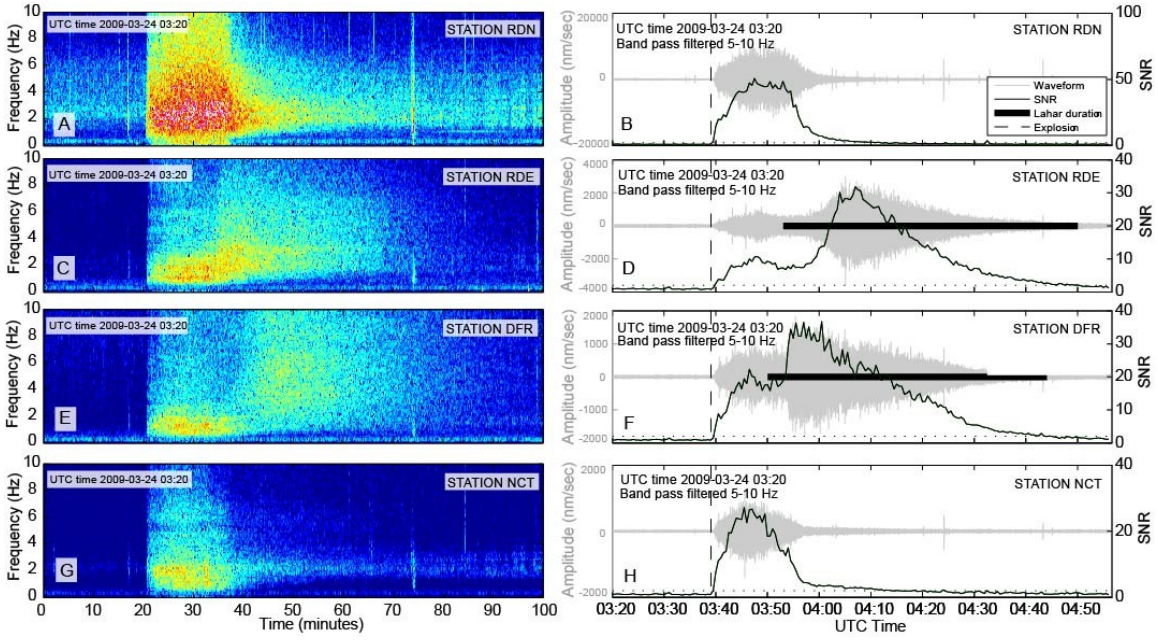

Figure 1.6 Lahar on March 24 recorded at 4 stations on the Redoubt network. Panels A, C, E and G show the spectra of the signals at stations RDN, RDE, DFR and NCT respectively. Panels B,D,F and H show the waveforms for the same event in grey, filtered between 5-10 Hz, and the signal to noise ratio (SNR) in black. Lahar durations are shown in black horizontal bars for stations RDE and DFR. The explosion onset is indicated by the dashed vertical line.

Table 1.1 The timing of the six seismic swarms identified during the 2009 Redoubt unrest. Also shown are the total number of earthquakes, earthquake rates per hour, and repeating earthquake rates per hour. The percent of earthquakes which repeat is calculated by dividing the total number of earthquakes in the swarm by the number of earthquakes which meet the similarity criteria discussed in section 3.

Swarm	Swarm start	Swarm end	duration (hours)	Total earthquakes	Maximum earthquake rate (per hour)	Maximum repeating earthquake rate (per hour)	Percent of earthquakes which repeat	Precedes explosion?
February 26	2/26/2009 6:00	2/27/2009 13:00	31	897	91	12	6	no
March 20	3/20/2009 12:00	3/23/2009 6:34	66	2000	82	54	68	yes
March 27	3/27/2009 0:00	3/27/2009 8:28	8	438	92	81	89	yes
March 29	3/29/2009 7:50	3/29/2009 9:00	1	37	32	32	100	no
April 2	4/2/2009 19:00	4/4/2009 13:58	43	1949	107	100	77	yes
May 2	5/2/2009 21:00	5/8/2009 1:00	123	7470	191	164	57	no

Table 1.2 Data for each of the 19 explosion events defined by Schaefer, 2012.
Total energy is calculated at station RDWB using the trace of the covariance matrix of the three component displacement waveforms in a moving time window, and the L/H ratio is the ratio between the energy in low and high frequency bands (0.3-25 Hz and 0.033-0.3 Hz respectively).

Event number[1]	Time (UTC)	Total energy	L/H ratio	duration at station SPU (min)[2]	Precursory swarm?	height (m)[3]
0	3/15/2009 21:05:00	0.7	23.8	-	no	4600
1	3/23/2009 6:34:00	1.3	1.6	2	yes	4500
2	3/23/2009 7:02:00	16.1	3.7	5	no	13400
3	3/23/2009 8:14:00	8.3	1.4	20	no	14600
4	3/23/2009 9:38:00	141.3	1.6	22	no	13100
5	3/23/2009 12:30:00	123.2	4.8	20	no	18300
6	3/24/2009 3:40:00	120.4	26.2	15	no	18300
7	3/26/2009 16:34:00	2.4	23.3	<1	no	8200
8	3/26/2009 17:24:00	43.2	6.7	11	no	18900
9	3/27/2009 7:47:00	10.4	11.3	<1	yes	12500
10	3/27/2009 8:28:00	24.3	11.2	5	no	14900
11	3/27/2009 16:39:00	50.5	11.2	8	no	15500
12	3/28/2009 1:34:00	76.5	60.2	2	no	14600
13	3/28/2009 3:24:00	31.9	29.2	4	no	15200
14	3/28/2009 7:19:00	23.1	28.7	2	no	14600
15	3/28/2009 9:19:00	7.9	54.1	2	no	14600
16	3/28/2009 21:40:00	6.8	1.8	6	no	5200
17	3/28/2009 23:29:00	13.1	9.6	9	no	12500
18	3/29/2009 3:23:00	13.1	21.9	10	no	14600
19	4/4/2009 13:58:00	15.8	2	31	yes	15200

[1]Schaefer, 2011; Buurman and Bull, 2012.

[2]Power et al., 2012.

[3]Schneider and Hoblitt, 2012.

Table 1.3 Lahar signal comparisons between stations RDE and DFR. Max amp is the mean amplitude in a 2 minute window around the peak signal to noise ratio (SNR); the onset time is the time when the SNR begins to increase following the decay from the explosion signal; the onset error is based on visual estimates; the end time is the time when the SNR drops below 2; and the end error is the number of minutes for the SNR to drop from 2 to 1.

Lahar number	RDE start time (UTC)	Onset error (min)	RDE end time (UTC)	RDE end error (min)	RDE duration (min)	RDE time since last explosion (min)	Follows explosion?	RDE Max amp (nm/s)	DFR start time (UTC)	Onset error (min)	DFR end time (UTC)	DFR end error (min)	DFR duration (min)	DFR time since last explosion (min)	Follows explosion ?	DFR Max amp (nm/s)	Max RDE / Max DFR	Max DFR / Max RDE
1	3/23/2009 8:40:00	4	39895.38264	17	31	26	yes	161	3/23/2009 8:33:00	6	3/23/2009 9:04:00	34	31	19	yes	94	1.7	0.6
2	3/23/2009 10:00:00	2	3/23/2009 11:50:00	34	110	12	yes	542	3/23/2009 9:58:00	6	3/23/2009 11:49:00	31	111	10	yes	427	1.3	0.8
3	3/23/2009 12:38:00	2	3/23/2009 13:23:00	11	45	8	yes	765	3/23/2009 12:39:00	10	3/23/2009 13:27:00	11	48	9	yes	638	1.2	0.8
4	3/24/2009 3:54:00	4	3/24/2009 4:51:00	15	57	14	yes	610	3/24/2009 3:51:00	6	3/24/2009 4:45:00	17	54	11	yes	349	1.7	0.6
5									3/26/2009 16:45:00	5	3/26/2009 17:23:00	1	38	11	yes	87		
6	3/26/2009 17:35:00	3	3/26/2009 18:35:00	14	60	11	yes	683	3/26/2009 17:33:00	1	3/26/2009 18:31:00	110	58	9	yes	454	1.5	0.7
7	3/27/2009 8:03:00	8	3/27/2009 8:29:00	1	26	16	yes	181	3/27/2009 8:03:00	4	3/27/2009 8:29:00	1	26	16	yes	209	0.9	1.2
8	3/27/2009 8:33:00	4	3/27/2009 9:28:00	31	55	5	yes	420	3/27/2009 8:36:00	2	3/27/2009 9:07:00	33	31	8	yes	260	1.6	0.6
9	3/27/2009 16:47:00	4	3/27/2009 17:35:00	39	48	8	yes	640	3/27/2009 16:45:00	1	3/27/2009 17:35:00	17	50	6	yes	287	2.2	0.4
10	3/28/2009 1:50:00	4	3/28/2009 2:22:00	27	32	16	yes	117	3/28/2009 1:43:00	1	3/28/2009 2:14:00	20	31	9	yes	150	0.8	1.3
11	3/28/2009 3:28:00	1	3/28/2009 3:41:00	7	13	4	yes	243	3/28/2009 3:36:00	1	3/28/2009 4:03:00	22	27	12	yes	65	3.7	0.3
12	3/28/2009 7:24:00	1	3/28/2009 7:41:00	5	17	5	yes	137										
13	3/28/2009 9:23:00	1	3/28/2009 9:31:00	10	8	4	yes	117										
14	3/28/2009 10:12:00	2	3/28/2009 10:36:00	61	24	12		98	3/28/2009 10:07:00	1	3/28/2009 11:10:00	107	63	7	yes	156	0.6	1.6
15	3/28/2009 16:51:00	4	3/28/2009 17:08:00	21	17	411	no	86	3/28/2009 16:37:00	6	3/28/2009 17:00:00	25	23	397	no	103	0.8	1.2
16	3/28/2009 23:33:00	1	3/29/2009 0:47:00	65	74	4	yes	224	3/28/2009 23:40:00	2	3/29/2009 0:37:00	65	57	11	yes	158	1.4	0.7
17	3/29/2009 3:45:00	3	3/29/2009 4:58:00	56	73	22	yes	187	3/29/2009 3:35:00	1	3/29/2009 4:45:00	45	70	12	yes	156	1.2	0.8
18	3/29/2009 21:18:00	4	3/29/2009 21:47:00	51	29	1075	no	156	3/29/2009 20:52:00	8	3/29/2009 21:30:00	43	38	1049	no	60	2.6	0.4
19	3/30/2009 8:31:00	4	3/30/2009 8:42:00	52	11	1748	no	104										
20	4/4/2009 14:30:00	8	4/4/2009 16:19:00	75	109	14	yes	986	4/4/2009 14:28:00	10	4/4/2009 15:46:00	85	78	12	yes	566	1.7	0.6

Max amp: mean amplitude in a 2 minute window around the peak signal to noise ratio
Onset: time when the signal to noise ratio begins to increase again following the explosion
End: time when the signal to noise ratio drops below 2
Onset error: visual estimate
End error: Number of minutes for the signal to noise ratio to drop from 2 to 1

Chapter 2 Using repeating volcano-tectonic earthquakes to track post-eruptive activity in the conduit system at Redoubt Volcano, Alaska[1]

2.1 Abstract

In the year following the end of the 2009 eruption of Redoubt Volcano, Alaska, four significant swarms of low-frequency, low magnitude ($M_L < 0.1$) earthquakes occurred at shallow depths beneath the summit. Because swarms of low-frequency (LF) earthquakes preceded eruptions in 1989 and 2009, the post-eruption swarms caused considerable concern and prompted the Alaska Volcano Observatory to raise the monitoring levels on three occasions. None of these swarms led to eruptions, however, and most observers—including the authors—initially concluded that the swarms had been caused by minor stress adjustments in the new lava dome or in the surrounding summit glaciers. New observations reveal that the shallow LF swarms were accompanied by two families of repeating earthquakes at depths between 3 and 6 km below sea level (bsl), where the magma storage region is thought to reside. These mid-crustal volcano-tectonic (VT) type earthquakes were identical to earthquakes recorded during the 2009 Redoubt eruption more than 6 months earlier. Focal mechanisms demonstrate that these earthquakes have thrust mechanisms inconsistent with the strike-slip nature of regional faulting. Based on these observations, we conclude that they are generated through processes occurring within the magma storage region. The concurrence of the repeating VT earthquakes with the shallow LF swarms indicates that the shallow LF earthquakes were also magmatically-driven. Our results emphasise that even brief episodes of low amplitude earthquake activity, such as the LF swarms observed at Redoubt following the 2009 eruption, can be indicative of magmatic activity. Perhaps more significant, however, is the demonstration that the conduit system at Redoubt remained active, intact, and capable

[1] Buurman, H., West, M.E., Roman, D.C., 2013. Using repeating volcano-tectonic earthquakes to track post-eruptive activity in the conduit system at Redoubt Volcano, Alaska: Geology, v. 41, p.511-514, doi:10.1130/G34089.1.

of transporting heat and fluids to the surface months after the eruption was considered over.

2.2 Introduction

Volcanic eruptions rarely occur without precursory seismicity. Precursory seismic swarms—increases in earthquake rate within a given volume over a concentrated period of time without a clear mainshock (Mogi, 1963)—have been documented on time scales of months to hours prior to eruptions (e.g. Endo et al., 1981; Yokoyama and de la Cruz-Reyna, 1990; Lahr et al., 1994; Jacobs and McNutt, 2010; Ruppert et al., 2011; Buurman et al., 2012). Most increases in volcanic seismicity do not lead to eruptions, however, since seismic swarms can be caused by both magmatic and non-magmatic processes. These include: dike injection into the shallow crust, such as that observed at Akutan Volcano, Alaska (Lu et al., 2005), Paricutin, Mexico (Gardine et al., 2011) and Iliamna Volcano, Alaska (Roman and Power, 2011); ice and debris avalanches on the steeper portions of volcanic edifices (Caplan-Auerbach and Huggel, 2007); and tectonically driven stress changes in the crust (e.g. Vidale and Shearer, 2006). Each of these processes generates distinct seismicity that varies both in location and waveform characteristics. The seismic record can therefore help constrain the source of earthquakes and assist with eruption forecasting.

Seismic swarms were frequently observed during the 1989 and 2009 eruptions of Redoubt Volcano, Alaska. During the 1989 eruption 14 of the 22 explosions or dome collapses were preceded by swarms of low frequency (LF) earthquakes (Power et al., 1994). Similarly, during the 2009 eruption three of the six seismic swarms noted by Buurman et al. (2012) preceded explosive activity. The 2009 eruption began on March 15, 2009, and for almost three weeks was characterised by large magmatic explosions, numerous lahars and episodic dome growth. The eruption entered an effusive phase following a final explosion on April 4, characterised by steady dome growth that

persisted until the end of June, 2009 (Schaefer, 2012). Seismicity at Redoubt remained elevated until the end of August 2009.

The recurrence of earthquake swarms at Redoubt in December 2009 and April 2010—six and ten months following the end of eruptive activity—prompted scientists to raise the alert level in anticipation of renewed eruptive activity (Power et al., 2012). These swarms were characterised by repeating LF earthquakes observed only at the summit stations, indicating that the events were small ($M_L < 0.1$) and that the source was high in the edifice (Figure 2.1). The source of these short-lived swarms was the subject of extensive debate among scientists at the Alaska Volcano Observatory because of Redoubt's well-documented history of seismic swarms preceding explosions and dome collapses. However, none of the swarms culminated in explosive activity. When it became clear that no eruption was imminent, the swarms were dismissed as having resulted from surficial processes: either stress adjustments from cooling and degassing within the new lava dome or creep in the summit ice fields.

We present evidence that the swarms were, in fact, magmatically driven. We examine the seismicity that occurred below the edifice in December 2009 and April 2010 and find repeating volcano-tectonic (VT) earthquakes that accompany the shallow LF swarms. These VT earthquakes share high degrees of waveform similarity with repeating earthquakes identified by Buurman et al. (2012) that occurred between 3-6 km below sea level (bsl) during the effusive phase of the 2009 eruption. We examine the shallow earthquake swarms and the deep repeating VT earthquakes in turn, before placing them in context with additional geophysical observations to show that 1) the two sets of earthquakes were related and 2) that they were both most likely driven by magmatic processes.

2.3 Shallow LF swarms in December 2009 and April 2010

Four episodes of summit seismicity, lasting between 1 and 80 hours, were recorded between December 2009 and April 2010. Each swarm episode began with a prolonged

event that lasted approximately 15 seconds and registered at stations within 5 km of the vent (Figure 2.1). These 'swarm onset events' lacked distinct P- and S-wave arrivals and were similar in frequency content to the repeating LF earthquakes that followed. All but the shortest swarm (on April 29, 2010) comprised more than one family of earthquakes, characterised by highly correlating waveforms (correlation values >0.8 over an 8 second waveform at station RSO) that occurred at rates of 1-2 per minute. The waveforms showed some similarity between the different swarms (correlation values up to 0.6), suggesting that the swarms shared a similar source mechanism and/or a similar location. The earthquakes were dominated by low frequencies between 1-6 Hz, were uniform in amplitude, and had durations at station RSO of approximately 8 seconds (Figure 2.2b).

There were no other notable changes in activity at Redoubt that coincided with the LF earthquake swarms. Both the geodetic record and the rate of earthquakes greater than M_L 0.1 remained unchanged during each swarm episode (Dixon et al., 2011; J. Freymueller, pers. comm., 2012). Gas emissions remained elevated for several years following the 2009 eruption (P. Kelly, pers. comm., 2012). However, sampling was sporadic and insufficient to determine whether there were changes in gas flux concurrent with the swarms (Werner et al., 2012). Heat flux also remained elevated, and incandescent areas on the surface of the dome were observed using a low-light time-lapse camera following the end of the eruption in July 2009 until the end of April 2010 (Figure 2.3).

2.4 VT earthquakes near the mid-crustal magma storage region

Significant VT earthquake activity occurred around the mid-crustal storage area, located between 3 and 10 km depth (Power et al., 2012, Coombs et al., 2012), during both the 1989 and 2009 eruptions at Redoubt. This activity has been broadly interpreted as the brittle response of the crust due to stresses induced by magma (e.g., Power et al., 2012). Buurman et al. (2012) demonstrated that a significant subset of this seismicity during the 2009 eruption was composed of four families of repeating VT earthquakes. Repeating VT earthquakes occur as a result of repeated slip on a fault, and have been documented in a number of volcanic areas including Mount St Helens (Frémont and Malone, 1987; Moran

et al., 2008), Augustine (Buurman and West, 2010), Bezymianny (Thelen et al, 2011) and Etna (Cannata et al., 2011).

The first of the repeating VT earthquakes occurred 12.5 hours prior to the last large magmatic explosion on April 4, 2009, after which they continued steadily through the effusive phase of the eruption (Figure 2.2a, 2.4a). We searched the continuous waveform data for other occurrences of these earthquakes using a master event cross correlation technique. We achieved this by cross correlating the four repeating VT earthquake families identified by Buurman et al. (2012) against the continuous seismic record from January 1, 2006 until January 1, 2012 at station REF. Events that correlated at 0.8 or better with 3-second waveform templates were included in the catalog of mid-crustal repeating VT earthquakes.

No earthquakes from these families occurred in the three years preceding the eruption. Commencing on April 4, 2009 and lasting throughout the dome-building phase of the eruption, 346 repeating VT earthquakes were recorded across the Redoubt seismic network. The four earthquake families contained 21 to 233 events. By June 2009, the rate of repeating VT earthquakes had tapered off contemporaneously with the rate of dome growth (Schaefer, 2012). The timing of these earthquakes strongly indicates that they were caused by the withdrawal of magma from the crustal reservoir during dome growth.

The two largest repeating VT families returned in short bursts in December 2009 and April 2010 (Figure 2.2), each time within 3 days of the shallow LF swarms. Because these earthquakes were known from the eruption period to be markers for magma withdrawal, their return months later suggested that magma was again moving at depth.

We calculated composite fault plane solutions and hypocenter relocations of the repeating VT earthquakes to investigate their relationship to the volcanic system at Redoubt. During the eruption, the seismic network consisted of 6 broadband and 8 short

period seismometers within 15 km of the vent, although at times the network was reduced to 11 operational stations (Dixon et al., 2010). Initial hypocenter locations were calculated with the GENLOC program (Pavlis et al., 2004) using the Redoubt velocity model (Figure 2.4a; Dixon et al., 2010). We then relocated the earthquakes using HypoDD, the double difference relocation algorithm of Waldhauser and Ellsworth (2000). The relocated repeating earthquakes occur within the main region of earthquake activity below the vent, and cluster into four earthquake families that are spread over a 3 km depth range (Figure 2.4a).

We attempted to calculate double-couple fault-plane solutions (FPS) based on P-wave first-motion polarities picked from waveform stacks for the four earthquake families, using the FPFIT program (Reasenberg and Oppenheimer, 1985). P-wave first motion polarities from stations with known reversed polarities were corrected before FPS calculation. We were able to obtain reliable FPS for the two largest families; graphical solutions are shown in Figure 2.4b and 2.4c and numerical descriptions, including error information, are given in Table 2.1. The FPS for the two largest earthquake families show similar oblique thrusting mechanisms with P-axes aligned approximately parallel to the regional orientation of maximum compression (Sánchez et al., 2004). The oblique thrust mechanism is inconsistent with the regional sense of slip which is predominantly strike-slip in the mid-crust (e.g., Ruppert 2008), indicating a reversal of the intermediate and minimum compressive stress axes for the VT earthquakes compared to background (tectonic) faulting. Sánchez et al., (2004) also found evidence for a reversal of intermediate and minimum compressive stress orientations between the active and inactive periods during and after the 1989 eruption of Redoubt, which implies that such a switch is characteristic of volcanic activity beneath Redoubt.

2.5 Discussion

The location of the mid-crustal repeating VT earthquakes and their presence during the period of sustained lava dome growth suggests that these earthquakes are related to activity in or around the magma storage area. The thrust-type focal mechanisms suggest

that there was a change in orientation of the minimum compressive stress from horizontal to vertical when these earthquakes occurred, although the maximum compressive stress remained consistent with the regional stress field (Figure 2.4b, 2.4c). There are three ways to interpret these fault plane solutions: 1) These earthquakes were caused by regional stresses, with no other (i.e. volcanic) influences; 2) They were generated by regional stresses combined with a reduction in normal stress on the fault(s), either from decompression of the rock around a magma chamber/conduit system or from increased gas and/or fluid pressure in the rock hosting the fault zone; and 3) The repeating VT earthquakes were caused by stresses from inflation of a dike-like conduit acting constructively with regional/tectonic stresses. Since the thrust mechanisms are inconsistent with the regional stress field, which appears to be characterised by horizontal maximum and minimum compressive stresses, we rule out hypothesis (1). We are not able to distinguish between hypotheses (2) and (3) with our data. Both of these hypotheses rely on activity in the conduit system, however, and both imply that the source of the repeating VT earthquakes is magmatically driven.

Armed with this conclusion, we now consider the shallow LF earthquake swarms in December 2009 and April 2010. These earthquake swarms coincided with the reappearance of the mid-crustal repeating VT earthquakes. On each occasion less than 10 repeating VT earthquakes were detected—far fewer than during the eruptive activity in April and May 2009. Their presence is nonetheless highly significant, as they indicate that the conduit system was once again active and-more importantly still-that the shallow LF swarms were driven by this same magmatic activity. We observe no consistent pattern in the timing between the mid-crustal VT earthquakes and the shallow low frequency swarms; in some instances the VT earthquakes preceded the shallow swarms, but this was not always true.

Although the shallow LF earthquake swarms were most likely driven by magmatic activity in the mid-crust, their exact source remains unclear. Repeating LF earthquake

swarms were observed during the 1989 and 2009 Redoubt eruptions, and were inferred to result from the resonance of fluid-filled cracks (e.g. Chouet 1996; Stephens and Chouet, 2001; Buurman et al., 2012). Given that no eruptive activity followed the shallow swarms in December 2009 and April 2010, the source of these events is likely to have been fluids (steam or gas) in cracks high in the edifice. We do not consider glacial sources for these LF earthquakes, since much of the crater glacier was removed during the 2009 eruption. The repeating VT earthquakes that occurred deeper in the conduit system are evidence of magmatically induced activity, either from small amounts of magma movement or from depressurisation around the magma storage area. The changes around the magma storage region could have produced a pulse of gas that manifested as repeating LF earthquakes as it travelled through the uppermost portions of the edifice. The prolonged larger event that occurred at the onset of each swarm (Figure 2.1) can be attributed to the reinitiation of the crack or pathway through which the ascending gas was able to escape.

It is also significant that the dome incandescence ceased concurrent with the last of the shallow swarms. The persistent thermal feature observed in the low-light camera was likely one of several degassing fumaroles on the lava dome (Wessels et al., 2012), and was visible in the majority of clear images following the end of the eruption until April 15, 2010 (Figure 2.3). In the next clear image of the dome taken on May 1, 2010, the hotspot feature had disappeared, and did not recur thereafter. We interpret this change as the final sealing of the shallow conduit system. It is noteworthy that this occurred in April 2010, ten months after the end of eruptive activity at the surface, as it demonstrates how long arc-volcanic systems can remain open following the end of eruptive episodes.

2.6 Acknowledgements

We are grateful for reviews from Wes Thelen and two anonymous reviewers that substantially improved the manuscript. We thank Ronni Grapenthin for insights into the deformation record, Peter Kelly for interpretation of the gas record, Rick Wessels for assistance with the low light camera data and Cyrus Read for his efforts in installing the campaign broadband instruments. The Alaska Volcano Observatory is a partnership

between the U.S. Geological Survey, the Geophysical Institute at the University of Alaska Fairbanks, and the Alaska Division of Geological and Geophysical Surveys.

2.7 References cited

Buurman, H. and West, M., 2010, Seismic precursors to volcanic explosions during the 2006 eruption of Augustine Volcano, *in* Power, J.A., Coombs, M.L., and Freymueller, J.T., eds., The 2006 eruption of Augustine Volcano: Menlo Park, California, U.S. Geological Survey Professional Paper 1769, p. 41-57.

Buurman, H., West, M.E., and Thompson, G., 2012, The Seismicity of the 2009 Redoubt eruption. Journal of Volcanology and Geothermal Research, doi: 10.1016/j.jvolgeores.2012.04.024.

Cannata, A., Alparone, S., Ferrari, F. and Ursino, A., 2011, Repeating volcano-tectonic earthquakes at Mt. Etna during 1999 – 2009, *in* Proceedings, Gruppo Nazionale di Geofisica della Terra Solida: Trieste, Italy, p. 23-27.

Caplan-Auerbach, J., and Huggel, C., 2007, Precursory seismicity associated with frequent, large ice avalanches on Iliamna volcano, Alaska, USA: Journal of Glaciology, v. 53, n. 180, p. 128-140.

Chouet, B.A. 1996, Long-period volcano seismicity; its source and use in eruption forecasting: Nature, v. 380, p. 309–316.

Coombs, M.L., Sisson, T. , Bleick, H. , Henton, S., Nye, C., Payne, A., Cameron, C., Larsen, J., Wallace, K. and Bull, K.F., 2012, Andesites of the 2009 eruption of Redoubt Volcano, Alaska. Journal of Volcanology and Geothermal Research, doi:10.1016/j.jvolgeores.2012.01.002.

Dixon, J.P., Stihler, S.D., Power, J.A., and Searcy, C., 2010, Catalog of earthquake hypocenters at Alaskan volcanoes: January 1 through December 31, 2009: U.S. Geological Survey Data Series 531.

Dixon, J.P., Stihler, S.D., Power, J.A., and Searcy, C.K., 2011, Catalog of earthquake hypocenters at Alaskan volcanoes: January 1 through December 31, 2010: U.S. Geological Survey Data Series 645.

Endo, E.T., Malone, S.D., Noson, L.L., and Weaver, C.S., 1981, Locations, magnitudes and statistics of the March 20- May 18 earthquake sequence, *in* Lipman, P.W. and Mullineau, D.R., eds., The 1980 Eruptions of Mt. St. Helens: Menlo Park, California, U.S. Geological Survey Professional Paper, No. 1250, p. 93-107.

Frémont, M.J., and Malone, S.D., 1987, High precision relative locations of earthquakes at Mount St. Helens, Washington: Journal of Geophysical Research, v. 92, p. 10223–10236.

Gardine, M., West, M.E., and Cox, T., 2011, Dike emplacement near Parícutin volcano, Mexico in 2006: Bulletin of Volcanology, v. 73, p. 123-132, doi: 10.1007/s00445-010-0437-9.

Jacobs, K.M., and McNutt, S.R., 2010, Using seismic b-values to interpret seismicity rates and physical processes during the preeruptive earthquake swarm at Augustine Volcano 2005-2006, chapter 3 of Power, J.A., Coombs, M.L., and Freymueller, J.T., eds., The 2006 eruption of Augustine Volcano, Alaska: U.S. Geological Survey Professional Paper 1769, p. 59-83.

Lahr, J., Chouet, B.A., Stephens, C.D., Power, J.A., Page, R.A., 1994. Earthquake classification, location and error analysis in a volcanic environment: implications for the magmatic system at Redoubt Volcano, Alaska. Journal of Volcanology and Geothermal Research 62, 137-151.

Lu, Z., Wicks, C., Kwoun, O., Power, J.A., and Dzurisin, D., 2005, Surface deformation associated with the March 1996 earthquake swarm at Akutan Island, Alaska, revealed by C-band ERS and L-band JERS radar interferometry: Canadian Journal of Remote Sensing, v. 31, p. 7-20.

Mogi, K., 1963, Some discussions on aftershocks, foreshocks and earthquake swarms, the fracture of a semi-infinite body caused by an inner stress origin and its relation to the earthquake phenomena (Third Paper): Bulletin of the Earthquake Research Institute-University of Tokyo, v. 41, p. 615-658.

Moran, S.C., Malone, S.D., Qamar, A.I., Thelen, W.A., Wright, A.K., and Caplan-Auerbach, J., 2008, Seismicity Associated with Renewed Dome Building at Mount St. Helens, 2004-2005, *in* Sherrod, D.R., Scott, W.E., and Stauffer, P.H., eds., A volcano rekindled: the renewed eruption of Mount St Helens, 2004-2006: Menlo Park, California, U.S. Geological Survey Professional Paper 1750, p. 27-60.

Pavlis, G. L., Vernon, F., Harvey, D., and Quinlan, D., 2004, The generalized earthquake-location (GENLOC) package: An earthquake-location library?: Computers and Geosciences, v.30, no. 9-10, p. 1079-1091, doi: 10.1016/j.cagea.2004.06.010.

Power, J. A., Lahr, J.C., Page, R.A., Chouet, B.A., Stephens, C.D., Harlow, D.H., Murray, T.L., and Davies, J.N., 1994, Seismic evolution of the 1989-1990 eruption sequence of Redoubt Volcano, Alaska, *in* Miller, T. P. and Chouet, B.A., eds., The 1989-1990 eruptions of Redoubt Volcano, Alaska. Journal of Volcanology and Geothermal Research, v. 62, no. 1, p. 69-94.

Power J., Stihler, S., Chouet, B.A., Haney, M.M., and Ketner, D.M., 2012, Seismic observations of Redoubt Volcano, Alaska—1989 – 2010 and a conceptual model of the Redoubt magmatic system. Journal of Volcanology and Geothermal Research, doi:10.1016/j.jvolgeores.2012.09.014.

Reasenberg, P., and Oppenheimer, D.H., 1985, FPFIT, FPPLOT, and FPPAGE, FORTRAN computer programs for calculating and displaying earthquake fault-plane Solutions: U.S. Geological Survey Open-File Report, 85-739.

Roman, D. C. and Power, J.A., 2011, Mechanism of the 1996-97 non-eruptive volcano-tectonic earthquake swarm at Iliamna Volcano, Alaska: Bulletin of Volcanology, v. 73, p. 143-153.

Ruppert, N.A., 2008, Stress map for Alaska from earthquake focal mechanisms. In, Active Tectonics and Seismic Potential of Alaska. Geophysical Monograph Series 179, AGU, p 351-367.

Ruppert, N.A., Prejean, S., and Hansen, R.A., 2011, Seismic swarm associated with the 2008 eruption of Kasatochi Volcano, Alaska: earthquake locations and source parameters: Journal of Geophysical Research, v. 116, B00B07, doi:10.1029/2010JB007435.

Sánchez, J.J., Wyss, M., and McNutt, S.R., 2004, Temporal-spatial variations of stress at Redoubt Volcano, Alaska, inferred from inversion of fault plane solutions. Journal of Volcanology and Geothermal Research, v. 130, p. 1-30.

Schaefer, J. G. (2012). The 2009 eruption of Redoubt Volcano, Alaska: Alaska Division of Geological and Geophysical Surveys Report of Investigation 2011-5.

Stephens, C. D., and Chouet, B. A., 2001, Evolution of the December 14, 1989 precursory long-period event swarm at Redoubt Volcano, Alaska: Journal of Volcanology and Geothermal Research, v. 109, n. 1, p. 133-148.

Thelen, W., Malone, S. and West, M.E., 2011, Multiplets: Their behavior and utility at dacitic and andesitic volcanic centers: Journal of Geophysical Research, v. 116, B08210, doi:10.1029/2010JB007924.

Vidale, J. E., and Shearer, P. M., 2006, A survey of 71 earthquake bursts across southern California: Exploring the role of pore fluid pressure fluctuations and aseismic slip as drivers: Journal of Geophysical Research, v. 111, B05312, doi:10.1029/2005JB004034.

Waldhauser, F., and Ellsworth, W.L., 2000, A double-difference earthquake location algorithm: Method and application to the northern Hayward fault, California: Bulletin of the Seismological Society of America, v. 90, p. 1353–1368.

Werner, C., Kelly, P., Doukas, M., Lopez, T., Pfeffer, M., McGimsey, G. and Neal, C., 2012, Degassing associated with the 2009 eruption of Redoubt Volcano, Alaska. Journal of Volcanology and Geothermal Research, doi:10.1785/0120000006.

Wessels, R. L., Vaughan, R. G., Patrick, M., Coombs, M., 2012, High-resolution satellite and airborne thermal infrared imaging of precursory unrest and 2009 eruption at Redoubt Volcano, Alaska. Journal of Volcanology and Geothermal Research doi:10.1016/j.volgeores.2012.04.012.

Yokoyama I, de la Cruz-Reyna S, 1990, Precursory earthquakes of the 1943 eruption of Parícutin volcano, Michoacan, Mexico. Journal of Volcanology and Geothermal Research, v. 44, p. 264–281.

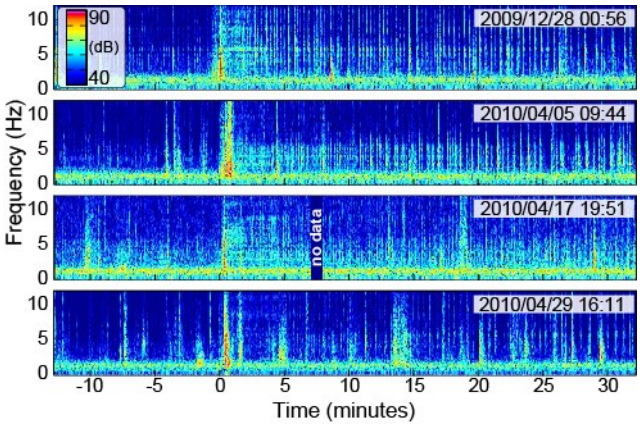

Figure 2.1 Spectrograms of each of the low frequency swarm onsets.
The time axis is relative to the onset of the swarm, each marked by a prolonged event lasting approximately 15 seconds in duration.

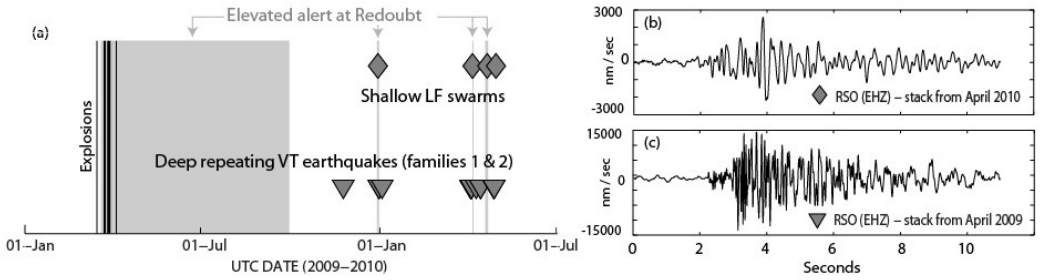

Figure 2.2 Eruption timeline and example waveforms.
(a) Schematic timeline of Redoubt unrest between January 1, 2009 and July 1, 2010. Periods when Redoubt Volcano was at elevated alert are indicated by the grey shaded areas. The shallow swarms are represented by diamonds and the repeating VT earthquakes by triangles. The explosions during the eruption are marked by vertical black lines (Schaefer, 2012). (b) Stack of 10 representative waveforms of the shallow swarms, recorded at station RSO on April 17, 2010. (c) Stack of 10 representative repeating VT waveforms from family 2, recorded at station RSO in April 2009.

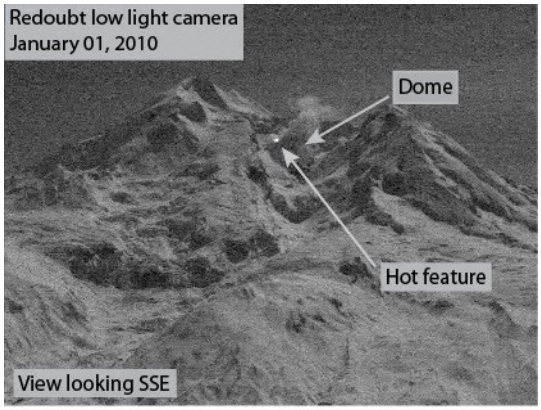

Figure 2.3 Clear image from the low light camera, showing the bright hotspot that represents a persistent thermal feature that persisted until late April 2010.

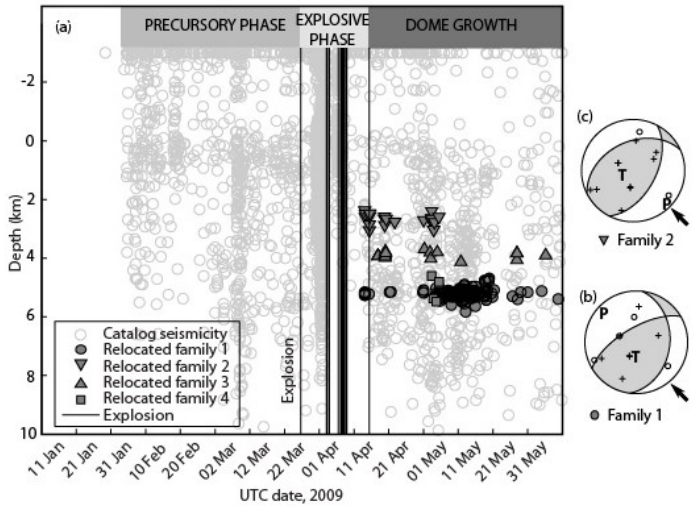

Figure 2.4 Earthquake depths as a function of time during the eruption.
(a) The four relocated families plotted with the catalog seismicity between January 1 and June 1, 2009. Explosions are indicated by vertical lines (Schaefer, 2012). (b) and (c) Composite fault plane solutions for families 2 and 1 respectively. Circles indicate dilatations and plus signs indicate compressions. Black arrows indicate the regional stress direction. The fault plane solutions are lower-hemisphere projections.

Table 2.1 Parameters (a) and formal errors (b) for cluster 1 and 2 fault plane solutions.

a)	#FM *	Strike – NP1*(°)	Dip – NP1(°)	Rake – NP1(°)	Strike – NP2(°)	Dip – NP2(°)	Rake – NP2(°)	P-axis Azimuth (°)	P-axis Dip (°)	T-axis Azimuth (°)	T-axis Dip (°)
Cluster 1	11	7	35	43	240	67	117	310	18	188	59
Cluster 2	12	28	54	66	245	42	119	135	6	242	70

*FM – First motions; NP1 – Nodal plane 1; NP2 – Nodal plane 2

b)	Misfit	STDR*	Strike Uncertainty (°)	Dip Uncertainty(°)	Rake Uncertainty (°)
Cluster 1	0.09	0.52	1	0	2
Cluster 2	0.00	0.60	7	6	4

*Station Distribution Ratio – A measure of polarity distribution with respect to nodal planes. A relatively high STDR indicates that polarities do not project near nodal planes.

Chapter 3 What controls volcano seismicity along the Aleutian arc?[1]

3.1 Abstract

We identify patterns in volcano seismicity along the Aleutian arc using nearly 10 years of seismic data published by the Alaska Volcano Observatory. The volcanoes in the central portion of the arc—those located from Aniakchak Peak to Mount Okmok—generate significantly more seismicity at depths below 15 km than those in the eastern and western regions of the arc. Most of the earthquakes that occur below 15 km depths are low frequency events, although we find some exceptions at the volcanoes in the western Aleutian Islands. We also examine the median weight percent SiO_2 compositions of the seismically monitored volcanoes by compiling published geochemical data. We find that the transition between felsic volcanism in the east to more mafic volcanism in the west occurs in the same region where the depth distribution of volcanic earthquakes changes.

Since deep volcanic earthquakes are most likely generated by the ascent of magma through the deep crust, our results suggest that magma ascent is more prolific in the central part of the arc compared to the western and eastern regions. This observation is in agreement with the location of the largest and most historically active volcanoes in the Aleutian arc, which are found in same region that generates abundant deep volcano seismicity.

We present two hypotheses to explain the variations in magmatic flux suggested by the patterns observed in deep volcanic earthquakes along the arc. The first hypothesis assumes that magma production rates are the same along the whole arc, and that the reduced magma flux in the eastern and western regions of the arc is due to changes in the upper plate that choke the ascent of magma. We propose that increased shear stresses which occur due to oblique subduction in the west and to far-field effects from the subduction of the Yakutat microplate in the east inhibit the rise of magma through the crust in these areas. We identify the Amlia fracture zone (AFZ) and the Becharof discontinuity—located in regions where the

[1] Buurman, H., Nye, C.J., West, M.E., Prepared for submission to *Geochemistry, Geophysics, Geosystems.*

depth range of volcanic earthquakes changes—as important tectonic features that facilitate these changes to the stress regimes. The second hypothesis assumes there are no differences in crust of the upper plate that could inhibit the ascent of magma, and that the observed variations in magmatic flux in the crust reflect variations in the generation of melt on the subducting plate. We propose that there are significant differences in the amount of H_2O subducted along the Aleutian arc which could account for the differences in melt production, and present two possible mechanisms for this model: 1) H_2O is transported into the mantle via sediments on the subducting plate, and 2) H_2O is transported into the mantle within areas of serpentinized crust that is found in fracture zones. We draw on observations of sediment thickness along the arc, and the location of the AFZ and the Aja fracture zone to support this hypothesis. Both of these hypotheses rely on common tectonic features such as the AFZ, suggesting that aspects from each model may play /important roles in controlling magmatism in the Aleutian arc.

3.2 Introduction

The Aleutian arc

The Aleutian arc has one of Earth's most active subduction zones. Stretching for over 4000 km between the Kamchatka Peninsula and mainland Alaska along the northern boundary of the Pacific Ocean, it marks the boundary where the Pacific plate subducts below the North American and Bering Sea plates at rates that vary from 54 mm per year in the east to 78 mm per year in the west (DeMets et al., 1990; Figure 3.1). The active volcanoes are located in the eastern 2500 km of the arc, where the Pacific plate motion is close to perpendicular to the trench. Subduction becomes progressively more oblique in the western arc, and the forearc crust west of 172 degrees W is broken into smaller crustal blocks that translate westward and rotate clockwise (Geist et al., 1988). A series of major back-arc faults dominate this region and accommodate the increasing strike-slip plate motion, and the plate boundary becomes predominantly right lateral strike-slip around 170 degrees E.

Volcanism in the Aleutian arc

The Aleutian volcanic arc is extremely active, averaging one eruption per year during historic time. Of the 142 known Quaternary volcanic centers, 94 have been active in the Holocene (Cameron, 2006). The most active volcanoes are found in the central and western portion of the volcanic arc, with Akutan Volcano in the eastern Aleutians setting the record of 33 eruptions in the past 250 years (Alaska Volcano Observatory unpublished data, 2005, available from www.avo.alaska.edu). Eruption style varies greatly along the arc, and in the past 10 years alone has included a violently explosive eruption at Kasatochi Volcano in 2008 that generated a series of ash plumes up to 18 km above sea level over 24 hours (Waythomas et al., 2010), 31 days of strombolian activity at Pavlof Volcano in 2007 (McGimsey et al., 2011), 5 weeks of sustained phreatomagmatic activity at Okmok Caldera in 2008 (McGimsey et al., 2011) and more than 2 months of both ash explosions and lava effusion at Augustine Volcano in 2006 (Power et al., 2006).

Volcano monitoring in the Aleutian arc

Although the Aleutian arc is sparsely populated, a highly focused volcano monitoring mission exists in Alaska owing to the large volume of air traffic—both as passenger flights and as air cargo—that passes directly over the volcanoes of the north Pacific on a daily basis. Since its formation in 1988, the Alaska Volcano Observatory (AVO) has monitored volcanic activity in the Aleutian arc primarily through seismic monitoring and satellite remote sensing techniques. Earthquake catalogs of both the eruptive and the non-eruptive volcano-seismic earthquake activity in the Aleutian arc are published each year as US Geological Survey reports, resulting in a remarkably complete history of Aleutian volcanic seismicity that spans the past 20 years (Dixon et al., 2012, and references therein). We refer to these collective publications throughout this study simply as the ‘earthquake catalogs’, and list those that are used in this study in the reference section.

Volcano seismicity in the Aleutian arc

The earthquake catalogs reveal a wide variety of non-eruptive volcano-seismic activity along the Aleutian arc. Volcanic earthquake rates range from less than 10 events per year at Pavlof Volcano to many hundreds of events per year at Mount Spurr. The spread of earthquakes around the vent varies greatly, from tightly clustered clouds as small as 3 km in diameter at Augustine Volcano to diffuse zones of seismicity as large as 34 km in diameter below Mount Veniaminof. The type of volcanic earthquakes also varies across the Aleutian arc. All of the earthquakes in the catalogs are assigned a type based on the characteristics of their seismograms. These event classifications include volcano-tectonic (VT), low frequency, shore-ice, and glacial, as well as a number of other signal types. Some Aleutian volcanoes such as Mount Gareloi generate almost exclusively low frequency earthquake activity, whereas earthquakes below the Katmai volcanic group are mostly VT earthquakes.

The goal of our study is to determine what controls these variations in the seismicity below Aleutian arc volcanoes. To do this we must first characterize Aleutian volcano seismicity, which is no small task given that 1) not all Aleutian volcanoes are monitored, 2) those volcanoes that are monitored are done so to varying degrees, with the magnitude of completeness varying from 0.1 to 1.7 along the arc according to the earthquake catalogs, and 3) inclement weather conditions can result in many months of compromised data, particularly on the remote islands of the western Aleutians. We therefore begin by assessing data quality and constructing a dataset that can be characterized at a regional scale. We then compare the seismic data to other parameters such as geographical setting, physical volcanic features and geochemical variations to determine whether they influence volcano seismicity at Aleutian volcanoes.

3.3 Characterizing volcano seismicity in the Aleutian arc

We use seismic data recorded between October 2002 and December 2011 to characterize Aleutian arc volcano seismicity. This nearly 10-year period spans the time during which the seismic network coverage was at its fullest along the Aleutian arc and continuous waveform data is available. We begin by identifying volcanoes that are seismically monitored and

subset the catalog around each edifice. Time periods of compromised data are then removed for each volcano, allowing us to make balanced comparisons along the entire arc.

We use our own naming conventions throughout this manuscript. Many Aleutian volcanoes are known by a number of different names; for example *Mount Spurr* is also recognised as *Spurr Volcano* and *Spurr Volcanic Complex* (AVO unpublished data, 2005, available from www.avo.alaska.edu). For the sake of simplicity and readability within the text, we refer to each volcano by the unique name and omit the *Mount, Mountain Crater, Peak* or *Volcano* part from the volcano names. We also divide the arc into regions as follows: the Cook Inlet region includes the volcanoes from Spurr to Augustine, which are situated along the western edge of the Cook Inlet; the Alaska Peninsula refers to the southwest coast of mainland Alaska and includes the volcanoes from Douglas to Dutton; the eastern Aleutians region spans the islands from Unimak Island to Umnak Island, which includes the volcanoes from Roundtop to Okmok; the central Aleutians encompasses the islands west of Unaska Island and east of Atka Island; and the western Aleutians includes all the islands west of Atka that have Holocene active volcanoes, reaching as far west as Buldir Island (Figure 3.1).

What defines an Aleutian arc volcano?

In this study of recent arc volcanism we consider only the 94 Aleutian volcanoes that have been active during the Holocene (Figure 3.1). There are two instances where we group vents together that are more commonly considered as separate volcanoes. We group Crater Peak and Spurr as one system: although these two vents erupt independently from one another, they are located within 3 km and form part of the same volcanic complex (Crater Peak is a satellite vent on the larger edifice of Spurr). Furthermore, their eruptive products have been shown to be at least partially interconnected (e.g., Nye and Turner, 1990). In the second instance we group Hague and Emmons together. As with the Spurr/Crater Peak case, Hague and Emmons are located within 7 km of each other within the same volcanic complex, although here the two volcanoes are more topographically distinct from one another. Their

eruptive products have also been shown to share a common magma source (Mangan et al., 2009).

Which Aleutian volcanoes are monitored?

In this study we define monitored volcanoes as Holocene active volcanoes that have 4 or more seismic stations within 30 km of the vent. The minimum requirement of 4 seismic stations reflects the threshold number of seismic stations used to calculate the hypocenters in the published AVO earthquake catalogs (Lahr, 1999). Similarly, the requirement of the stations to be located within 30 km of the volcano is based empirically on the scatter of hypocenters around the seismic stations in the earthquake catalogs. We exclude submarine volcanoes that would otherwise fit these criteria.

According to our definition, there are 47 monitored volcanoes in the Aleutian arc. The distribution of the monitored volcanoes results in a fairly complete coverage of the Aleutian arc, with the exception of the central Aleutians region (Figure 3.1). It should be noted that, based on the same seismic data, AVO reports to monitor only 33 volcanoes. The main reason for this discrepancy is that the AVO number of 33 is loosely based on the number of real-time seismic monitoring networks that operate along the arc in relation to the closest major volcanic edifice. The majority of seismic networks monitor only one volcano (for example the Gareloi, Iliamna, and Redoubt networks). However, a number of the networks have the capability of monitoring more than one volcano, due either to a large spread in station spacing or to tightly clustered volcanoes. Examples include the Katmai network, which monitors 11 volcanoes, and the Emmons network, which monitors 3 volcanoes.

Defining the volcanic-seismic dataset

At most volcanoes earthquakes occur in a diffuse circular zone below the edifice. For this reason we use circles centered on the summit of each volcano to delineate the extent of each earthquake catalog. The circles also encompass all Holocene vents associated with the volcano. At volcanoes where the zone of seismicity is either elongate or offset from the main

summit, such as at Makushin or at Atka, we extend the radius of the circle to include this activity (see Appendix 3.A). We truncate the circles at some of the more closely spaced volcanoes to ensure that there is no overlap between the catalogs (such as at Kliuchef, Appendix 3.A-10). Care is also taken to omit tectonically-driven hypocenters. This is particularly important at Spurr, Bobrof, Great Sitkin, Takawangha and Gareloi, all of which are located within 20 km of known zones of tectonic seismicity (e.g., Ruppert et al., 2012).

The resulting earthquake catalogs, included in Appendix 3.A, vary widely both with the geographical extent and with the number of hypocenters. The geographical spread of hypocenters ranges from a radius of 1 km at Novarupta to a radius of 17 km at Veniaminof, although at more than 75% of the volcanoes the radius of the hypocenter spread is 8 km or less (Figure 3.2). The catalog for Spurr is by far the largest, containing over 7000 events, although many of these earthquakes are small ($M_L < 0$). Other catalogs contain very little activity (for example < 10 earthquakes total were recorded at Pavlof Sister, Table Top, Wide Bay, Moffett and Bobrof), and in one case (at Gilbert) no earthquakes were recorded during the period of study.

Assessing data quality

Due to the nature of remote volcano monitoring in the Aleutian arc, data outages—periods when the continuous flow of seismic data is interrupted—are common. Data transfer from seismic stations can fail for numerous reasons that include damage to the instrumentation, insufficient power supply, and disrupted radio links. These problems are more prevalent during the months of November through March, when winter storms sweep across the arc bringing strong winds, heavy snowfall and extreme temperature lows.

It is important that we identify periods when data flow was compromised, so that we do not mistake a decrease or absence of seismicity for a change in volcanic activity. We assess data quality on the vertical component of each station on a day-by-day basis by examining the continuous waveform data. Data is considered compromised if the range of the daily time series is less than 100 times bigger than the standard deviation of the time series. A

day that has data gaps for more than 6 hours is also regarded as having insufficient data quality. We combine data quality information for every station located within 30 km of each volcano and identify days on which the network data was compromised—i.e. days when there were less than 4 stations in operation. These times are recorded as 'daily station outages'. We then assess network quality on a weekly basis, and weeks with more than 3 days of daily station outages are flagged as 'network outages'. Episodes when daily station outages occurred more than 2-3 days per week for more than 4 consecutive weeks were also flagged as times when the earthquake monitoring was compromised.

While this method is successful in identifying bad data at the majority of the networks, it performs less well at networks that experience unusual data quality issues such as regular noise spikes. In these situations it is often still possible to locate earthquakes despite the noise present within the data. We therefore include a manual quality check of the daily station outages that were identified during days when earthquakes were successfully located, and override the algorithm in cases where less than 25% of the daily time series is compromised.

The network outages for each volcano are shown in Appendix 3.A. The Akutan, Makushin and Katmai networks were the most robust, with no outages occurring during our period of study. We calculate a median of 74 weeks of data outages during our study period across the Aleutian arc volcanoes, although some networks fared particularly poorly. Based on our data quality assessment, we exclude Adagdak from the study as it has only 209 days of data that meets our data quality criteria. All other volcanoes in this study have at least one year of acceptable monitoring data. This leaves us with 46 monitored volcanoes in the Aleutian arc.

We remove earthquakes that were located during network outages from the catalogs. This eliminates any bias towards larger earthquakes in the catalogs, since it is often still possible to locate larger earthquakes at a volcano with compromised data quality by using stations on adjacent volcano networks.

Depth distributions of volcanic seismicity

Our final challenge is to present the 46 earthquake catalogs in such a way that they can be readily compared across the whole arc. Since the spread of the seismicity at each volcano is already known—defined by the radius of the earthquake catalog as described in section 3.3.3—we now characterize the depth distribution of seismicity below each volcano. We divide each catalog into 3 km depth bins and calculate the cumulative energy within each bin. We then divide the cumulative energy by the number of years that the network was fully operational, and use these values to calculate the cumulative magnitude *per year of data* for each depth bin of the catalog, following the methods of Thelen et al., 2010.

Along-arc variations in the spread of volcanic earthquakes

We find no correlation between the spread of earthquakes around Aleutian volcanoes and their geographical location along the arc (Figure 3.2). In general, the spread of volcano seismicity is distributed between 2 and 10 km, although several outliers have seismicity distributed up to 17 km around the edifice (see section 3.3 for further discussion). Similarly, we find no correlation between the spread of seismicity around the Aleutian volcanoes and volcano elevation (Appendix 3-B).

Along-arc variations in the depth distribution of volcanic earthquakes

Our results indicate that the depth distribution of volcanic earthquakes does vary along the Aleutian arc. In Figure 3.3 we plot the cumulative magnitude per year of data (see section 3.3) as a function of depth below each volcano, ordered from west to east along the arc. We find that there is significantly more earthquake activity below 15 km depth in the central portion of the arc—below the Alaska Peninsula and the eastern Aleutians—than in the easternmost and westernmost regions of the arc.

The western transition from shallow to deeper earthquake activity occurs between Korovin to the west, where activity extends down to 15 km, and Okmok to the east, where seismicity persists down to depths of 30 km. While the offset in earthquake depths between

Korovin and Okmok appears abrupt, it is important to note that they are separated by a distance of 250 km containing a number of unmonitored volcanoes (Figure 3.1).

The eastern transition from deep to shallow earthquake activity occurs between the Peulik-Ugashik area and Aniakchak. We observe significant seismic energy (cumulative yearly magnitude of 2) down to 30 km depth below Aniakchak, and cumulative yearly magnitudes less than 1 occurring below Ukinrek Maars in the Ugashik area down to only 18 km depth. East of the Ugashik area, seismicity is typically limited to the top 10 km of crust, although some deeper activity occurs below the Katmai/Novarupta/Trident cluster of volcanoes.

Figure 3 shows significant seismic energy below Redoubt and Spurr in the easternmost portion of the arc. All of the seismic activity at depths greater than 14 km below Redoubt occurred during the precursory phase of the 2009 eruption, and was interpreted as the crustal response to the ascent of magma from these depths (Power et al., 2013; Appendix 3.A-45). The activity below Spurr has also been attributed to the crustal response to the depressurization of the shallower portions of the Crater Peak magmatic system following the 1992 eruptive sequence and the 2004-2005 unrest below Spurr (Power et al., 2002; George, 2010). By contrast, those volcanoes in the central region of the arc that have erupted within our study period show no such correlation between deep earthquakes and eruptive activity (for example, Appendix 3-A.12, Appendix 3-A.20).

Variations in earthquake type along the Aleutian arc

Since VT earthquakes are by far the most common earthquake type in the Aleutian arc, we examine the distribution of VT earthquake types as a percentage of all earthquake activity. Of the other remaining categories of earthquake type, low frequency events are the most common, so we infer from this distribution that a low percentage of VT activity indicates predominantly low frequency earthquake activity. We divide the earthquake catalogs into 3 km depth bins, similar to the method described in section 3.3. Figure 3.4 confirms that the majority of volcanic earthquakes in the Aleutian arc are VT, and their rate

drops of considerably below about 12 km depth. There are several instances where the shallow earthquake activity is notably lacking in VT earthquakes: at Gareloi and Shishaldin; within the Emmons volcanic cluster (Pavlof, Pavlof Sister and Hague); and somewhat at Iliamna. The majority of earthquakes deeper than 12 km are low frequency type earthquakes. This result is true for almost the entire arc, with the notable exception of the volcanoes west of Bobrof in the western Aleutians where the VT activity extends to depths as deep as 25 km.

3.4 Comparing volcano seismicity and geochemistry along the Aleutian arc

If the trends in volcano seismicity truly reflect broad differences in Aleutian volcanoes, we ought to be able to find corresponding differences within other volcanic datasets. An excellent candidate for such an analysis is the geochemical dataset for Aleutian volcanoes. Magma composition is directly related to magma viscosity, and is a control on how easily magma can move through the crust. It therefore also has the strong potential to influence how much and what type of seismicity a volcano produces.

The geochemical composition of the Aleutian volcanoes has been studied to varying degrees along the arc. Numerous geochemical studies have been undertaken at volcanoes like Spurr, which erupt frequently and are (relatively) easily accessible. Data is sparser in the remote regions of the arc (with Okmok and Adak being notable exceptions), particularly in the western Aleutians. The geochemical data are limited for several volcanoes: Takawangha; Table Top; Wide Bay; Gilbert; and Roundtop. We assume similar geochemical compositions at Tanaga and Takawangha, since the two peaks are thought to belong to the same volcanic complex. Similarly, we assume a shared composition between Pavlof and Pavlof Sister, since they are both part of the extra-caldera products from the Emmons volcanic complex.

Variations in SiO_2 content across the Aleutian arc

We used the published whole-rock weight percent SiO_2 compositions for the seismically monitored volcanoes in this study. We calculate the median value of the weight percent SiO_2 from the available data at each volcano, shown in Table 3.1, and used these

values to examine the relationship between composition and the distribution of earthquake depths below each edifice.

The median SiO_2 compositions of the seismically monitored Aleutian volcanoes are plotted against along-arc distance in Figure 3.5. These results show a bimodal distribution in SiO_2 composition that varies with distance. In the eastern part of the arc—in the Cook Inlet, Katmai and northern Alaska Peninsula regions—the average SiO_2 composition is close to 61%. In the western 1500 km of the arc this number is much lower, at around 55%. The transition between these two distributions is sharp, and occurs arc in the region between Peulik and Veniaminof. The transition also has a curious overlap: Ukinrek Maars, west of Peulik, has the lowest SiO_2 composition of the whole arc; and Aniakchak—to the west of Ukinrek Maars—has a notably felsic composition above 63%, one of the highest values along the arc. The Ukinrek Maars craters are thought to have been generated by magma that was sourced directly from the mantle via a discontinuity that runs through the depth of the crust (see discussion in section 3.6.2; Decker et al., 2008).

Comparing SiO_2 content and seismicity

There is a correlation between SiO_2 composition and the distribution of earthquake depths along the arc. Figure 6 shows the distribution in SiO_2 composition for each volcano superimposed on top of the seismicity depth distribution along the arc. The abrupt change from solely andesitic magmas in the east to more diverse, but dominantly more mafic magmas in the west (discussed in section 3.3) occurs in the same region where the depth distribution of seismicity changes from more shallow depth ranges in the eastern section of the arc to a much greater range in earthquake depths in the central part of the arc (see section 3.2). This suggests that there may be a common process that controls both the seismicity and the geochemical composition in this region of the arc.

We find limited correlation between the lateral spread of earthquakes and SiO_2 composition in the Aleutian arc, although the most felsic systems tend to have more tightly clustered seismicity with radii of less than 5 km (Appendix 3.C).

3.5 What generates volcano seismicity along the Aleutian arc?

The sources of volcanic earthquakes have often been inferred from the frequency content of the seismograms, meaning that the assigned earthquake type given in the earthquake catalogs (which is based on waveform characteristics) can be used as a proxy for the earthquake source. VT earthquakes are most commonly thought to result from the brittle failure of rock within the volcanic edifice. Several mechanisms have been proposed for low frequency earthquake mechanisms, including oscillatory pressure changes within magma conduits (Ukawa and Ohtake, 1987), unsteady nonlinear fluid flow (Julian, 1994), and resonance of fluid-filled cracks (Chouet et al., 1994). These earthquakes commonly accompany volcanic activity and have, at times, been used as indicators of impending eruptions (e.g. Chouet, 1996).

With these definitions in mind, we re-examine the depth distribution of VT and low frequency earthquakes along the Aleutian arc (Figure 3.3). The majority of the seismic activity in the arc is restricted to the upper 12 km of the crust and occurs as VT earthquakes, suggesting that the crust below this depth is more ductile. Although the transition between continental crust and oceanic crust occurs below Unimak Island, we do not observe a corresponding change in the depth of the brittle-ductile transition inferred from our dataset of volcanic earthquakes. Studies of the transition between oceanic and continental crust in the Aleutian arc (e.g. Fliedner and Klemperer, 1999) have found only a minor change in the depth of the Moho, so it is possible that there is correspondingly little variation in the brittle-ductile transition on the arc-wide scale.

Explaining the presence of earthquake activity—especially VT earthquake activity—below the brittle-ductile transition is challenging, since a region that deforms plastically should not in general generate seismic energy. Although the majority of earthquakes below 12 km depth are low frequency earthquakes and are therefore probably generated by the movement of fluids that are most likely ascending magma, VT earthquakes are also present at these depths (e.g. Power et al., 2004). Fractures within mantle-derived xenoliths provide

evidence that brittle failure is still possible at depths between 20 and 65 km, however, and studies of these rocks have shown that such fracturing is most likely driven by the exsolution of CO2-rich fluids from ascending basaltic magma (Wilshire and Kirby, 1989). Alternatively, deep VT earthquakes may result as a product of transient elevated strain rates related to the movement of magma within the lower crust.

We conclude that the earthquake activity below 15 km depth in the Aleutian arc is generated by rising magma. This hypothesis is not particularly remarkable until we consider that deep volcanic earthquakes are absent in the easternmost and westernmost regions of the active volcanic arc (Figure 3.3), suggesting that more magma rises through the central part of the arc and/or that the deep magmatic processes in the central region are more seismogenic. A greater flux of magma in the central region of the arc suggests that there ought to be bigger more eruptive activity in this region, and this is not evident in our dataset. However, our dataset spans only 10 years and the eruptive cycles of volcanoes occur on timescales extending over thousands of years. When we consider the historical eruptive activity in the Aleutian arc—i.e. eruptive activity over the past 250 years—we find that 8 out of the 10 most active volcanoes are located in the region with deeper earthquakes, with the remaining 2 located in the western Aleutian Islands (AVO unpublished data, 2005, available from www.avo.alaska.edu).

The occurrence of deep earthquakes below Redoubt in the months prior to the 2009 eruptive activity is also noteworthy for a number of reasons. First, it supports the hypothesis that deep earthquake activity is generated by rising magma, since it immediately preceded eruptive activity. More importantly, however, it demonstrates that the crust in the eastern section of the arc is capable of generating deep seismic activity (as opposed to being aseismic) but that at least over the past 10 years it hasn't done so. We interpret this as further evidence that shows that there is less magmatic flux in this region of the arc. The reduced magmatic flux in this portion of the arc could give magma bodies that are ponded in the mid- to upper-crust more opportunity to evolve, a hypothesis that is supported by our geochemical results, which demonstrate that the volcanism to the east is more felsic.

We also note that the largest Holocene calderas in the arc are located within the region where volcanic earthquakes are deepest. Aniakchak, Emmons, Fisher and Okmok each are 10 km wide calderas indicative of high levels of magma flux through the crust. With the exception of Ugashik, located at the eastern edge of the region of deep volcanic seismicity, there are no similar calderas in the eastern or western regions of the arc, further supporting our hypothesis for greater magmatic flux in the central region of the Aleutian arc.

3.6 Aleutian arc geodynamics

We are left with a leading question that forms the crux of this study: what is different about the central region of the Aleutian arc that causes the observed increase in magmatic flux? In addressing this problem we present two end-member hypotheses that draw on observations from a number of studies across a variety of other disciplines (Figure 3.7).

Regional stresses in the overriding plate as a control on arc magmatism

Our first hypothesis considers the role that regional stresses could play in controlling the ascent of magma through the upper (North American) plate (Figure 3.7a). In this scenario we assume that magma generation is constant along the length of the Aleutian arc, and that the observed variations in magma flux are due to stress conditions in the crust which control the rate of magma ascent. To develop this hypothesis, we consider the tectonic stresses along the arc and identify features of the arc that could influence the regional stress regime.

Regional stresses in the western Aleutian arc

Oblique subduction dominates the western region of the Aleutian arc. Slip partitioning of the oblique subduction (McCaffrey, 1992; McCaffrey, 2002) has been shown through various paleomagnetic, geomorphological and seismic studies to have broken the crust west of 172 degrees W into a number of blocks that rotate clockwise and translate westwards (e.g. Geist et al., 1988; Krutikov et al., 2008). This leads to a stress field that is has less of a convergent component and more of a strike-slip (arc-parallel shear) component compared to the region further to the east. We propose that this increased transpressional

stress regime could choke the ascent of magma through the crust in this region, resulting in reduced magmatic flux and consequently fewer deep earthquakes.

An important tectonic feature in this area is the Amlia Fracture zone (AFZ), which is a bathymetric high on the Pacific Plate that subducts below the central Aleutian Islands at approximately 173˚W (Figure 3.1). The fracture zone forms a 1-km-high, 20- 40-km-wide ridge that offsets 57 m.y. oceanic crust to the west with 65 m.y. oceanic crust to the east (Ryan et al., 2012). The AFZ appears to mark a transition in regional seismicity, with abundantly more earthquakes with magnitudes greater than 6 occurring in the region immediately to the west compared with the same area to the east (Ekstrom and Engdahl, 1989). Lu and Wyss (1996) calculated stress inversions from focal mechanisms to show that major changes in stress directions occur across the fracture zone, and Freymueller et al. (2008) note that the boundary between strongly coupled and weakly coupled regions in the Andreanof Islands coincides approximately with the AFZ. Studies since the early 1980s have hypothesized a tear in the plate along the AFZ (e.g. House and Jacob, 1983; Ekstrom and Engdahl, 1989; Singer et al., 2007; Ryan et al., 2012) that could account for the variations in stresses due to the increasing subduction obliquity, earthquake focal mechanisms in the vicinity and even the altered chemistry of the volcanics on Seguam Island (which are not included in our study as Seguam is not seismically monitored).

The location of the AFZ coincides with the change from shallow volcano-seismic activity in the west to deep volcano-seismic activity in the east. This observation leads us to speculate that the AFZ marks the change in regional stress regime, isolating the crust to the east from the increased transpression to the west. Magma is able to ascend more easily through the crust to the east, where the regional transpressional stresses are weaker.

Regional stresses in the eastern Aleutian arc

The tectonic stress regime in the eastern region of the arc is complicated due to the flat-slab subduction of the buoyant Yakutat microplate (e.g. Haeussler, 2008). Deformation attributed to the Yakutat microplate has been measured on faults as far north as the Tintina fault, and is also thought to be translated westwards along the Denali and Castle Mountain

faults (e.g., Haeussler, 2008; Figure 3.1). We propose that these wide-spread additional compressive stresses from the collision of the Yakutat microplate also affect the crust below the eastern volcanic arc and constrict the ascent of magma in that area, resulting in fewer deep volcanic earthquakes.

We identify the Becharof discontinuity, located in the Ugashik-Becharof Lakes region along the northern Alaska Peninsula (Figure 3.1), as an important tectonic feature that could influence the stress regime in this portion of the arc. The Becharof discontinuity (BD) is defined through aeromagnetic and geomorphologic data as a tectonic feature that runs transverse to the subduction zone across the Alaska Peninsula. It also marks the location where the Bruin Bay fault—a 515 km-long transpressional fault that was most active in the late Tertiary and a major tectonic structure in southern Alaska—converges with the Ugashik Lakes fault system (ULFS), a north-northeast trending fault zone to the south of Becharof Lake dominated by normal faulting (Figure 3.1; Decker et al., 2008). These three tectonic features converge under the southern shore of Becharof Lake, below the vents of mantle-derived CO_2 at Gas Rocks, and less than 2 km from the Ukinrek Maars craters (Figure 3.1, inset). The confluence of these tectonic features, as well as the energetic earthquake swarm that occurred along the BD in 1998 (McGimsey et al., 2003), led Decker et al. (2008) to speculate that the BD marks a persistent zone of weakness that extends through the full extent of the crust.

The transition between deep and shallow volcanic earthquakes occurs in the region of the BD, leading us to speculate that the two are related. The transpressional sense of slip on the Bruin Bay fault that extends to the northeast of the Becharof-Ugashik Lake region demonstrates that the state of stress in the crust has been compressional over a long period of geologic time, dating back at least 26 m.y. when the fault was the most active (Detterman and Reed, 1980; Detterman and Hartsock, 1966). It is likely that this compression is primarily driven by the larger subduction zone processes involving the collision of the Yakutat Block in southcentral Alaska, which arrived at the Aleutian trench approximately 23 m.y. ago (Chapman et al., 2008). The extensional setting that is mapped by Decker et al. (2008) to the south of the Becharof discontinuity and within the ULFZ indicates that the crustal stresses are

significantly different to the south of the Becharof-Ugashik region. This suggests that the BD marks a change in the regional stress regime, where the region to the south is isolated from the compressive stresses driven by the Yakutat collision in the northwest. Further evidence of this change in stress field can be observed in the subsidence of the Bristol Bay basin to the north of the ULFS (Figure 3.1). It is possible that a break in the crust along the BD facilitates the normal faulting in the ULFS and the extension in the Bristol Bay basin. The reduced transpressional stresses in the crust south of the BD could then allow magma to ascend more easily through the crust, explaining the increase in deep earthquake activity in that region.

Similar stress regimes in the eastern and western Aleutian arc?

We propose a similar model for the reduction of magma flux in the eastern and western regions of the arc, despite the two areas having vastly different tectonic settings. The orientation of the regional stress regime in both areas ought to be evident in moment tensor solutions to earthquakes in the upper plate along the arc. However, very little data exists for earthquakes in the upper plate along the Aleutian arc (Appendix 3-D). The only region of the arc with significant earthquake activity in the upper plate is the western Aleutians, west of the AFZ, which has been subject to numerous studies and is consequently reasonably well understood in terms of regional stresses (e.g., Ekstrom and Engdahl, 1989; Ruppert et al., 2012). There is insufficient data along the rest of the arc for us to draw meaningful conclusions about the present-day stress regime using moment tensor solutions.

Variations in magma production along the down-going plate as a control on arc magmatism

Our alternate hypothesis assumes that the magma can ascend through the overriding plate with similar ease along the length of the arc, and that the observed differences in magmatic flux stem from variations in the rate of magma production along the subduction zone (Figure 3.7b). The introduction of H_2O into the mantle is the main mechanism by which magma is thought to be generated (Coats, 1962). This hypothesis suggests that more H_2O is introduced into the subduction zone in the central region of the arc, which exhibits the greatest magmatic flux and a corresponding increase in deep volcanic earthquakes. We

consider two processes that could facilitate the introduction of H_2O into the mantle: 1) transport within water-laden sea-floor sediments, and 2) transport within zones of serpentinization that are associated with fracture zones.

Water transport into the mantle via sediment flux

The thickness of sediments in the Aleutian trench varies significantly along the arc. Most of the material in the Aleutian trench is comprised of turbidites composed of sediments shed off of the Alaska Range, although some of the older sediments are derived from the Chugach, Wrangell and St Elias mountains (Kelemen et al., 2003). Additional sediment is delivered to the trench via sedimentary fans that cross the Gulf of Alaska, originally sourced from southeast Alaska. Sediment thickness increases gradually from east to west between 160 and 172 ˚ W, and, after an abrupt thinning by about 30% between 173 and 174 ˚ W, they thin more gradually to near zero at 190 ˚ W (Singer et al., 2007). The sudden thinning of sediments at 173 degrees W is due to the influence of the AFZ, which acts as barrier to the westward transport of turbidite sediment (Scholl et al., 1982). In addition, Singer et al. (2007) note that the AFZ has served to focus the peak sediment flux beneath the arc. This is an important observation in terms of arc volcanism, since the region with the highest rate of deep volcanic earthquakes extends east of the AFZ, but not to the west. Furthermore, studies that examine variations in the geochemistry of Aleutian volcanic products have suggested that sediments play an important role in generating melt in the mantle (e.g. Kelemen et al., 2003; Kay et al., 1978; Class et al., 2000).

Given the influence that the AFZ has on sediment flux, its location where the rate of deep volcanic earthquake activity suddenly changes, and the role that sediments are thought to have in generating melt in the mantle, it is reasonable that sediment flux could influence volcano seismicity. In this model, the increase in deep volcanic seismicity in the central region of the arc is caused by the elevated sediment flux in that area. West of the AFZ, where there are significantly less sediments present in the trench, there are correspondingly fewer volcanic earthquakes. The increasing obliquity of subduction to the west of the AFZ reduces the trench-normal convergence rate, which means that the sediment volume flux to the mantle decreases systematically to the west. In the westernmost islands of the arc

(Komandorsky islands, Russia), the plate motion is nearly trench-parallel, and almost no sediment is being delivered to the mantle at present.

Water transport into the mantle via fracture zones

An alternate process that introduces H_2O into the mantle is through the subduction of serpentine, a mineral rich in H_2O and stable to depths of 120-200 km within subducted oceanic crust (Singer et al., 2007). The highly fractured and faulted oceanic crust that is associated with fracture zones can expose large areas of peridotite to seawater hydrothermal alteration that creates large amounts of serpentine close to the plate surface (Kerrick, 2002). Subducting fracture zones therefore have the potential to transport and release large volumes of water deep into the mantle, which increase the amount of melt and magma flux through the crust and, presumably, increase the rate of deep volcanic earthquake activity.

The AFZ, described in detail in section 3.6, is an obvious candidate for this mechanism in the western Aleutians. Its westward migration over time could explain why volcanoes to the east exhibit greater magmatic flux than those to the west, and could also account for the increased deep volcanic seismicity to the east. A similar process may be occurring in the eastern Aleutian arc from the subduction of the Aja fracture zone, which subducts under the Alaska Peninsula in the same region where we observe the transition from deep to shallow volcanic earthquakes (Figure 3.1). The Aja fracture zone migrates to the east, and could therefore explain the presence of deep volcanic earthquake activity to the west and account for the lack of deep volcanic seismicity to the east.

Subducting sediment or subducting fracture zones?

It is likely that both the increase of sediment into the mantle and the subduction of fracture zones play important roles in this model for controlling arc magmatism, since each process by itself can not sufficiently explain the observed variations in magmatic processes. If subducting fracture zones alone were at play, we might only expect to see deep volcanic earthquakes in the immediate vicinity and not extending for hundreds of km along the arc. If sediment flux alone was the key mechanism, then how do we explain the abrupt transition from shallow to deep volcanic earthquake activity in the eastern Aleutian arc? Similarly, it is

not clear how long the effects of a subducted fracture zone could persist: although the central region of the arc generates abundant deep seismicity, there have been no subducting fracture zones there for millions of years.

Comparing hypotheses: upper plate stress changes versus varying lower plate magma genesis

While our hypotheses each rely on very different processes in order to explain the variations in magmatism along the Aleutian arc, they share some significant common features. The AFZ plays a role in both models: in the stress-driven hypothesis it marks a regional stress boundary, while in the melt-driven hypothesis it provides a mechanism with which to increase the amount of H_2O into the mantle. Subduction obliquity is also important in both models: it enhances the transpressional stresses within the crust in the stress-driven hypothesis, and controls the rate of fracture zone migration along the trench in the melt-driven model. This overlap between models is a strong indication that aspects of both hypotheses may be important. Given the speculative nature of our models and the limits of our seismic dataset, however, we refrain from further conjecture to which aspects of the two models play the most important roles in controlling arc magmatism.

3.7 Additional considerations

The active western Aleutians paradox

Our stress-based model (section 3.6) model links the decrease in eruptive activity in the western regions of the Aleutian arc to crustal stresses associated with the increasing subduction obliquity. In the melt-based model we propose that there is reduced magma production in this region, due to a decrease in sediment thickness on the down-going slab. While there is a general reduction in the amount of volcanic activity in the western Aleutians, the eruptive records show that some volcanoes in this region (namely Gareloi and Great Sitkin) are among the most active in the arc. There are several possible explanations for this. For the stress-based model, the rotating crustal blocks may in some places be able to accommodate enough of the increased stresses to allow for long-lived magma ascent below certain volcanoes. However, these more active volcanoes are located along the edges of the

rotating blocks and along the back-arc transform faults, where we would expect to find a larger concentration of stresses, so this explanation is unlikely (Figure 3.1). Given that the back-arc transform faults accommodate the wider-scale westward translation of crust in the fore-arc, it is possible that the back-arc transform faults mark zones of weakness that extend through the length of the brittle crust, that could facilitate the easier rise of magma. Both Gareloi and Great Sitkin are located along the Adak to Atka shear zone (Ryan and Scholl, 1993), suggesting that it is a zone of weakness along which magma can more readily ascend through the lithosphere. It fails to explain, however, why Moffet, Kanaga and Kliuchef do not show the same high levels of volcanic activity. For the melt-based model, it is possible that sediment is able to accumulate locally within smaller bathymetric features on the down-going plate, although it is unclear exactly which bathymetric features would be capable of this.

The influence of earthquake swarms and eruptions

The earthquake catalogs that we constructed in section 3.3 contain seismicity that was generated during episodes of volcanic unrest, which include seismic swarms and eruptive activity. 26 of the 46 monitored volcanoes have experienced episodes of seismic unrest, which we define as periods when the rate of seismicity was more than triple the mean earthquake rate, and 8 of these volcanoes have also erupted during our period of study (volcanic unrest at each volcano is included in Appendix 3-A). The majority of seismicity generated during volcanic unrest is limited to the shallowest 10 km of crust, and is most likely generated by the brittle response of the crust to intruding magma (e.g., Hill, 1977). Some volcanoes, most notably Redoubt and Iliamna, also generate earthquakes between 15 and 30 km depth during unrest that is probably associated with magma flux in the lower crust.

We find little change to the overall depth distribution of volcanic earthquakes when we remove events associated with episodes of volcanic unrest (see comparison in Appendix 3-E). This confirms that the trends we observe in the depth distribution of volcanic earthquakes are generally independent of eruptive activity

The effects of varying network aperture

It is possible that some deeper earthquakes recorded at networks with small apertures get excluded from the published AVO earthquake catalogs because of their large horizontal errors. The networks with the smallest apertures are those located on the volcanic islands of the Western Aleutians, while the largest networks are located along the Alaska Peninsula and in the Cook Inlet region. Given that the majority of the networks in the eastern portion of the arc are spread over distances greater than 40 km around the volcanoes, we can be confident that the lack of deep seismicity in this region is not an effect of network aperture. We cannot be as certain in the western Aleutians, but we do note that the spacing of the networks is close enough that stations on adjacent networks are often used in locating deeper seismicity, effectively increasing the network aperture in these areas.

Magnitude of completeness considerations

The arc-wide magnitude of completeness for our study period is 1.4, although when we exclude Aniakchak, Fisher and Tanaga this number drops to 1.0. We exclude earthquake below ML 1.4 in Appendix 3-F and find that the depth distribution of volcanic earthquakes does not change appreciably: the central portion of the arc still contains more deep seismicity than either the east or west. This further confirms that our results are unaffected by biases within the dataset.

3.8 Conclusion

Our seismic characterizations of Aleutian volcanism have brought forth some interesting trends that have not previously been identified in the Aleutian arc. The volcanoes in the central region of the arc—from Okmok on Umnak Island up to and including Aniakchak on the Alaska Peninsula—generate more deep seismicity than those to the east or west. The majority of earthquakes below 12 km depths are low frequency events, with the exception of the volcanoes in the western Aleutians. The eastern limit to the deep earthquake activity occurs in approximately the same region where previous studies have shown that the volcanism becomes more felsic.

We propose that most deep volcanic earthquakes are generated by the ascent of magma through the lower crust. The more energetic deep seismicity in the central Aleutians suggests that these volcanoes should be more prolific than those to the east or west. This hypothesis is in agreement with the location of the largest and most historically active volcanoes in the Aleutian arc, which are found in same region of the central Aleutians that generates abundant deep volcano seismicity.

To explain the variations in deep volcanic earthquakes—and the magma flux they represent—we present two parallel hypotheses. The first assumes that magma production rates are the same along the whole arc, and that the reduced magma flux in the eastern and western regions of the arc is due to changes in the upper plate that choke the ascent of magma. This hypothesis suggests stresses due to oblique subduction in the west and far-field effects from the subduction of the Yakutat microplate in the east inhibit the rise of magma through the crust in these areas. We identify the AFZ and the BD—located in the regions where the depth range of volcanic earthquakes changes—as important tectonic features that mark these changes to the stress regimes. The second hypothesis assumes that there are no differences in crust of the upper plate that could inhibit the ascent of magma, and that the observed variations in magmatic flux in the crust reflect variations in the generation of melt on the subducting plate. We propose that there are significant differences in the amount of H_2O that is subducted along the Aleutian arc which could account for the differences in melt production, and present two possible mechanisms for this model: 1) H_2O is transported into the mantle via sediments on the subducting plate, or 2) H_2O is transported into the mantle within areas of serpentinized crust that is found in fracture zones. We draw on observations of sediment thickness along the arc, the changes in trench-normal convergence rates, and the location of the AFZ and the Aja fracture zone to support this hypothesis.

Both of these hypotheses rely on common tectonic features such as the AFZ, suggesting that aspects from each model may play equally important roles in controlling magmatism in the Aleutian arc.

3.9 Acknowledgements

We thank Dave Scholl, Dan Dzurisin, Bob Gillis and Rich Koehler for their insightful discussions and ideas, Cheryl Cameron for her expertise on Alaskan volcanoes, and X, X, and X for their reviews of this manuscript. Janet Schaefer provided the map in Figure 1. This study was possible thanks to the dedicated work of a number of individuals: Scott Stihler, Mitch Robinson and Jim Dixon maintained the near real-time database of earthquake locations; John Paskievitch, Guy Tytgat, Steve Estes, Tim Plucinski, Cyrus Read, Ed Clark and Dane Ketner kept the continuous real-time seismic data flowing. The Alaska Volcano Observatory is a partnership between the U.S. Geological Survey, the Geophysical Institute at the University of Alaska Fairbanks, and the Alaska Division of Geological and Geophysical Surveys.

3.10 References

Cameron, C.E., 2006. An updated count of historic eruptions and volcanoes in Alaska [abs]: Geological Society of America – Abstracts with Programs, v. 38, n. 5, p. 75.

Chapman, J. B., T. Pavlis, S. Gulick, A. Burger, L. Lowe, J. Spotila, R. Bruhn, M. Vorkink, P. Koons, A. Barker, K, Picornel, K. Ridgeway, B. Hallet, J. Jaeger, and J. McAlpin, 2008, Neotectonics of the Yakutat collision: Changes in deformation driven by mass redistribution, AGU Chapman volume Active Tectonics and Seismic Potential of Alaska.

Chouet, B.A., Page, R.A., Stephens, C.D., Lahr, J.C., Power, J.A., 1994. Precursory swarms of long-period events at Redoubt Volcano (1989–1990), Alaska; their origin and use as a forecasting tool. J. Volcanol. Geotherm. Res. 62, 95– 136.

Chouet, B.A., 1996, Long-period volcano seismicity; its source and use in eruption forecasting: Nature, v. 380, p. 309–316, doi:10.1038/380309a0.

Class, C., Miller, D.M., Langmuir, C.H., 2000, Distinguishing melt and fluid subduction components in Emnak volcanic, Aleuitan arc: Geochem. Geophys. Geosyst., v. 1 6, doi: 10.1029/1999GC000010.

Coats, R.R., 1962, Magma type and crustal structure in the Aleutian arc, *in* MacDonald, G.A. and Kuno, H., eds., The Crust of the Pacific Basin: Geophys. Monogr. Ser., v. 6, p. 92-109.

Decker, P.L., Reifenstuhl, R.R., and Gillis, R.J., 2008, Structural linkage of major tectonic elements, Ugashik Lakes - Becharof Lake region, northeastern Alaska Peninsula (presentation): DNR Spring Technical Review Meeting, Anchorage, Alaska, March 26-27, 2008: Alaska Division of Geological & Geophysical Surveys, 18 p.

DeMets, C., Gordon, R.G., Argus, D.F. & Stein, S., 1990. Current plate motions, *Geophys. J. Int.* **101,** 425–478.

Detterman, R.L., and Hartsock, J.K., 1966, Geology of the Iniskin–Tuxedni region, Alaska: U.S. Geological Survey Professional Paper 512, 78 p., 6 plates, scale 1:63,360.

Detterman, R.L., and Reed, B.L., 1980, Stratigraphy, structure, and economic geology of the Iliamna Quadrangle, Alaska: U.S. Geological Survey Bulletin 1368-B, 86 p., 1 plate, scale 1:250,000.

Dixon, J.P., Stihler, S.D., Power, J.A., and Searcy, C.K., 2012, Catalog of earthquake hypocenters at Alaskan volcanoes: January 1 through December 31, 2011: U.S. Geological Survey Data Series 730, 82 p., available online at http://pubs.usgs.gov/ds/730/pdf/ds730.pdf.

Ekstrom, G., and Engdahl, E.R., 1989, Earthquake source parameters and stress distribution in the Adak Island region of the central Aleutian Islands, Alaska: Journal of Geophysical Research, v. 94, p. 15,499–15,519, doi:10.1029/JB094iB11p15499.

Fliedner, M.M. and S.L. Klemperer, 1999, Composition of an island-arc: wide-angle studies in the eastern Aleutian islands, Alaska. J. Geophys. Res., v. 104, pp. 10,667-10,694.

Freymueller, J.T., Woodard, H., Cohen, S.C., Cross, R., Elliott, J., Larsen, C.F., Hreinsdottir, S., and Zweck, C., 2008, Active deformation processes in Alaska, based on 15 years of GPS measurements, *in* Freymuller, J.T., Haeussler, P.J., Wesson, R., and Ekstrom, G., eds., Active Tectonics and Seismic Potential of Alaska: American Geophysical Union Geophysical Monograph 179, p. 1–42.

Geist, E.L., Childs, J., and Scholl, D., 1988, The origin of summit basins of the Aleutian ridge: Implications for block rotation of an arc massif: Tectonics, v. 7, p. 327–341, doi:10.1029/TC007i002p00327.

George, O., 2010, Relating deep magmatic processes to eruptive behavior beneath arc volcanoes through an analysis of deep seismicity: University of Alaska MS thesis, 101 p.

Haeussler, P.J., 2008, An Overview of the Neotectonics of Interior Alaska: Far-Field Deformation From the Yakutat Microplate Collision, *in* Freymueller, J.T., Haeussler, P.J., Wesson, R., and Ekstrom, G., eds., Active Tectonics and Seismic Potential of Alaska: American Geophysical Union Geophysical Monograph 179, p. 83–108.

Hill, D. P., l977, A model for earthquake swarms: Jour. Geophys. Res. v. 82, pp. 1347-135l.

House, L.S., and Jacob, K.H., 1983, Earthquakes, plate subduction, and stress reversals in the eastern Aleutian arc: Journal of Geophysical Research, v. 88, no. B11, p. 9347–9373, doi:10.1029/JB088iB11p09347.

Julian, B.R., 1994. Volcanic tremor: nonlinear excitation by fluid flow. J. Geophys. Res. 99, 11135–11150.

Kay, R.W., Sun, S.-S, and Luu-Hu, C.-N, 1978, Pb and Sr isotopes in volcanic rocks from the Aleutian Islands and Pribilof Islands, Alaska: Geochim. Cosmochim. Acta, 42, p. 263-273.

Kelemen, P.B., Yogodzinski, G.M., and Scholl, D.W., 2003, Along strike variation in the Aleutian Island arc— Genesis of high Mg# andesite and implications for continental crust, *in* Eiler, J., ed., The Subduction Factory: American Geophysical Union Geophysical Monograph 138, p. 223–276.

Kerrick, D., 2002, Serpentine Seduction: Science, v. 298, P. 1344-1345.

Krutikov, L., Stone, D., and Minyuk, P., 2008, New Paleomagnetic data from the Central Aleutian Island Arc: Implications for Block Rotations, in: Active Tectonics and Seismic Potential in Alaska, edited by: Eds. Freymueller, J. T., Haeussler, P. J., Wessone, R. L., and Ekstrom, G., AGU Geophysical Monograph, 179, 135–149.

Lahr, J.C., 1999, HYPOELLIPSE: A computer program for determining local earthquake hypocentral parameters, magnitude, and first motion pattern; U.S. Geological Survey Open-File Report 99-23, 116 p.

Lu, Z., and Wyss, M., 1996, Segmentation of the Aleutian plate boundary derived from stress direction estimates based on fault plane solutions: Journal of Geophysical Research, v. 101, no. B1, p. 803–816, doi:10.1029/95JB03036.

Mangan, M, Miller, T, Waythomas, C., Trusdell, F., Calvert, A., and Layer, P., 2009, Diverse lavas from closely spaced volcanoes drawing from a common parent: Emmons Lake Volcanic Center, Eastern Aleutian Arc: Earth and Planetary Science Letters, v. 287, p. 363-372, doi:10.1016/j.epsl.2009.08.018 .

McCaffrey, R., 1992, Oblique plate convergence, slip vectors, and forearc deformation: J. Geophys. Res. 97:8905–15.

McCaffrey, R., 2002, Crustal block rotations and plate coupling, *in* Stein, S., Freymueller, J., eds, Plate Boundary Zones: A.G.U. Geodyn. Ser. 30:101–22.

McGimsey, R.G., Neal, C.A., and Girina, O., 2003, 1998 volcanic activity in Alaska and Kamchatka: summary of events and response of the Alaska Volcano Observatory: U.S. Geological Survey Open-File Report 03-423, 35 p.

McGimsey, R.G., Neal, C.A., Dixon, J.P., Malik, Nataliya, and Chibisova, Marina, 2011, 2007 Volcanic activity in Alaska, Kamchatka, and the Kurile Islands: Summary of events and response of the Alaska Volcano Observatory: U.S. Geological Survey Scientific Investigations Report 2010–5242, 110 p.

Nye, C. J., and Turner, D. L., 1990, Petrology, geochemistry, and age of the Spurr volcanic complex, eastern Aleutian arc: Bulletin of Volcanology, v. 52, n. 3, p. 205-226.

Power, J.A, Stihler, S.D., White, R.A., and Moran, S.C., 2004, Observations of deep long-period (DLP) seismic events beneath Aleutian Arc volcanoes: 1989-2002: Journal of Volcanology and Geothermal Research, v. 138, p. 243-266.

Power, J.A., Nye, C.J., Coombs, M.L., Wessels, R.L., Cervelli, P.F., Dehn, J., Wallace, K.L., Freymueller, J.T., and Doukas, M.P., 2006, The reawakening of Alaska's Augustine Volcano: Eos, v. 87, n. 37, p. 373, 377.

Power, J.A., Jolly, A.D., Nye, C.J., Harbin, M.L., 2002, A conceptual model of the Mount Spurr magmatic system from seismic and geochemical observations of the 1992 Crater Peak eruption sequence, Bull. Volcanol. 64, 206-218.

Power, J.A., Stihler, S.D., Chouet, B.A., Haney, M.M., and Ketner, D.M., 2013, Seismic observations of Redoubt Volcano, Alaska—1989–2010 and a conceptual model of the Redoubt magmatic system: Journal of Volcanology and Geothermal Research, doi:10.1016/j.jvolgeores.2012.09.014.

Ruppert, N.A., Kozyreva, N.P., and Hansen, R.A., 2012, Review of crustal seismicity in the Aleutian Arc and implications for arc deformation: Tectonophysics, v. 522-523, p. 150-157, doi:10.1016/j.tecto.2011.11.024.

Ryan, H.F., Amy E. Draut, Katie Keranen, and David W. Scholl, 2012, Influence of the Amlia fracture zone on the evolution of the Aleutian Terrace forearc basin, central Aleutian subduction zone, Geosphere; v. 8; no. 6; p. 1254–1273; doi:10.1130/GES00815.1.

Ryan, H.F., and Scholl, D.W., 1993, Geologic Implications of Great Interplate Earthquakes along the Aleutian Arc, Journal of Geophysical Research, V 98, no. B12, P. 134-146.

Scholl, D.W., Vallier, T.L., and Stevenson, A.J., 1982, Sedimentation and deformation in the Amlia fracture zone sector of the Aleutian trench: Marine Geology, v. 48, p. 105–134, doi:10.1016/0025-3227(82)90132-3.

Singer, B.S., Jicha, B.R., Leeman, W.P., Rogers, N.W., Thirlwall, M.F., Ryan, J., and Nicolaysen, K.E., 2007, Along-strike trace element and isotopic variation in Aleutian Island arc basalt: Subduction melts sediments and dehydrates serpentine: Journal of Geophysical Research, v. 112, p. B06206, doi:10.1029/2006JB004897.

Thelen, W.A., Malone, S.D., and West, M.E., 2010, Repose time and cumulative moment magnitude: a new tool for forecasting eruptions?: Geophysical Research Letters, v. 37, L18301, 5 p. doi: 10.1029/2010GL044194, 2010.

Ukawa, M., Ohtake, M., 1987. A monochromatic earthquake suggesting deep-seated magmatic activity beneath the Izu-Ooshima Volcano, Japan. J. Geophys. Res. 92, 12649–12663.

Waythomas, C.F., Scott, W.E., Prejean, S.G., Schneider, D.J., Izbekov, Pavel, and Nye, C.J., 2010, The 7-8 August 2008 eruption of Kasatochi Volcano, central Aleutian Islands, Alaska: Journal of Geophysical Research, v. 115, n. B00B06, 23 p., doi:10.1029/2010JB007437.

Wilshire, H.G., and Kirby, S.H., 1989, Dikes, joints and faults in the upper mantle, Tectonophysics, 161: 23-31.

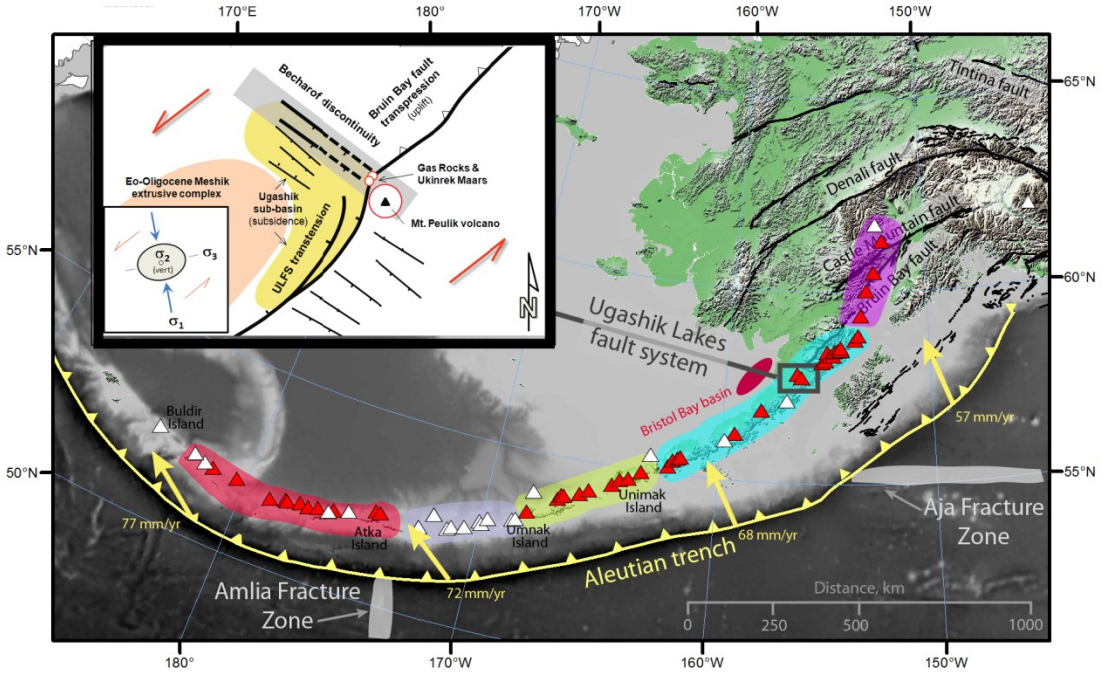

Figure 3.1 Map of the Aleutian arc and schematic of the Ugashik Lakes fault system (inset). Monitored Holocene volcanoes are represented by red triangles, Holocene active volcanoes without seismic networks are white triangles. Subduction direction is indicated by yellow arrows, and the associated relative plate velocity is indicated in yellow text (after DeMets et al., 1990). Colored areas indicate the different geographical regions: Cook Inlet (purple), Alaska Peninsula (cyan), eastern Aleutians (yellow), central Aleutians (blue) and western Aleutians (red). Black lines indicate major tectonic faults. The inset show a schematic of the Ugashik Lakes fault system, from Decker et al., 2008.

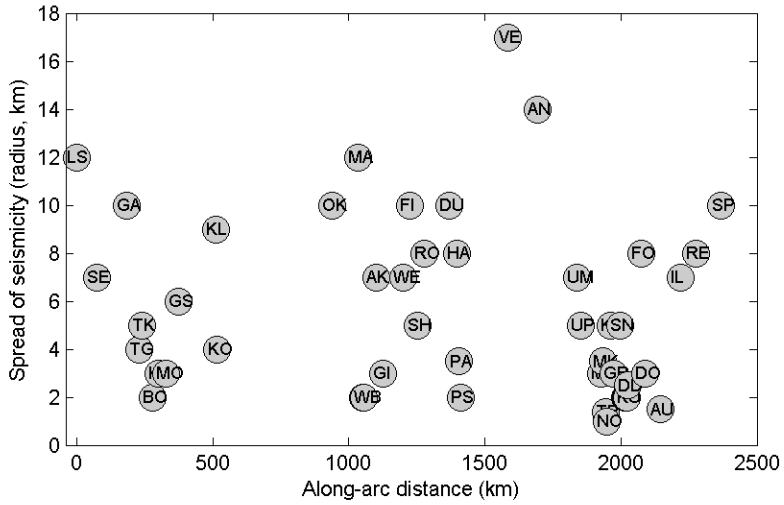

Figure 3.2 Relative along-arc distance, ordered from west to east, as a function of the spread of seismicity around the edifice (defined as a radius centered on the peak).

Codes: LS-Little Sitkin; SE-Semisopochnoi; GA-Gareloi; TG-Tanaga; TK-Takawangha; BO-Bobrof; KA-Kanaga; MO-Moffett; GS-Great Sitkin; KO-Korovin; KL-Kliuchef; OK-Okmok; MA-Makushin; TT-Table Top; WB-Wide Bay; AK-Akutan; GI-Gilbert; WE-Westdahl; FI-Fisher; SH-Shishaldin; RO-Roundtop; DU-Dutton; HA-Hague; PA-Pavlof; PS-Pavlof Sister; VE-Veniaminof; AN-Aniakchak; UM-Ukinrek Maars; UP-Ugashik-Peulik; MA-Martin; MK-Mageik; TR-Trident; NO-Novarupta; KT-Katmai; GR-Griggs; SN-Snowy; DE-Denison; ST-Steller; KU-Kukak; DD-Devil's Desk; FO-Fourpeaked; DO-Douglas; AU-Augustine; IL-Iliamna; RE-Redoubt; SP-Spurr.

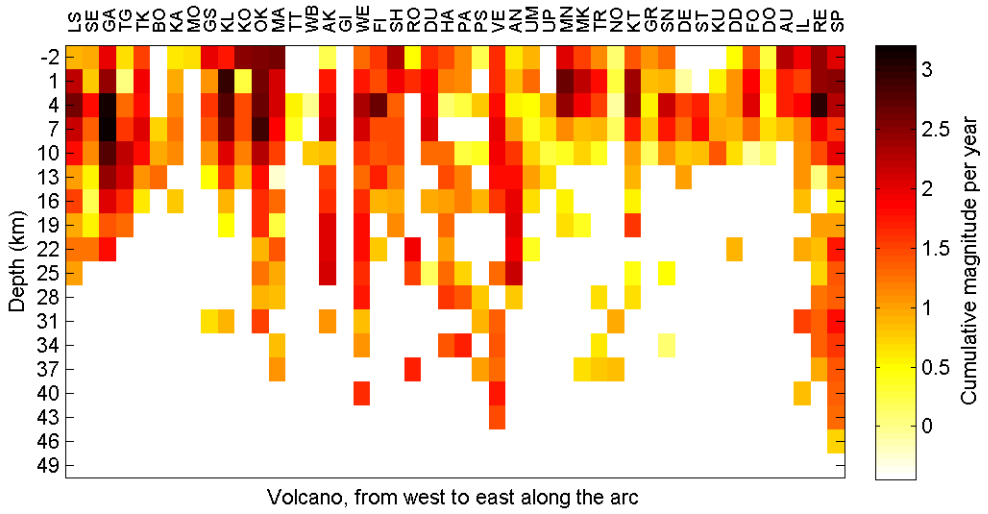

Figure 3.3 Distribution of cumulative earthquake magnitude per year of data within 3 km depth bins below each volcano, ordered east to west.

Codes: LS-Little Sitkin; SE-Semisopochnoi; GA-Gareloi; TG-Tanaga; TK-Takawangha; BO-Bobrof; KA-Kanaga; MO-Moffett; GS-Great Sitkin; KO-Korovin; KL-Kliuchef; OK-Okmok; MA-Makushin; TT-Table Top; WB-Wide Bay; AK-Akutan; GI-Gilbert; WE-Westdahl; FI-Fisher; SH-Shishaldin; RO-Roundtop; DU-Dutton; HA-Hague; PA-Pavlof; PS-Pavlof Sister; VE-Veniaminof; AN-Aniakchak; UM-Ukinrek Maars; UP-Ugashik-Peulik; MA-Martin; MK-Mageik; TR-Trident; NO-Novarupta; KT-Katmai; GR-Griggs; SN-Snowy; DE-Denison; ST-Steller; KU-Kukak; DD-Devil's Desk; FO-Fourpeaked; DO-Douglas; AU-Augustine; IL-Iliamna; RE-Redoubt; SP-Spurr.

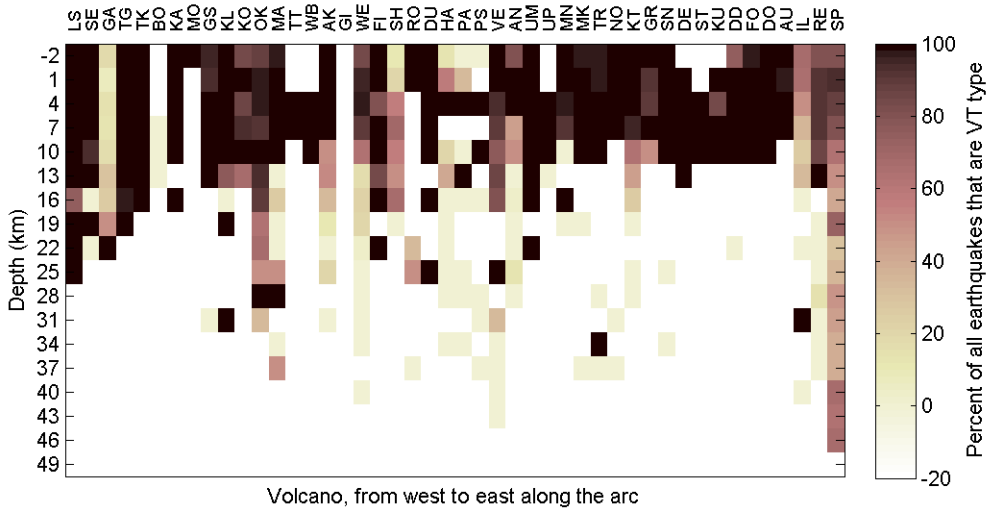

Figure 3.4 Distribution of earthquake type within 3 km depth bins below each volcano, ordered east to west.
Earthquake type is expressed as a percentage of all earthquakes recorded within each depth bin that are VT type.
Codes: LS-Little Sitkin; SE-Semisopochnoi; GA-Gareloi; TG-Tanaga; TK-Takawangha; BO-Bobrof; KA-Kanaga; MO-Moffett; GS-Great Sitkin; KO-Korovin; KL-Kliuchef; OK-Okmok; MA-Makushin; TT-Table Top; WB-Wide Bay; AK-Akutan; GI-Gilbert; WE-Westdahl; FI-Fisher; SH-Shishaldin; RO-Roundtop; DU-Dutton; HA-Hague; PA-Pavlof; PS-Pavlof Sister; VE-Veniaminof; AN-Aniakchak; UM-Ukinrek Maars; UP-Ugashik-Peulik; MA-Martin; MK-Mageik; TR-Trident; NO-Novarupta; KT-Katmai; GR-Griggs; SN-Snowy; DE-Denison; ST-Steller; KU-Kukak; DD-Devil's Desk; FO-Fourpeaked; DO-Douglas; AU-Augustine; IL-Iliamna; RE-Redoubt; SP-Spurr.

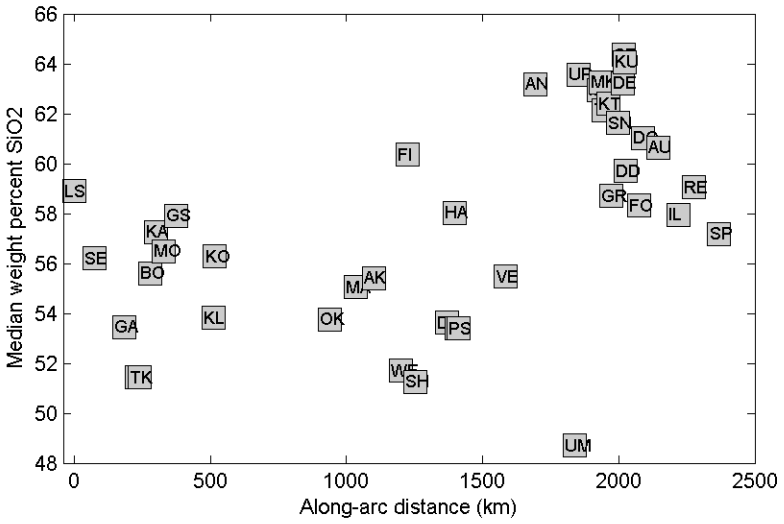

Figure 3.5 Relative along-arc distance, ordered from west to east, as a function of the median weight percent SiO_2 content.
Codes: LS-Little Sitkin; SE-Semisopochnoi; GA-Gareloi; TG-Tanaga; TK-Takawangha; BO-Bobrof; KA-Kanaga; MO-Moffett; GS-Great Sitkin; KO-Korovin; KL-Kliuchef; OK-Okmok; MA-Makushin; TT-Table Top; WB-Wide Bay; AK-Akutan; GI-Gilbert; WE-Westdahl; FI-Fisher; SH-Shishaldin; RO-Roundtop; DU-Dutton; HA-Hague; PA-Pavlof; PS-Pavlof Sister; VE-Veniaminof; AN-Aniakchak; UM-Ukinrek Maars; UP-Ugashik-Peulik; MA-Martin; MK-Mageik; TR-Trident; NO-Novarupta; KT-Katmai; GR-Griggs; SN-Snowy; DE-Denison; ST-Steller; KU-Kukak; DD-Devil's Desk; FO-Fourpeaked; DO-Douglas; AU-Augustine; IL-Iliamna; RE-Redoubt; SP-Spurr.

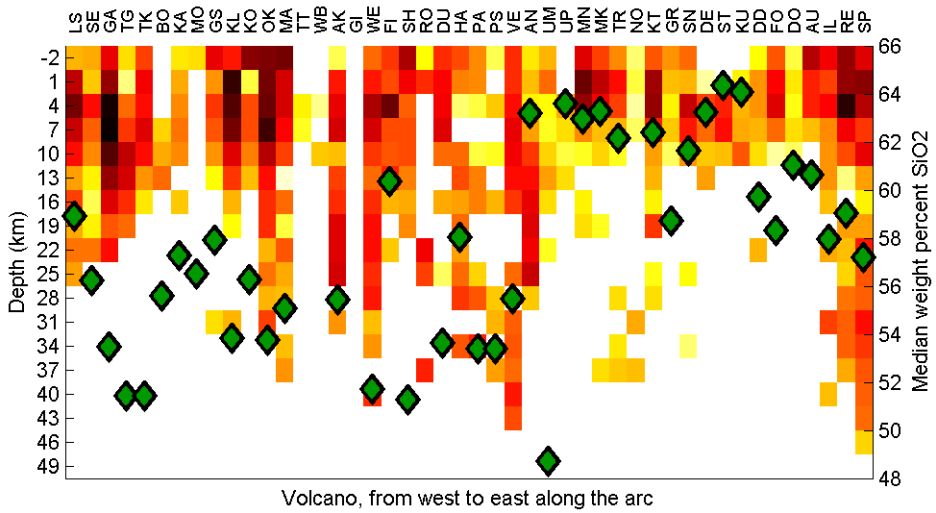

Figure 3.6 Median weight percent SiO_2 of each volcano (green diamonds), ordered west to east, plotted on top of the cumulative earthquake magnitude per year of data within 3 km depth bins below each volcano.

Codes: LS-Little Sitkin; SE-Semisopochnoi; GA-Gareloi; TG-Tanaga; TK-Takawangha; BO-Bobrof; KA-Kanaga; MO-Moffett; GS-Great Sitkin; KO-Korovin; KL-Kliuchef; OK-Okmok; MA-Makushin; TT-Table Top; WB-Wide Bay; AK-Akutan; GI-Gilbert; WE-Westdahl; FI-Fisher; SH-Shishaldin; RO-Roundtop; DU-Dutton; HA-Hague; PA-Pavlof; PS-Pavlof Sister; VE-Veniaminof; AN-Aniakchak; UM-Ukinrek Maars; UP-Ugashik-Peulik; MA-Martin; MK-Mageik; TR-Trident; NO-Novarupta; KT-Katmai; GR-Griggs; SN-Snowy; DE-Denison; ST-Steller; KU-Kukak; DD-Devil's Desk; FO-Fourpeaked; DO-Douglas; AU-Augustine; IL-Iliamna; RE-Redoubt; SP-Spurr.

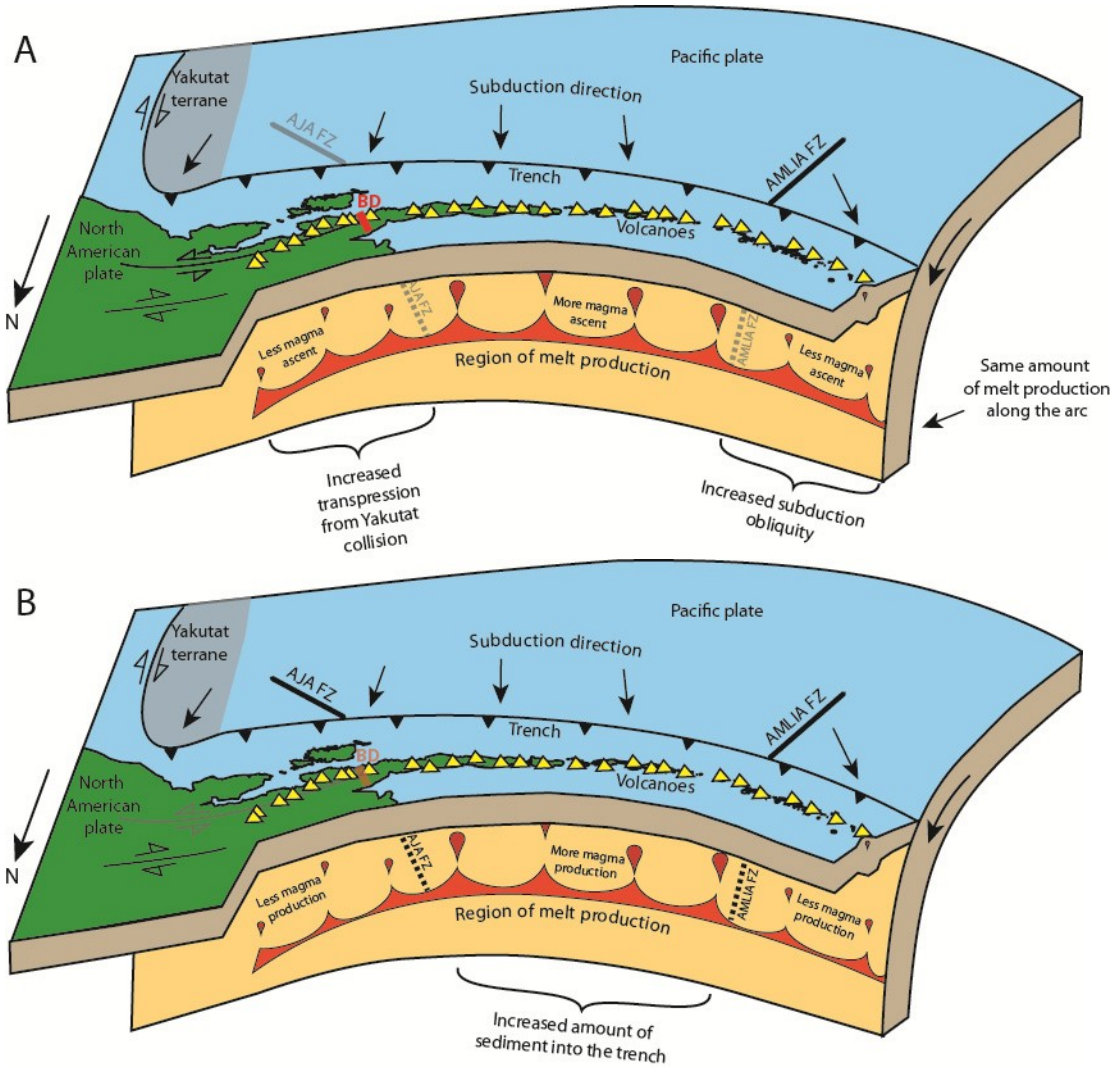

Figure 3.7 Cartoon depictions of both models that explain variations in volcanism in the Aleutian arc. A: The stress-based model, in which variations in transpressional stresses control the rate at which magma can ascend through the crust of the upper plate. B: The melt-based model, where variations in arc magmatism are due to differing rates of magma production along the Aleutian arc.

Table 3.1 Median weight percent SiO_2 of the study volcanoes.

Volcano	Median SiO2
Little Sitkin	58.9
Semisopochnoi	56.21
Gareloi	53.45
Tanaga	51.43
Takawangha	51.43
Bobrof	55.6
Kanaga	57.25
Moffett	56.49
Great Sitkin	57.92
Kliuchef	53.82
Korovin	56.27
Okmok	53.76
Makushin	55.05
Table Top	
Wide Bay	
Akutan	55.42
Gilbert	
Westdahl	51.7
Fisher	60.36
Shishaldin	51.26
Roundtop	
Dutton	53.63
Hague	58.02
Pavlof	53.4
Pavlof Sister	53.4
Veniaminof	55.47
Aniakchak	63.19
Ukinrek Maars	48.7
Ugashik-Peulik	63.57
Martin	62.96
Mageik	63.25
Trident	62.15
Novarupta	
Katmai	62.4
Griggs	58.7
Snowy	61.62
Denison	63.22
Steller	64.36
Kukak	64.07
Devil's Desk	59.7
Fourpeaked	58.31
Douglas	61.02
Augustine	60.64
Iliamna	57.95
Redoubt	59.04
Spurr	57.19

Appendix 3.A-1

Volcano: Little Sitkin

Latitude: 51.9531 N

Longitude: 178.5356 E

Elevation (m): 1188

Number of Holocene vents: 2

Radius of catalog (km): 12

Number of earthquakes: 548

Days of good data: 1500

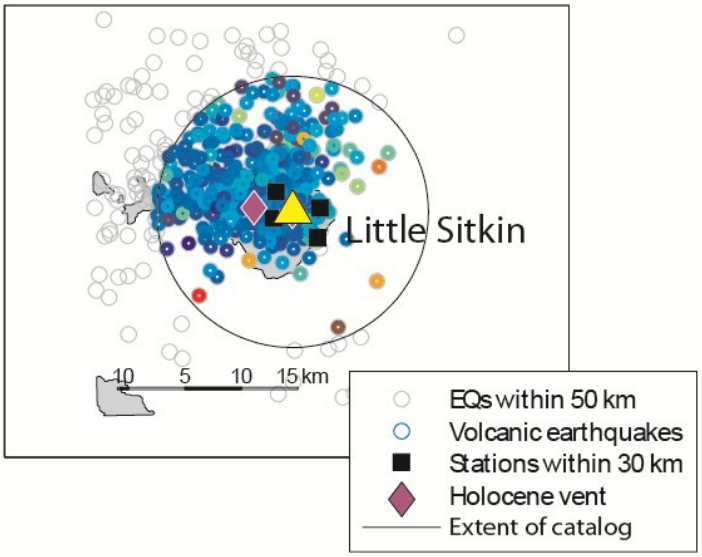

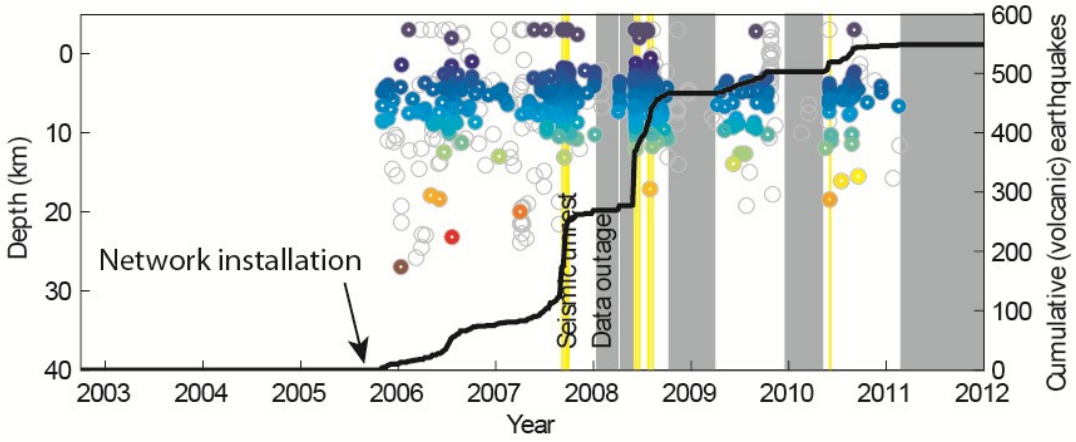

Appendix 3.A-2

Volcano: Semisopochnoi
Latitude: 51.9288 N
Longitude: 179.5977 E
Elevation (m): 800
Number of Holocene vents: 8
Radius of catalog (km): 7
Number of earthquakes: 104
Days of good data: 1500

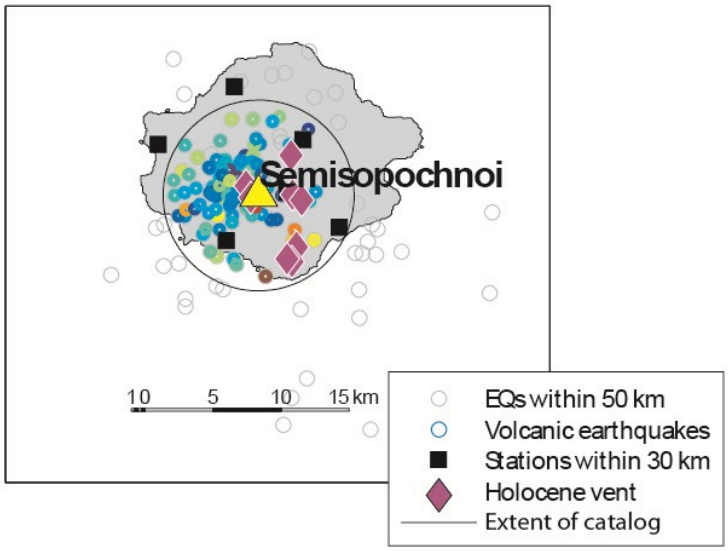

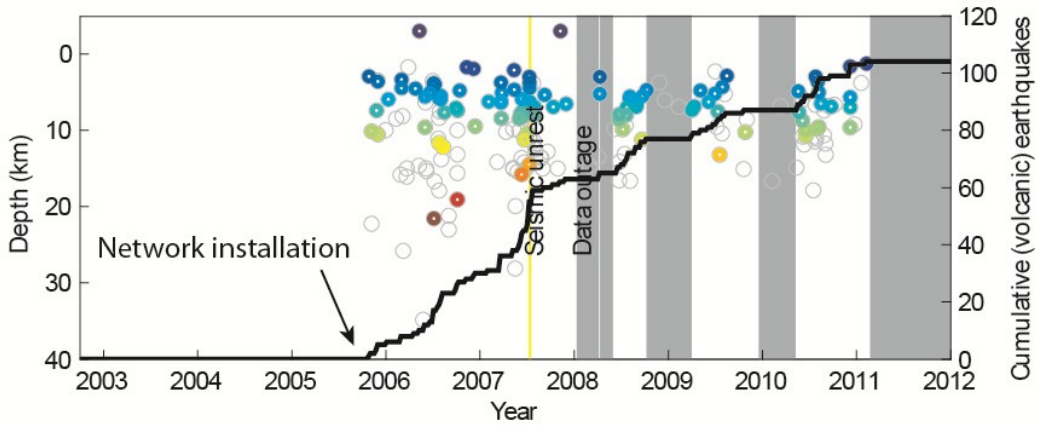

Appendix 3.A-3

Volcano: Gareloi

Latitude: 51.7889 N

Longitude: -178.7937 E

Elevation (m): 1573

Number of Holocene vents: 17

Radius of catalog (km): 10

Number of earthquakes: 2606

Days of good data: 392

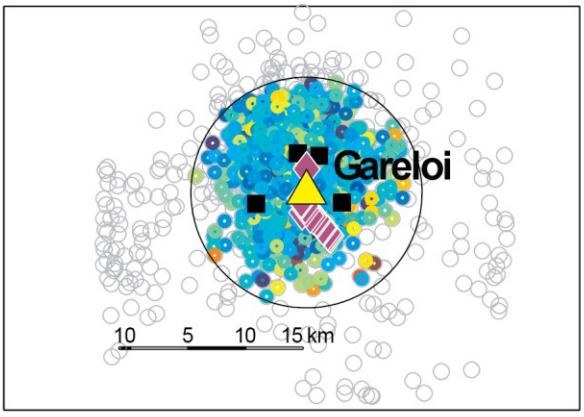

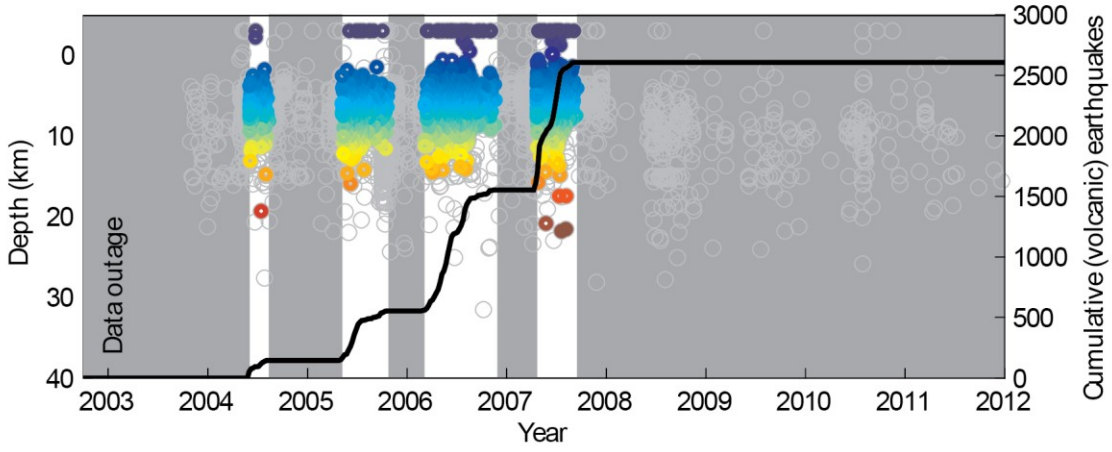

Appendix 3.A-4

Volcano: Tanaga
Latitude: 51.884 N
Longitude: -178.143 E
Elevation (m): 1806
Number of Holocene vents: 4
Radius of catalog (km): 4
Number of earthquakes: 309
Days of good data: 2538

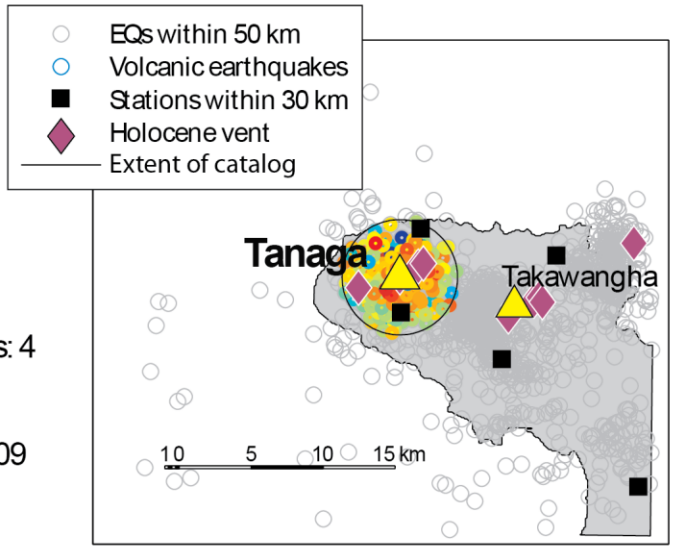

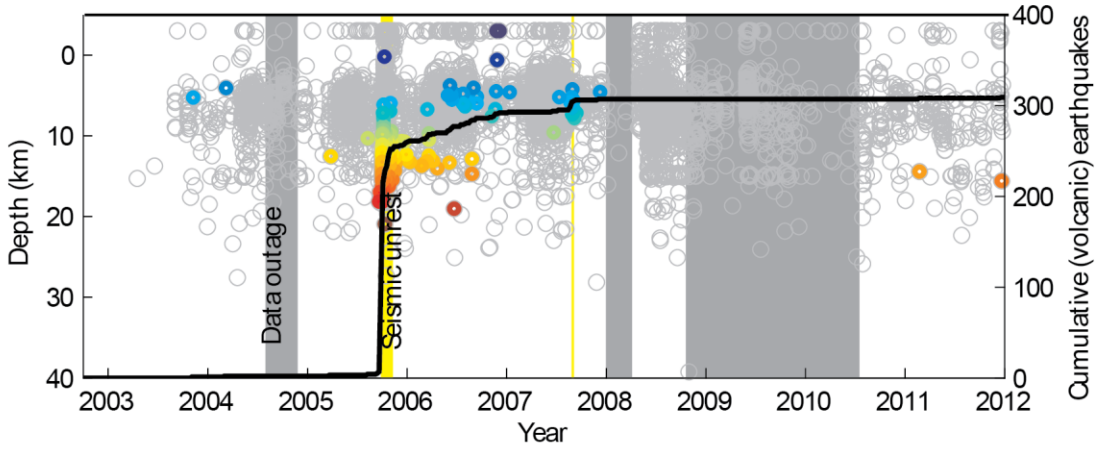

Appendix 3.A-5

Volcano: Takawangha

Latitude: 51.867 N

Longitude: -178.027 E

Elevation (m): 1449

Number of Holocene vents: 5

Radius of catalog (km): 5

Number of earthquakes: 305

Days of good data: 2538

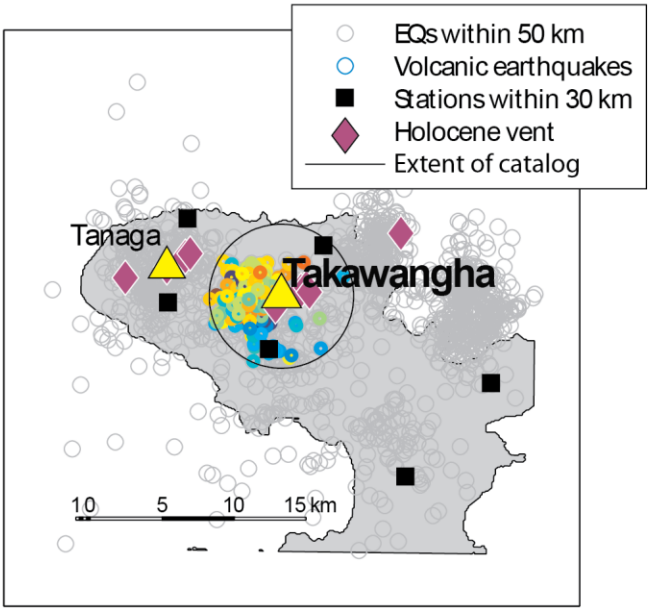

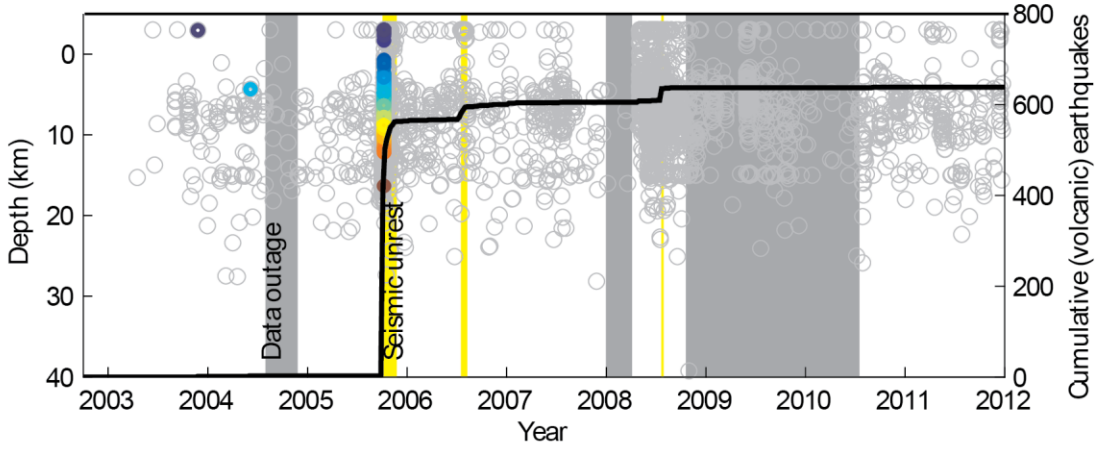

Appendix 3.A-6

Volcano: Bobrof
Latitude: 51.9072 N
Longitude: -177.4409 E
Elevation (m): 738
Number of Holocene vents: 1
Radius of catalog (km): 2
Number of earthquakes: 5
Days of good data: 2679

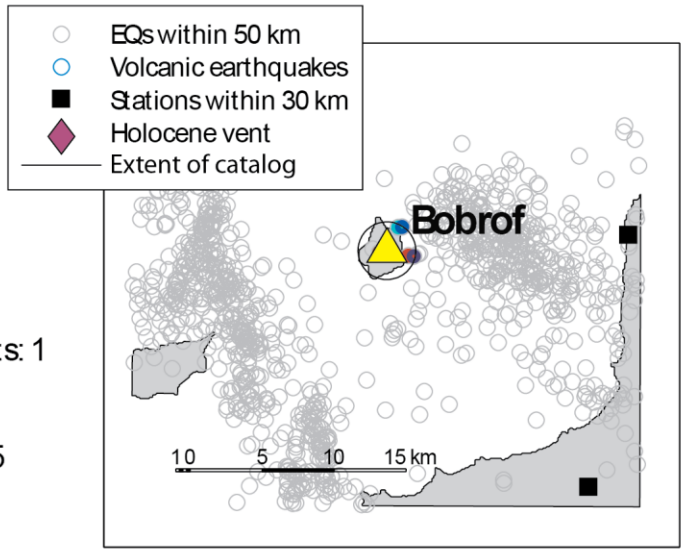

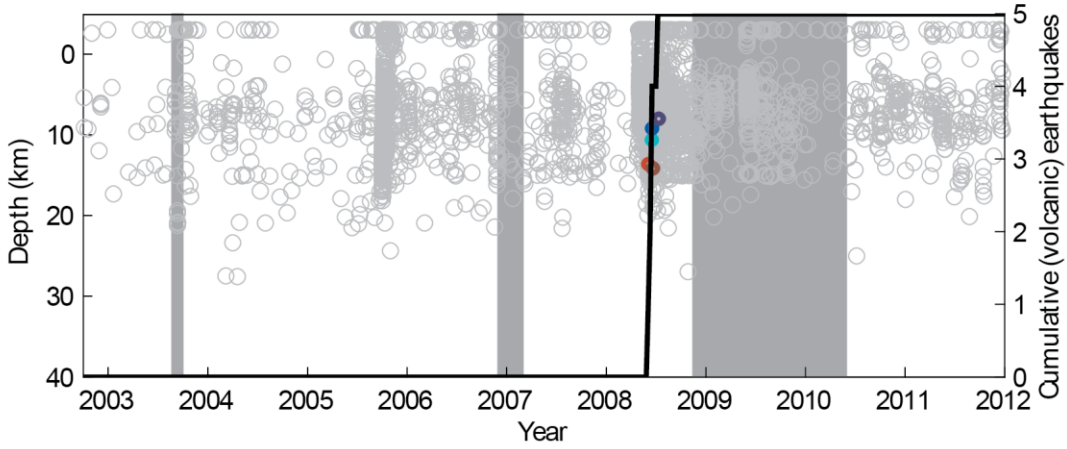

Appendix 3.A-7

Volcano: Kanaga
Latitude: 51.9242 N
Longitude: -177.1623 E
Elevation (m): 1307
Number of Holocene vents: 4
Radius of catalog (km): 3
Number of earthquakes: 42
Days of good data: 2362

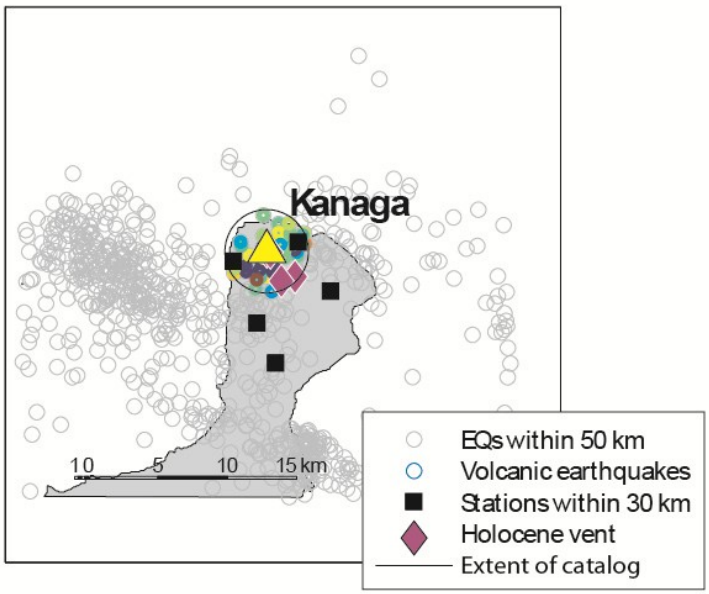

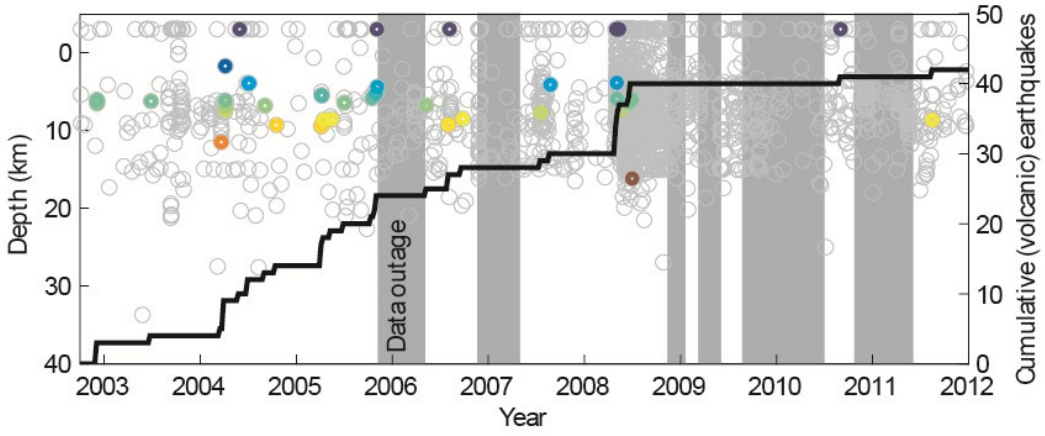

Appendix 3.A-8

Volcano: Moffett
Latitude: 51.937 N
Longitude: -176.741 E
Elevation (m): 1196
Number of Holocene vents: 1
Radius of catalog (km): 3
Number of earthquakes: 1
Days of good data: 2469

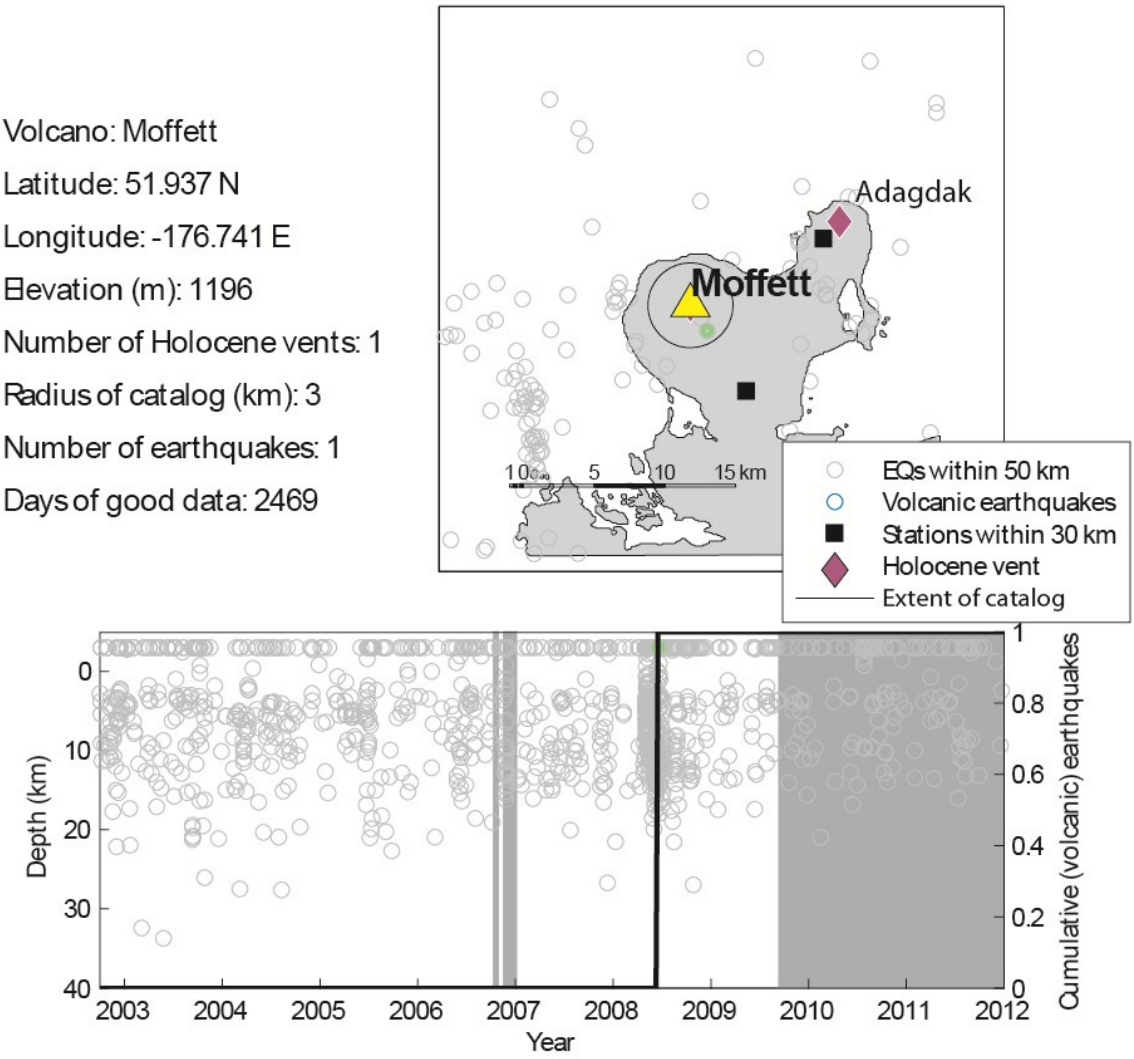

Appendix 3.A-9

Volcano: Great Sitkin
Latitude: 52.0765 N
Longitude: -176.1109 E
Elevation (m): 1740
Number of Holocene vents: 14
Radius of catalog (km): 6
Number of earthquakes: 328
Days of good data: 2959

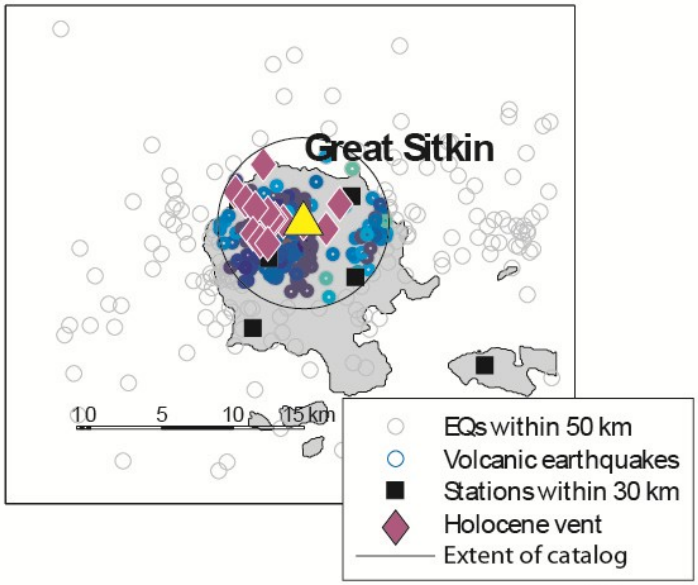

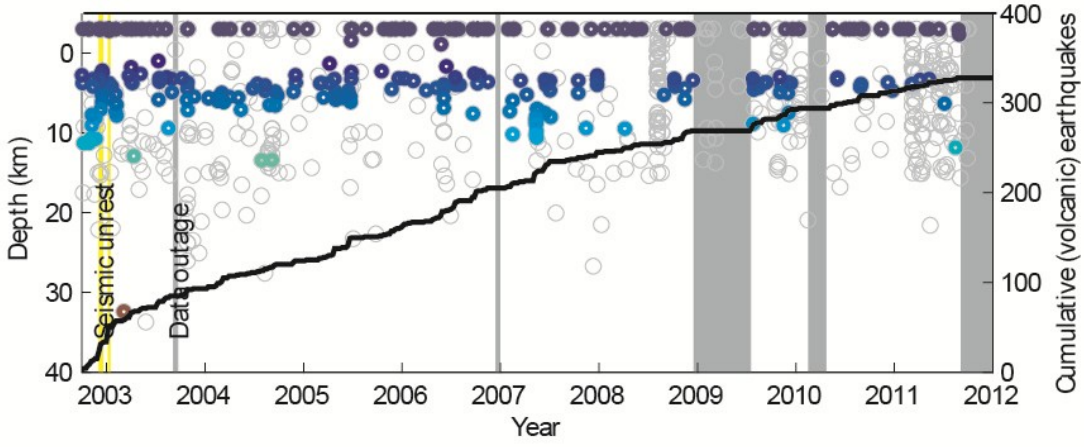

Appendix 3.A-10

Volcano: Kliuchef
Latitude: 52.3309 N
Longitude: -174.139 E
Elevation (m): 1533
Number of Holocene vents: 2
Radius of catalog (km): 9
Number of earthquakes: 874
Days of good data: 2861

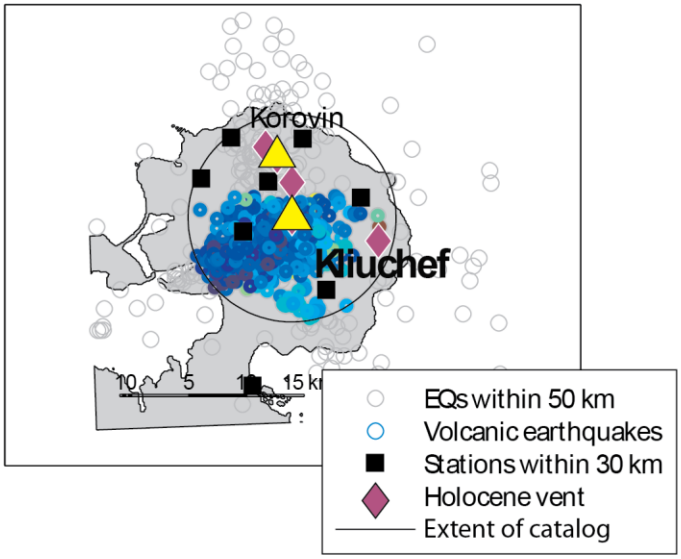

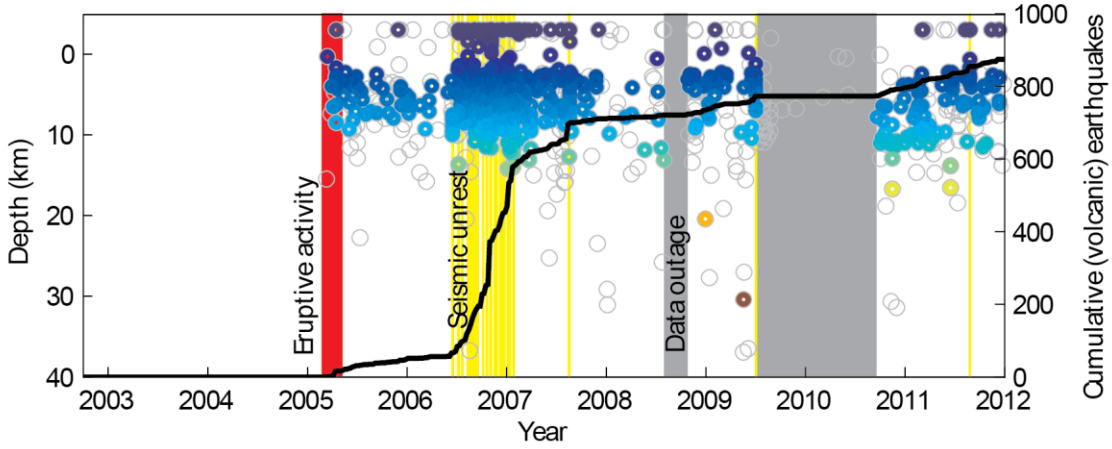

Appendix 3.A-11

Volcano: Korovin

Latitude: 52.3793 N

Longitude: -174.1548 E

Elevation (m): 1533

Number of Holocene vents: 3

Radius of catalog (km): 4

Number of earthquakes: 78

Days of good data: 1734

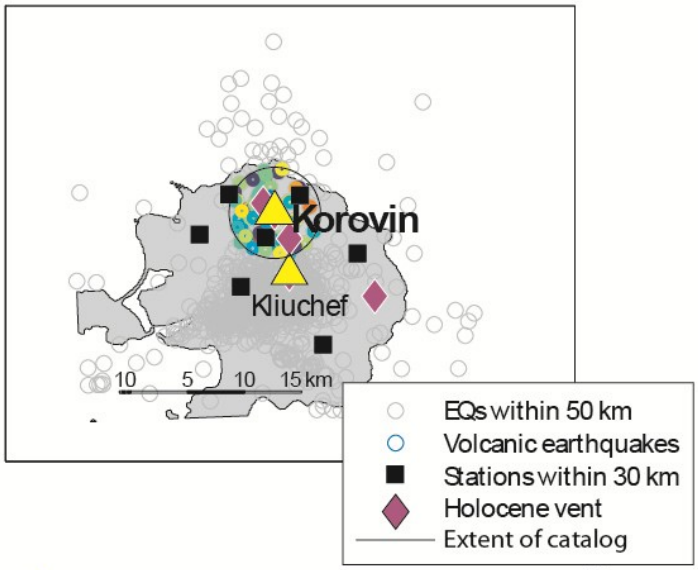

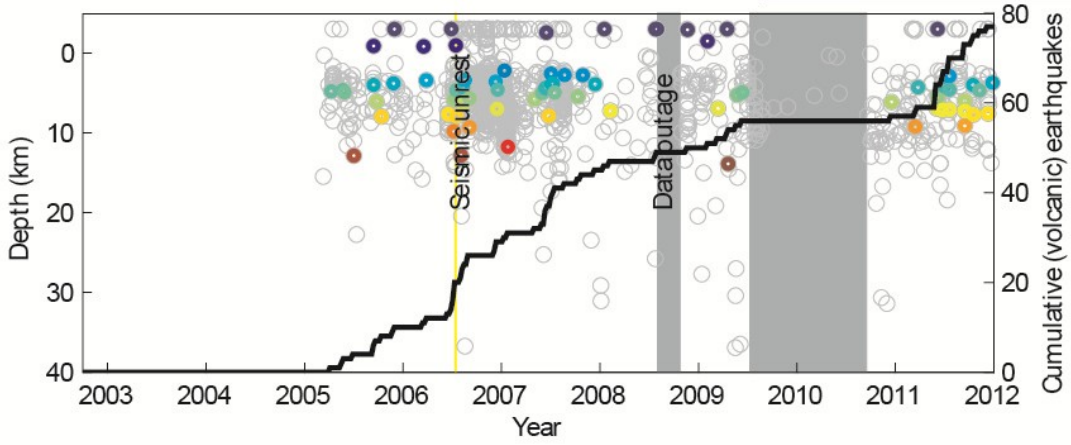

Appendix 3.A-12

Volcano: Okmok
Latitude: 53.419 N
Longitude: -168.132 E
Elevation (m): 1073
Number of Holocene vents: 18
Radius of catalog (km): 10
Number of earthquakes: 782
Days of good data: 3138

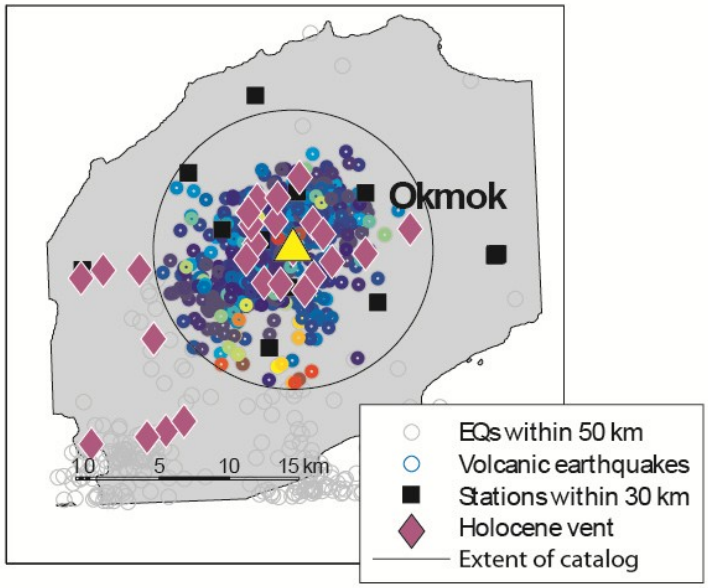

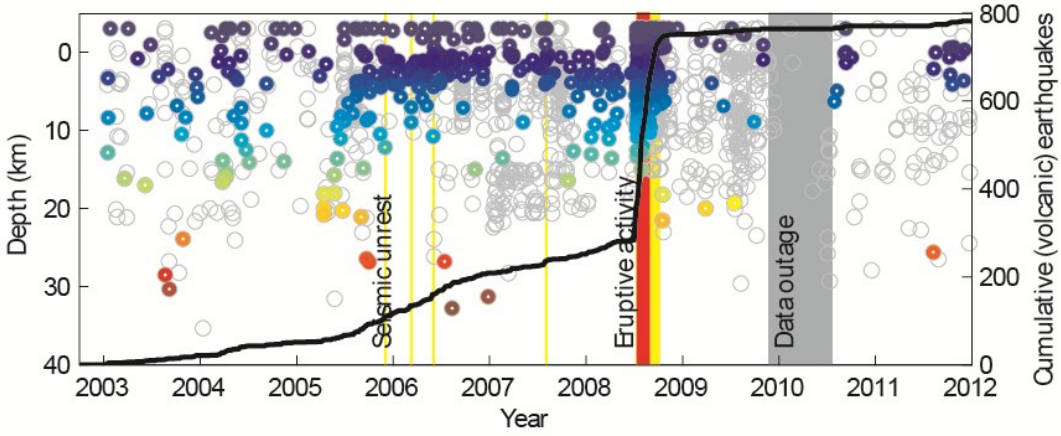

Appendix 3.A-13

Volcano: Makushin
Latitude: 53.8871 N
Longitude: -166.932 E
Elevation (m): 1800
Number of Holocene vents: 12
Radius of catalog (km): 12
Number of earthquakes: 914
Days of good data: 3379

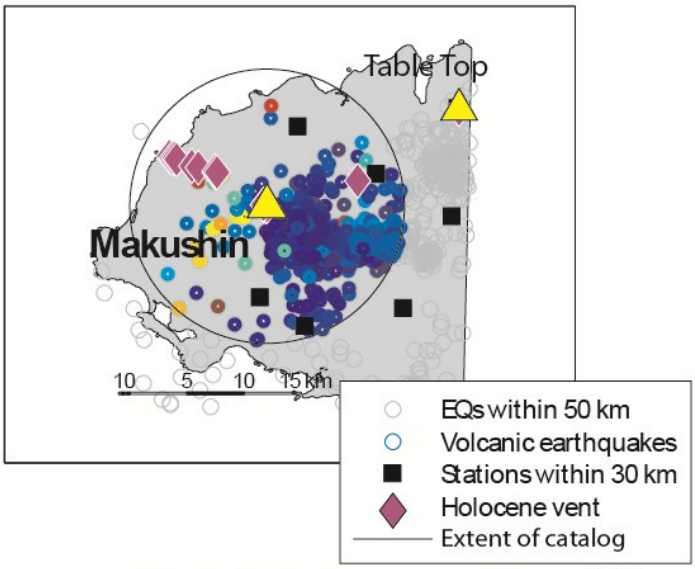

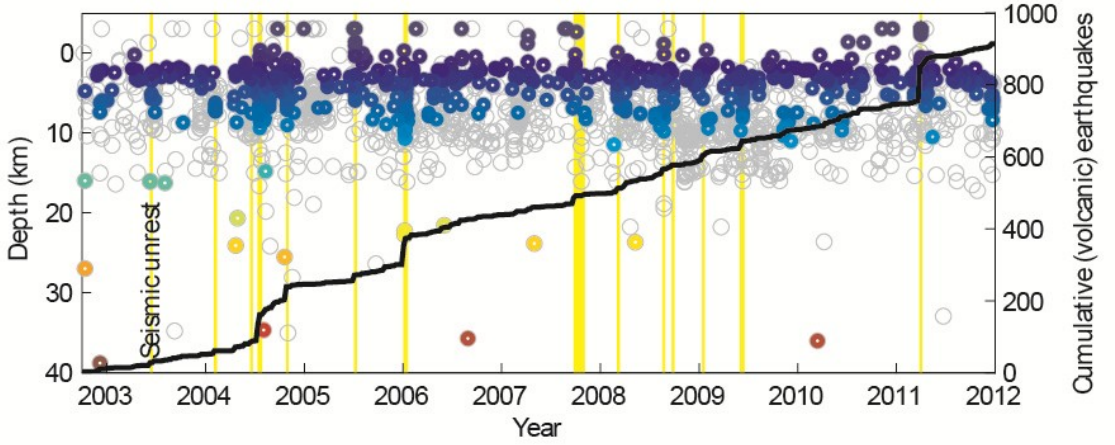

Appendix 3.A-14

Volcano: Table Top
Latitude: 53.9671 N
Longitude: -166.679 E
Elevation (m): 792
Number of Holocene vents: 1
Radius of catalog (km): 2
Number of earthquakes: 6
Days of good data: 3379

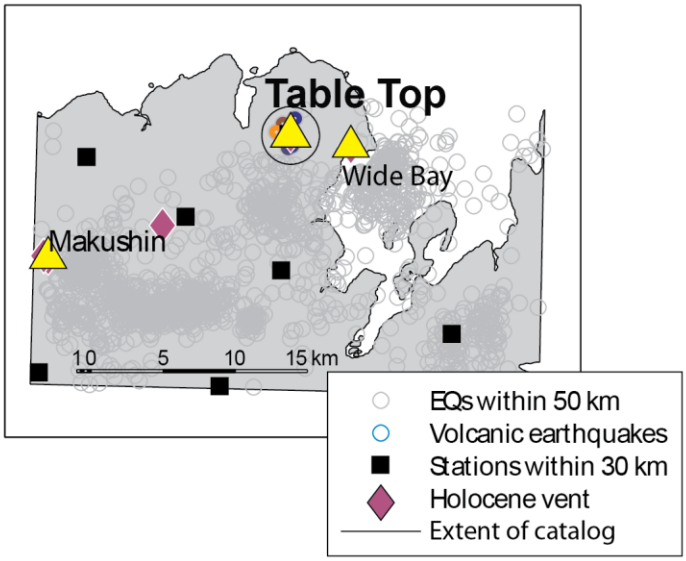

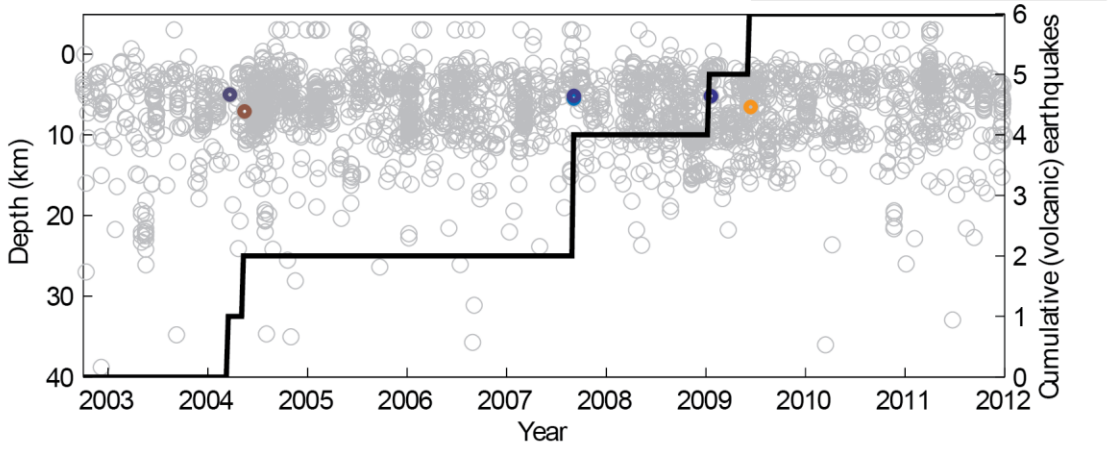

Appendix 3.A-15

Volcano: Wide Bay

Latitude: 53.9611 N

Longitude: -166.615 E

Elevation (m): 640

Number of Holocene vents: 1

Radius of catalog (km): 2

Number of earthquakes: 9

Days of good data: 3379

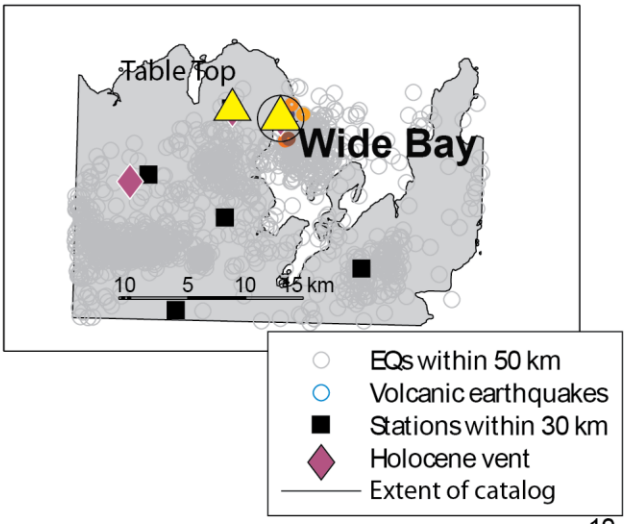

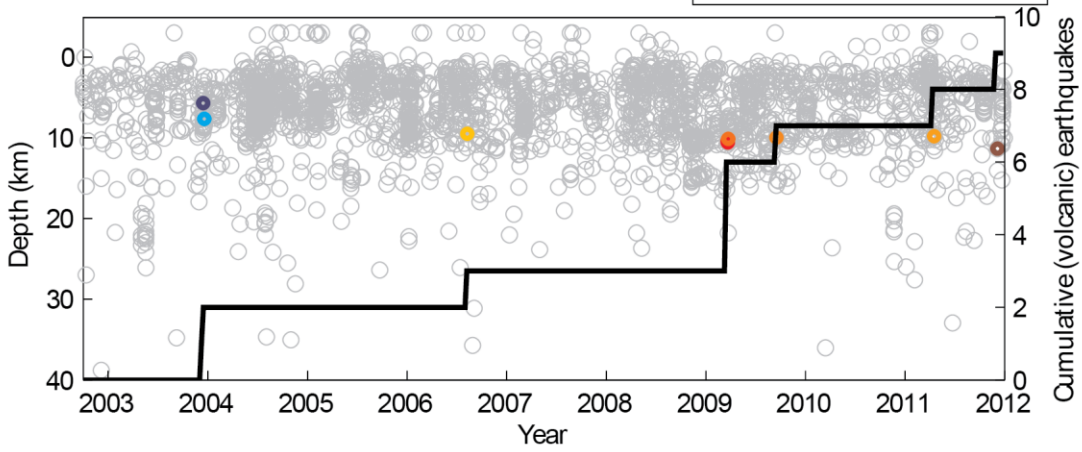

Appendix 3.A-16

Volcano: Akutan

Latitude: 54.1331 N

Longitude: -165.9855 E

Elevation (m): 1303

Number of Holocene vents: 3

Radius of catalog (km): 7

Number of earthquakes: 641

Days of good data: 3379

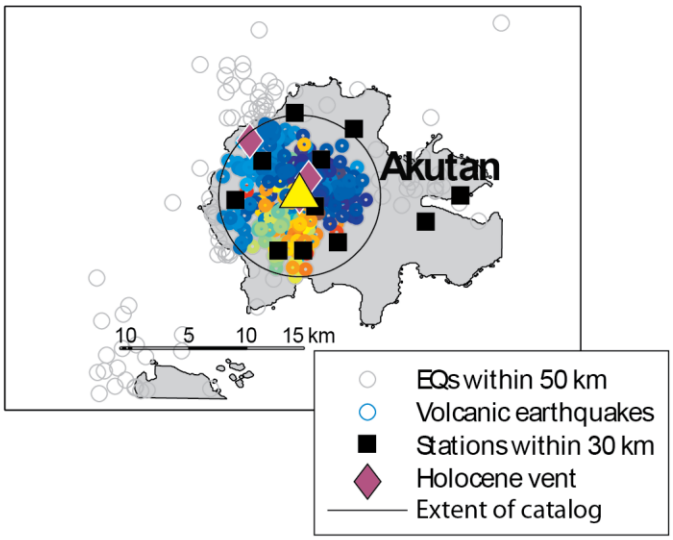

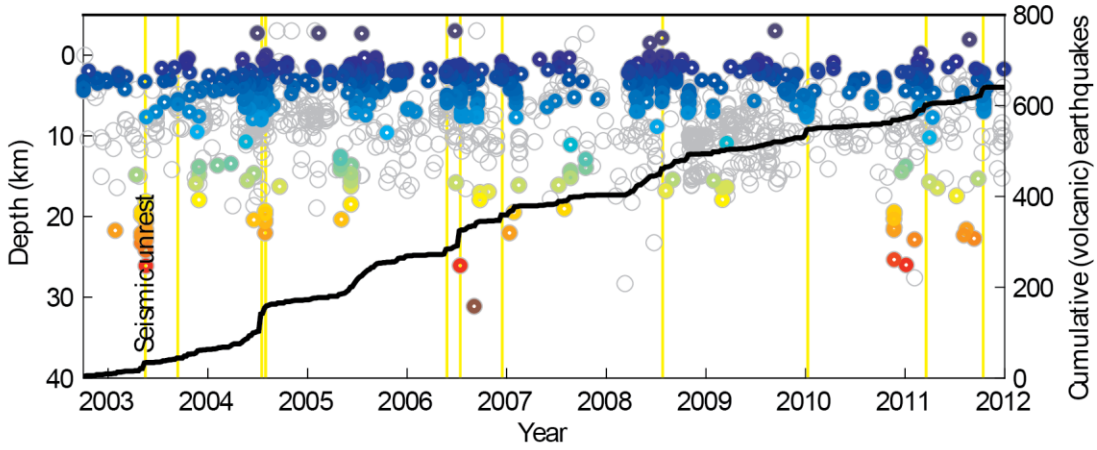

Appendix 3.A-17

Volcano: Gilbert

Latitude: 54.2522 N

Longitude: -165.6605 E

Elevation (m): 818

Number of Holocene vents: 1

Radius of catalog (km): 3

Number of earthquakes: 0

Days of good data: 3379

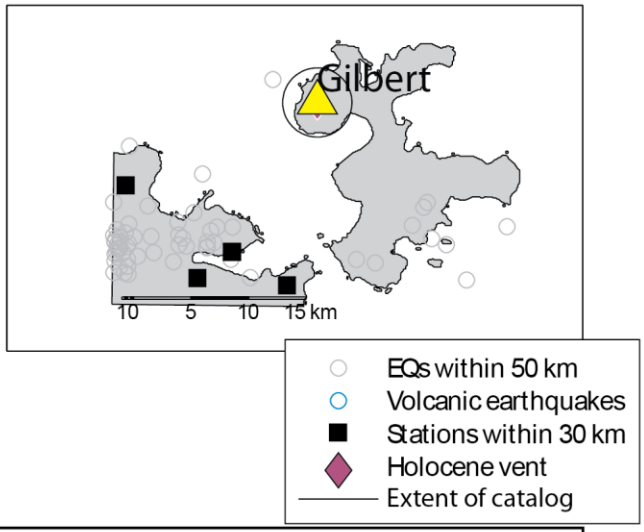

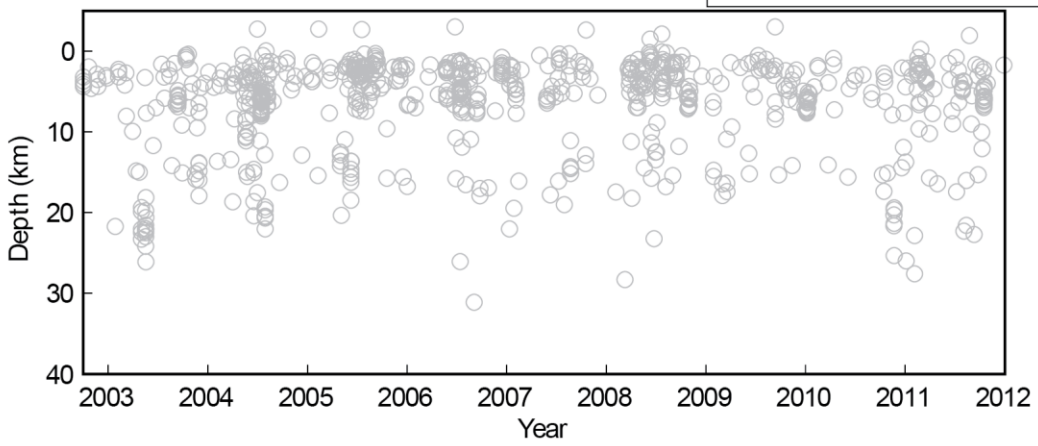

Appendix 3.A-18

Volcano: Westdahl
Latitude: 54.5171 N
Longitude: -164.6476 E
Elevation (m): 1560
Number of Holocene vents: 5
Radius of catalog (km): 7
Number of earthquakes: 455
Days of good data: 2373

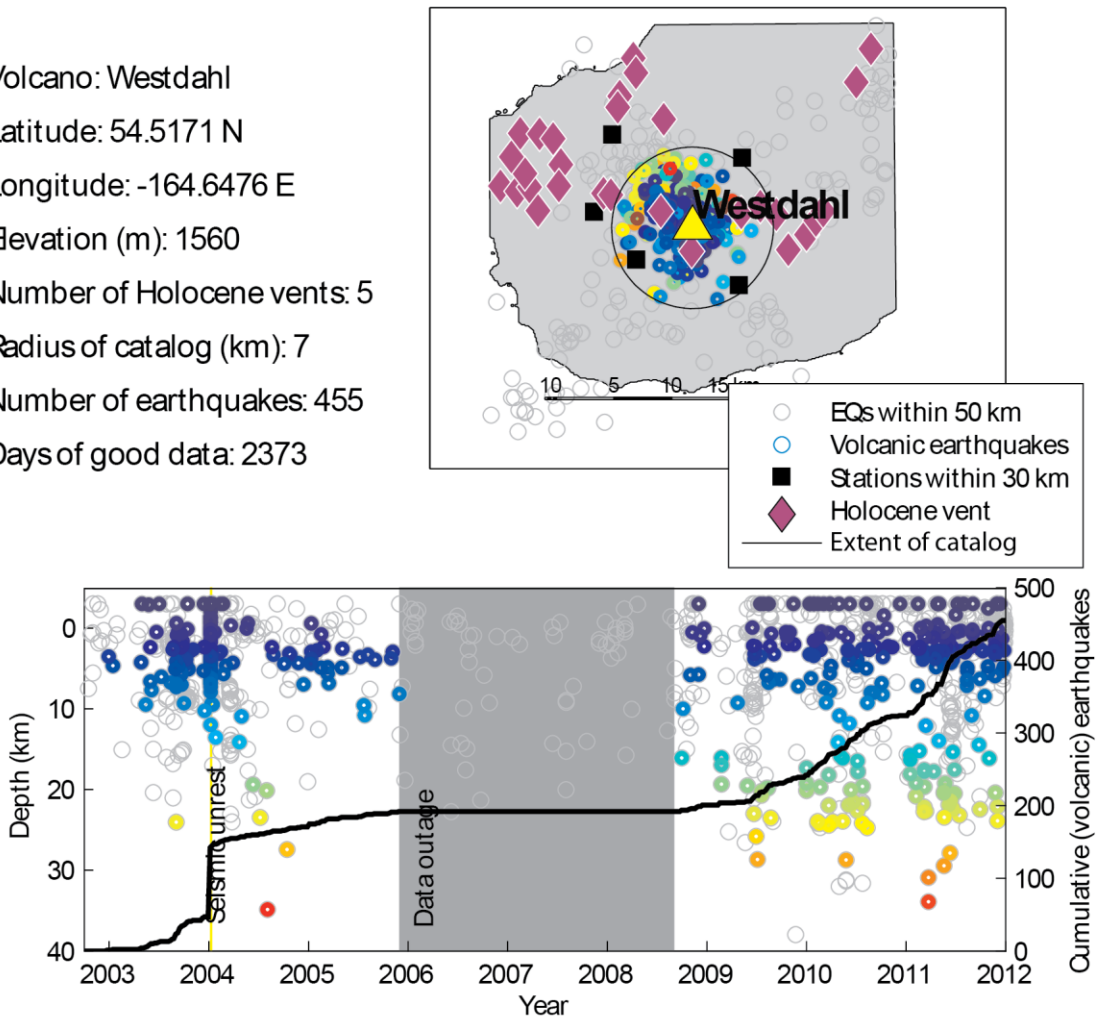

Appendix 3.A-19

Volcano: Fisher

Latitude: 54.6692 N

Longitude: -164.3524 E

Elevation (m): 1112

Number of Holocene vents: 20

Radius of catalog (km): 10

Number of earthquakes: 33

Days of good data: 3085

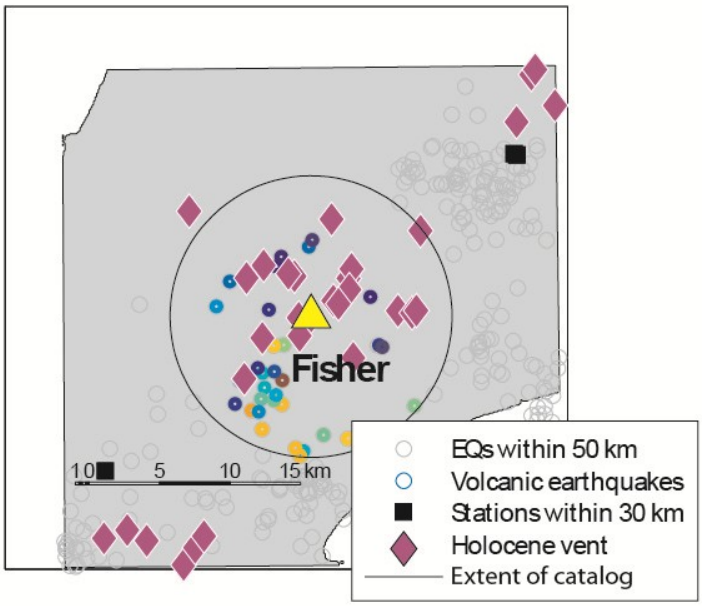

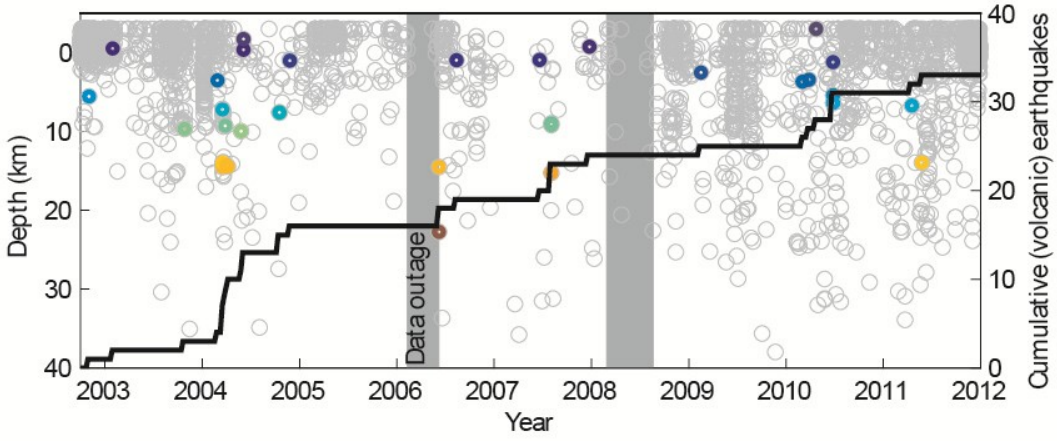

Appendix 3.A-20

Volcano: Shishaldin
Latitude: 54.7554 N
Longitude: -163.9711 E
Elevation (m): 2857
Number of Holocene vents: 9
Radius of catalog (km): 5
Number of earthquakes: 1886
Days of good data: 2836

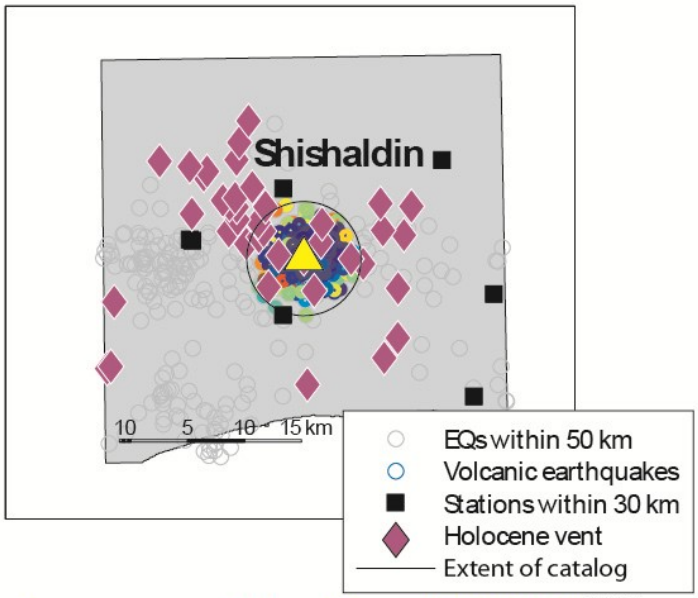

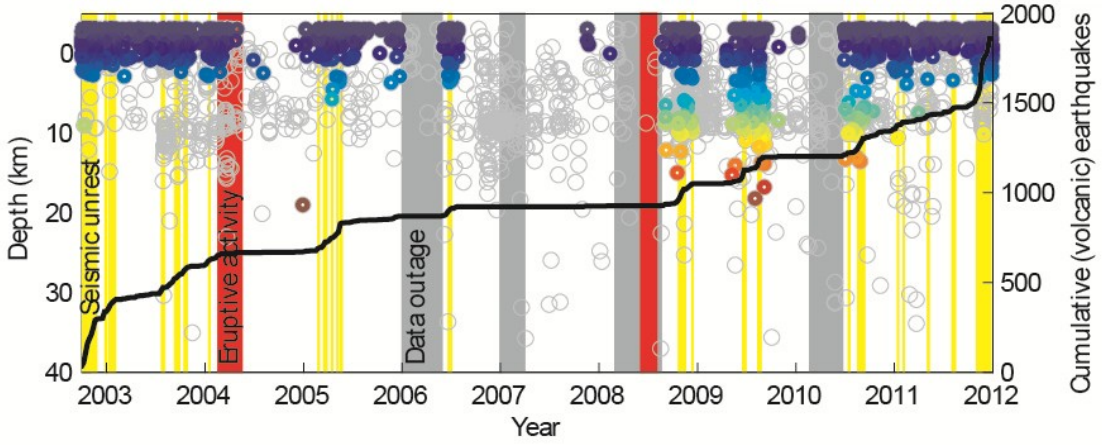

Appendix 3.A-21

Volcano: Roundtop
Latitude: 54.7992 N
Longitude: -163.5914 E
Elevation (m): 1871
Number of Holocene vents: 1
Radius of catalog (km): 8
Number of earthquakes: 9
Days of good data: 1050

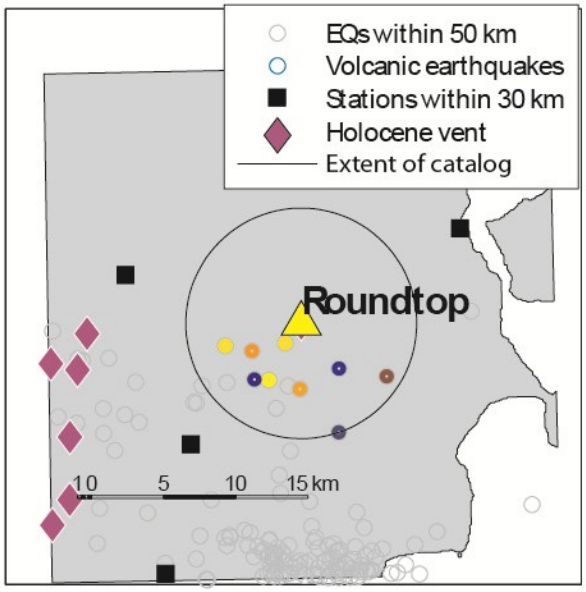

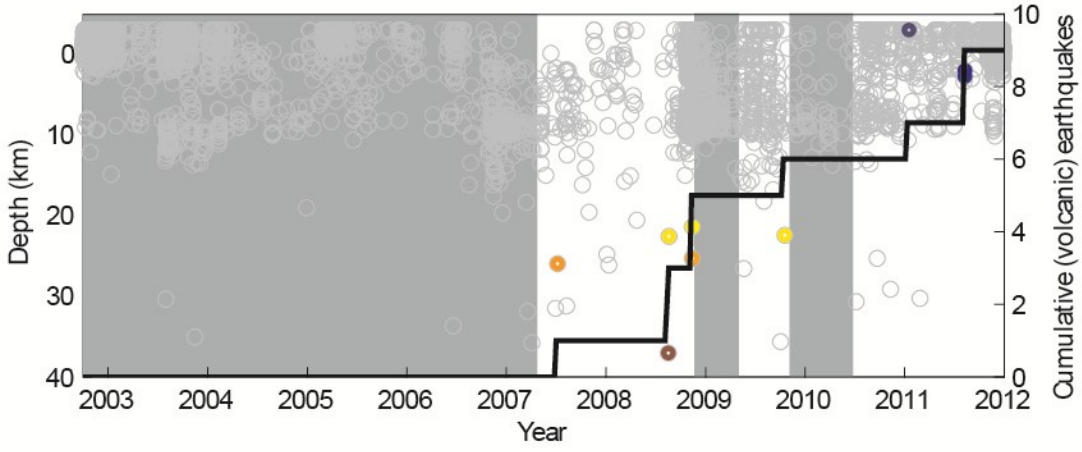

Appendix 3.A-22

Volcano: Dutton
Latitude: 55.1867 N
Longitude: -162.2744 E
Elevation (m): 1473
Number of Holocene vents: 3
Radius of catalog (km): 10
Number of earthquakes: 187
Days of good data: 3116

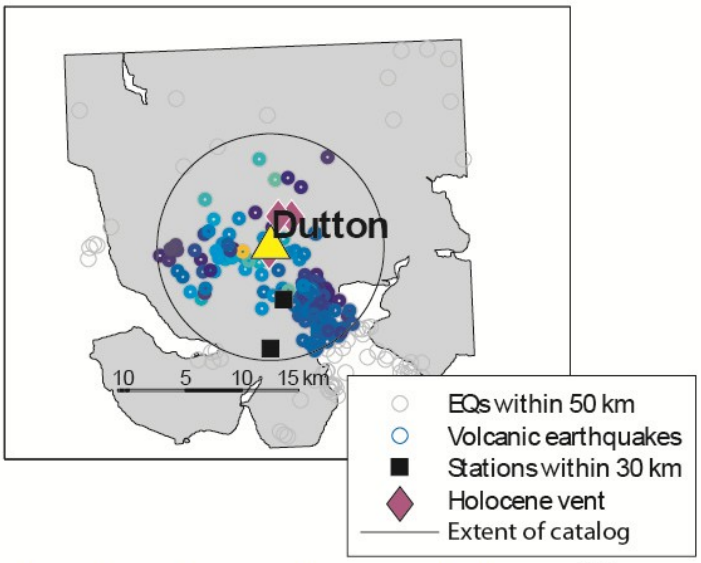

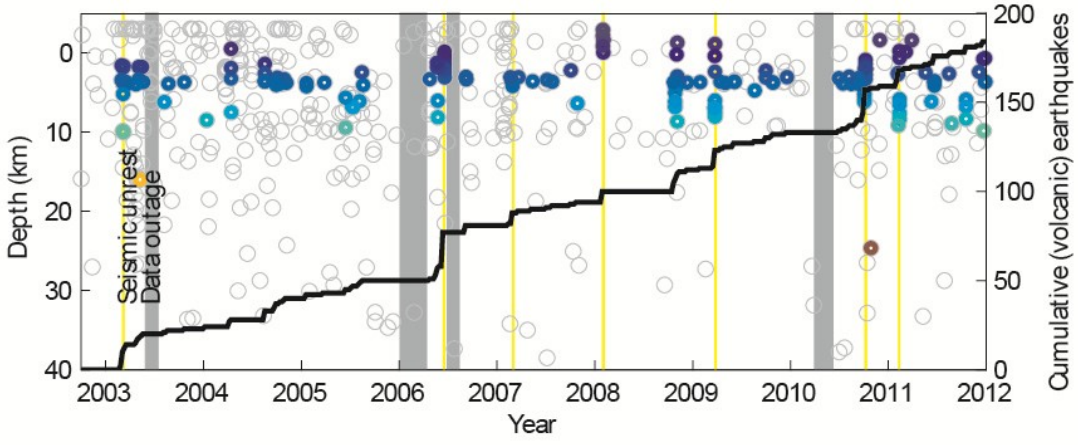

Appendix 3.A-23

Volcano: Hague

Latitude: 55.3672 N

Longitude: -161.994 E

Elevation (m): 1341

Number of Holocene vents: 8

Radius of catalog (km): 8

Number of earthquakes: 102

Days of good data: 2978

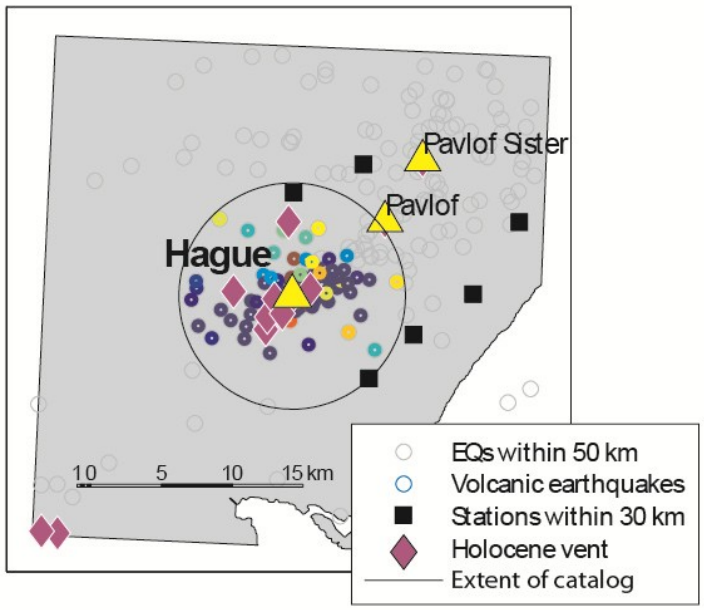

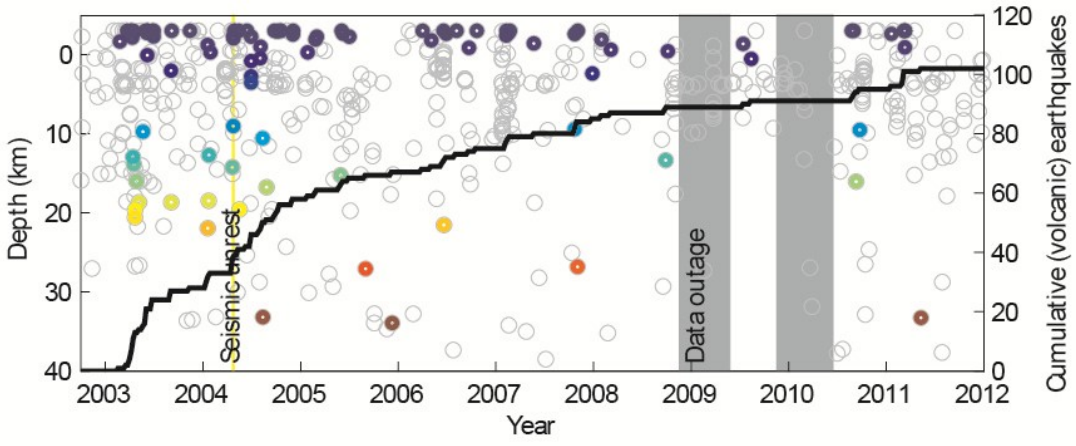

Appendix 3.A-24

Volcano: Pavlof
Latitude: 55.4173 N
Longitude: -161.8937 E
Elevation (m): 2518
Number of Holocene vents: 1
Radius of catalog (km): 3.5
Number of earthquakes: 24
Days of good data: 2978

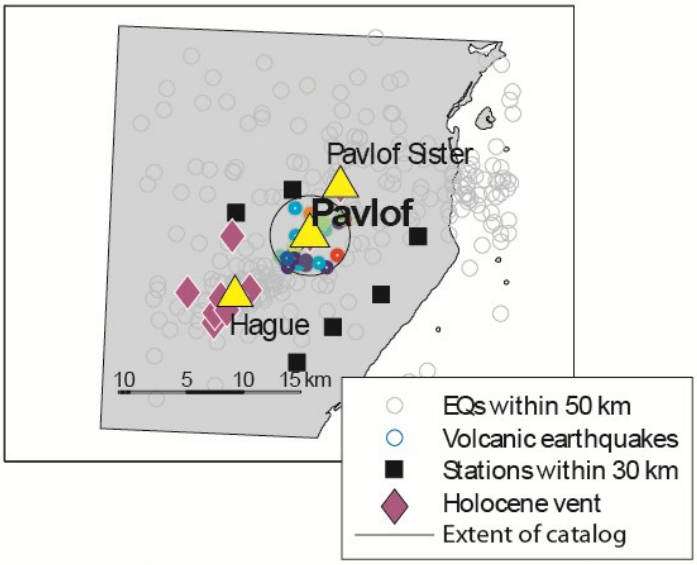

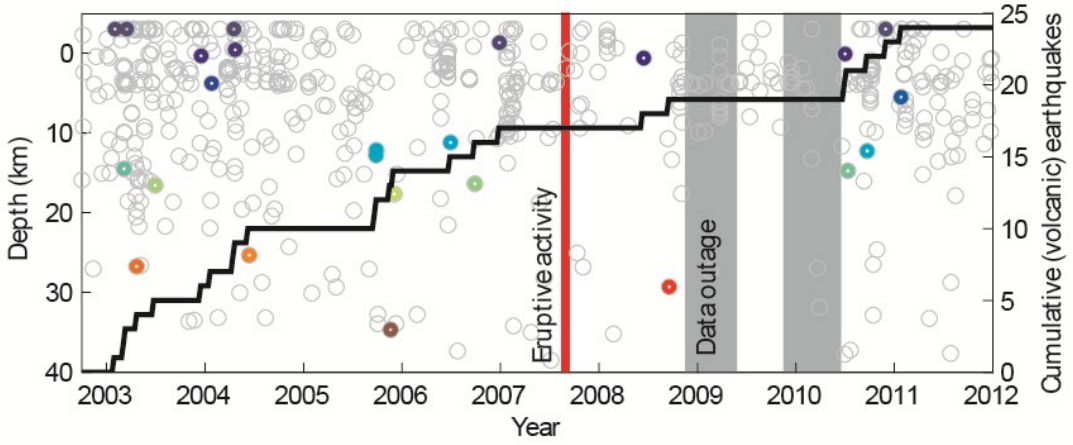

Appendix 3.A-25

Volcano: Pavlof Sister
Latitude: 55.4569 N
Longitude: -161.8544 E
Elevation (m): 2142
Number of Holocene vents: 1
Radius of catalog (km): 2
Number of earthquakes: 8
Days of good data: 2978

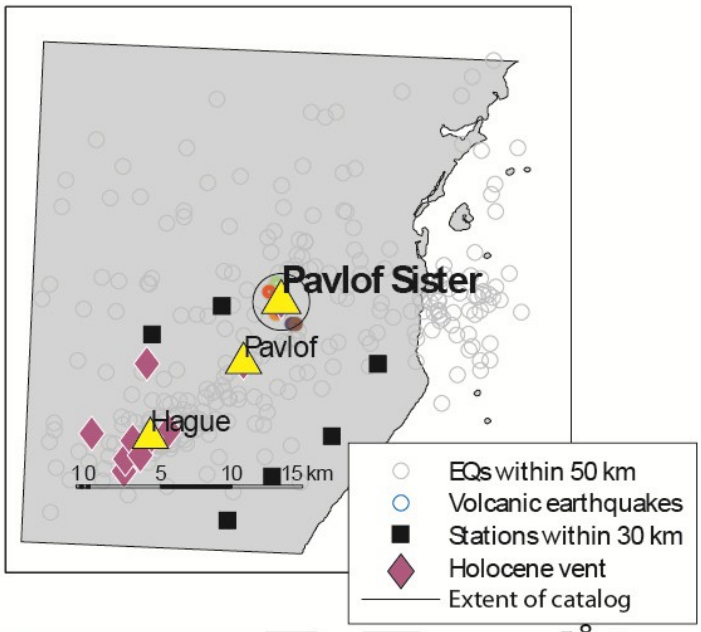

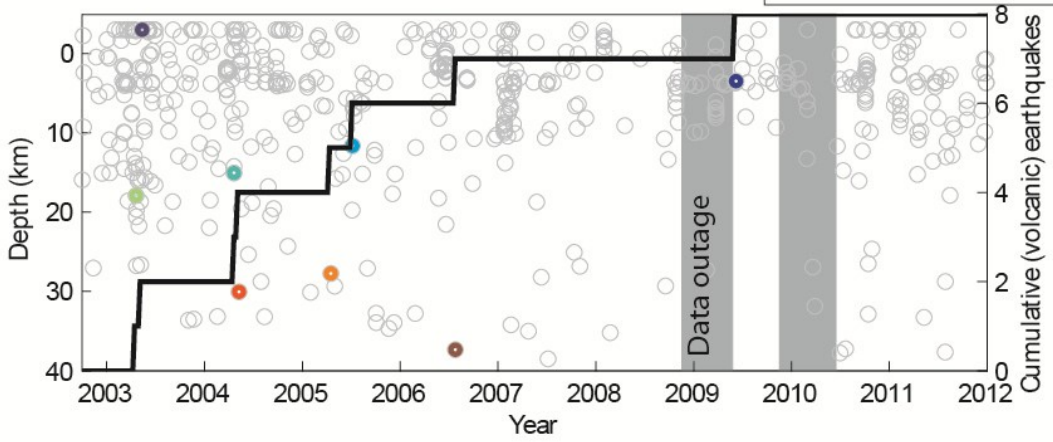

Appendix 3.A-26

Volcano: Veniaminof
Latitude: 56.1979 N
Longitude: -159.3931 E
Elevation (m): 2507
Number of Holocene vents: 8
Radius of catalog (km): 17
Number of earthquakes: 138
Days of good data: 3011

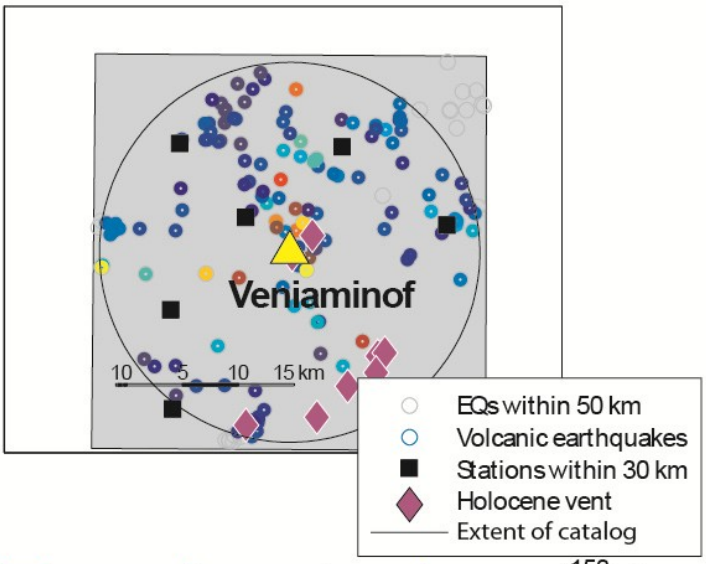

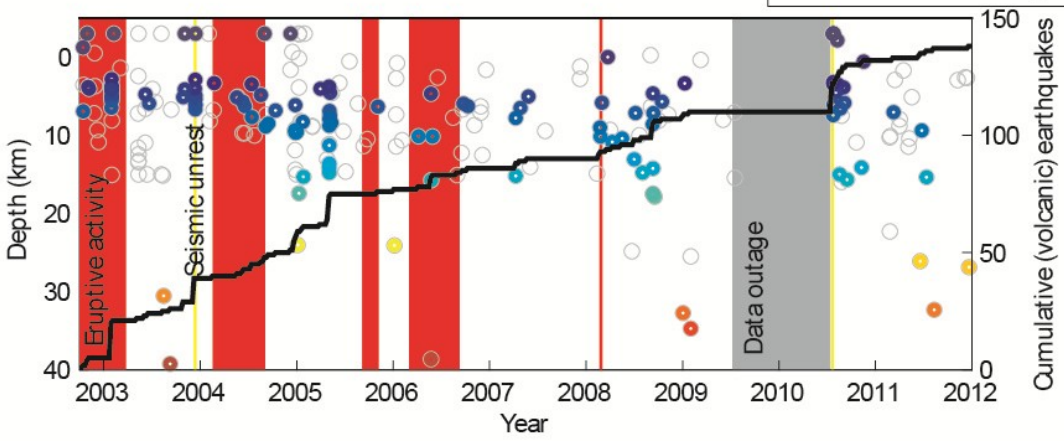

Appendix 3.A-27

Volcano: Aniakchak

Latitude: 56.9058 N

Longitude: -158.209 E

Elevation (m): 1341

Number of Holocene vents: 13

Radius of catalog (km): 14

Number of earthquakes: 146

Days of good data: 2121

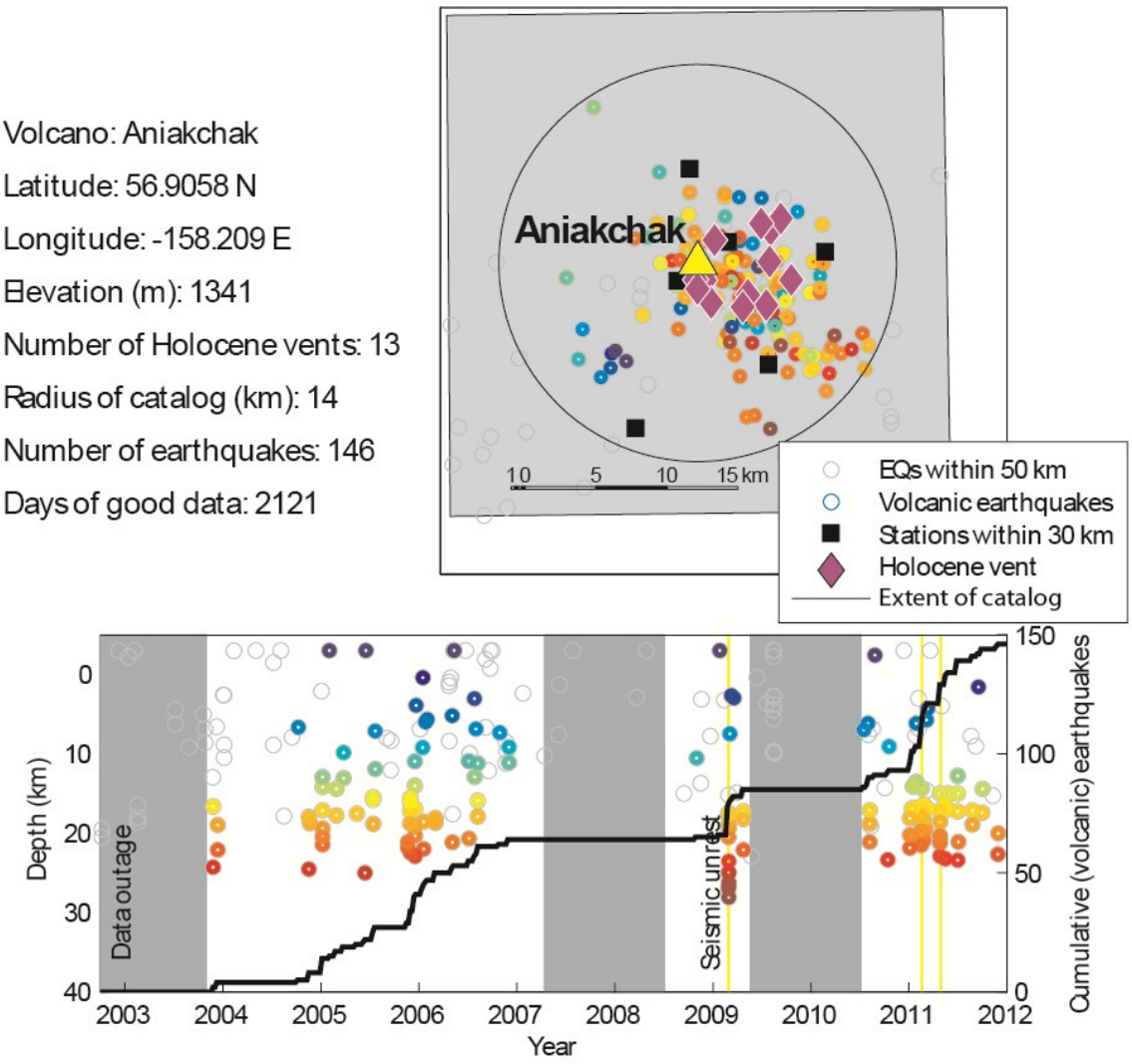

Appendix 3.A-28

Volcano: Ukinrek Maars

Latitude: 57.8338 N

Longitude: -156.5139 E

Elevation (m): 91

Number of Holocene vents: 3

Radius of catalog (km): 7

Number of earthquakes: 18

Days of good data: 3243

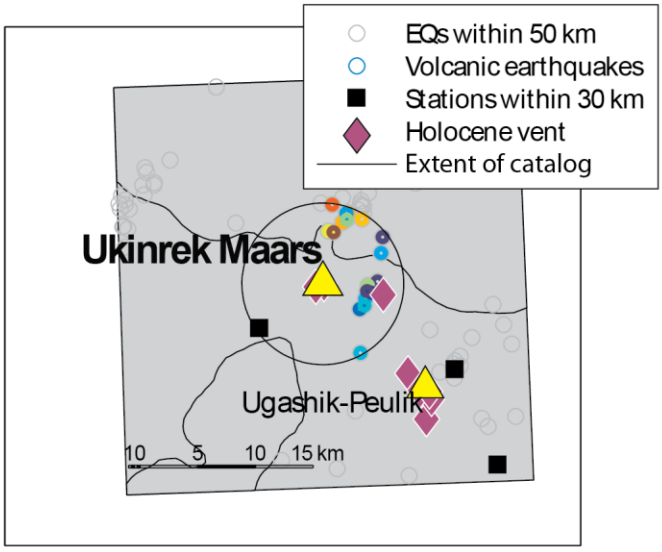

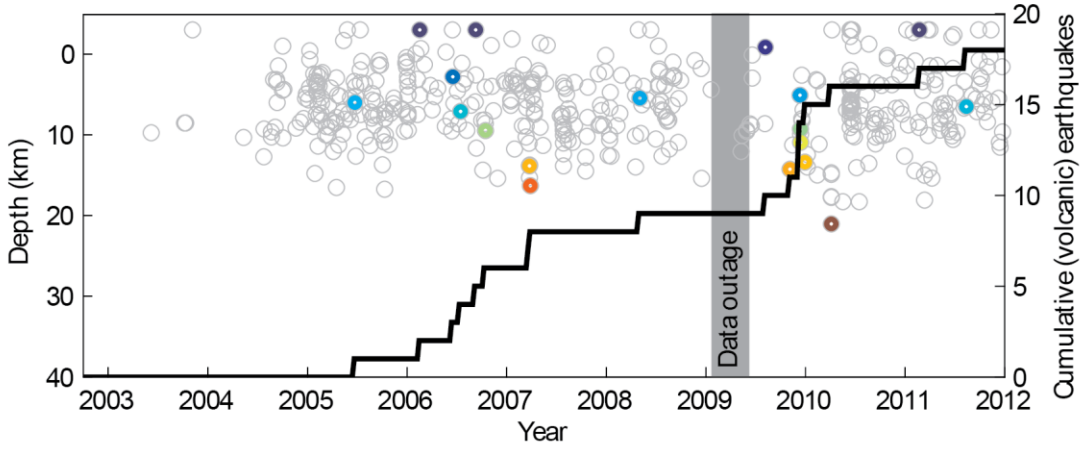

Appendix 3.A-29

Volcano: Ugashik-Peulik
Latitude: 57.7503 N
Longitude: -156.37 E
Elevation (m): 1474
Number of Holocene vents: 6
Radius of catalog (km): 5
Number of earthquakes: 10
Days of good data: 3243

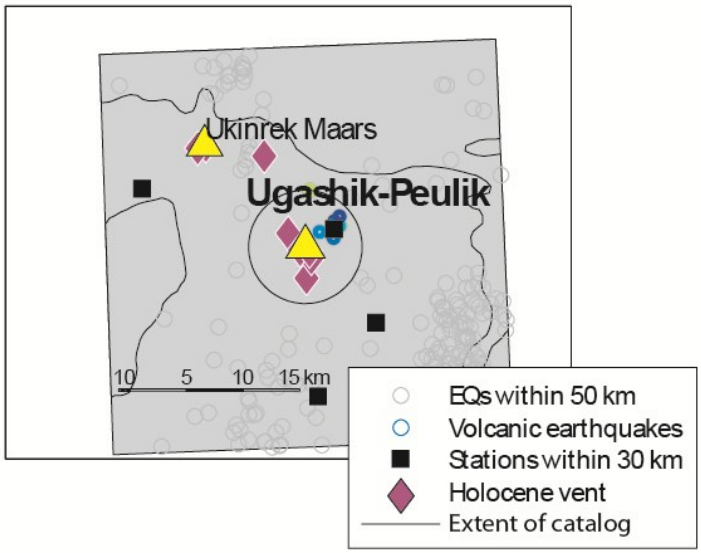

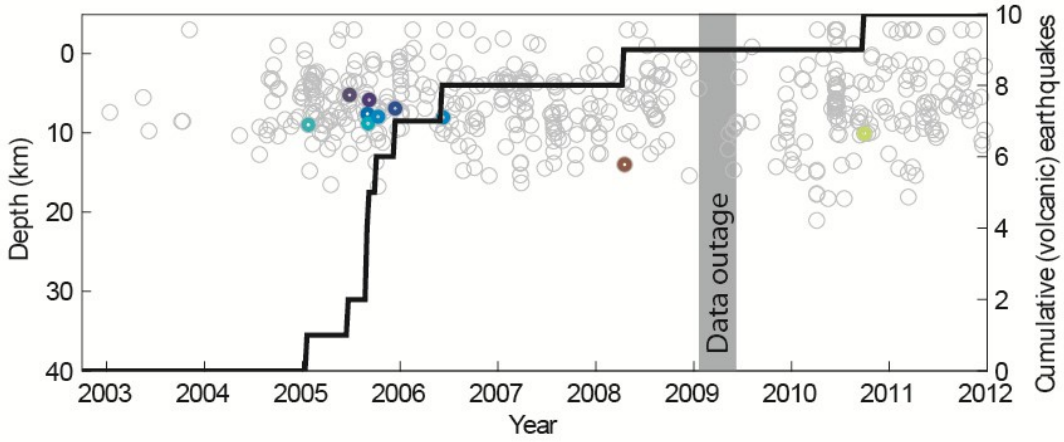

Appendix 3.A-30

Volcano: Martin
Latitude: 58.1692 N
Longitude: -155.3566 E
Elevation (m): 1860
Number of Holocene vents: 1
Radius of catalog (km): 3
Number of earthquakes: 3781
Days of good data: 3351

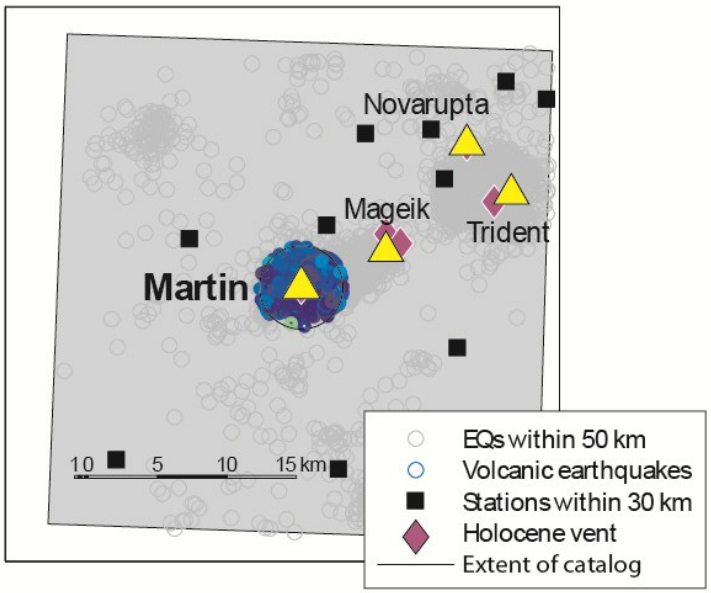

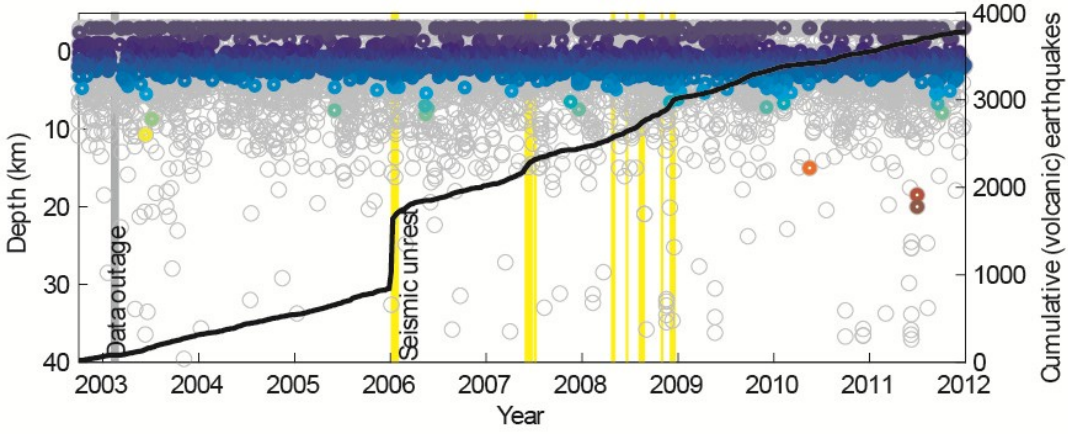

Appendix 3.A-31

Volcano: Mageik
Latitude: 58.1946 N
Longitude: -155.2544 E
Elevation (m): 2165
Number of Holocene vents: 2
Radius of catalog (km): 3.5
Number of earthquakes: 1206
Days of good data: 3351

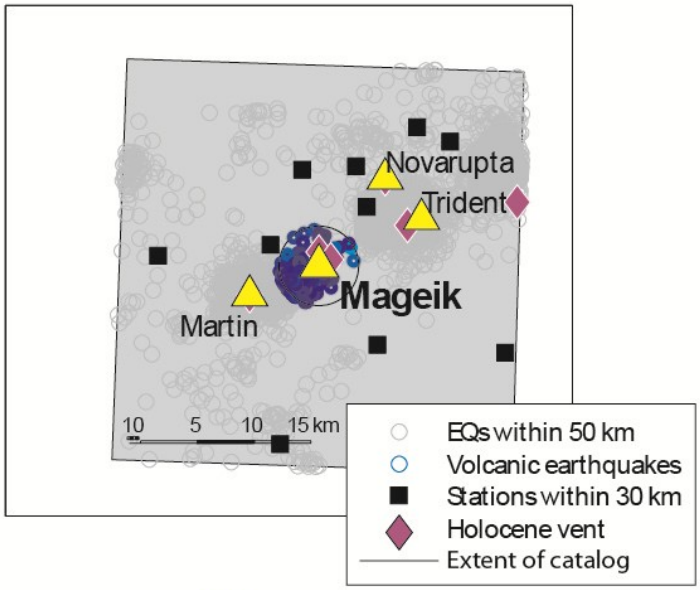

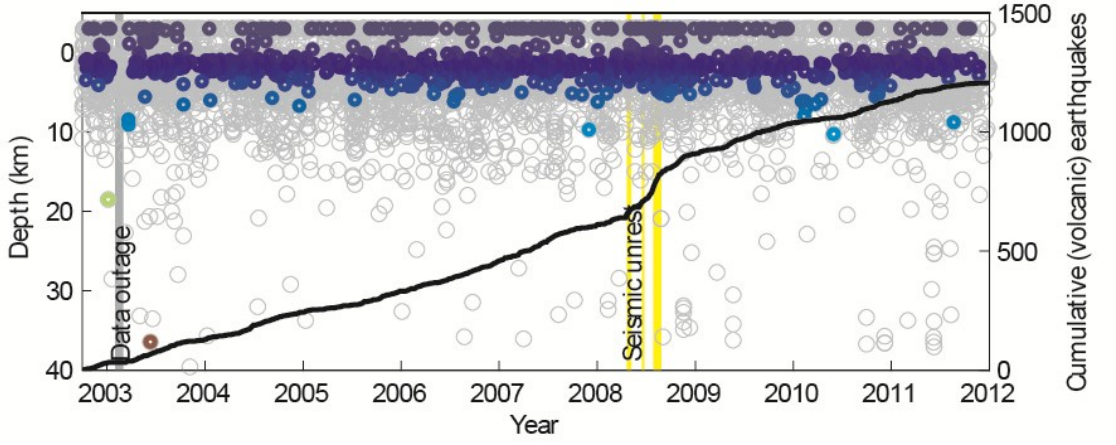

Appendix 3.A-32

Volcano: Trident

Latitude: 58.2343 N

Longitude: -155.1026 E

Elevation (m): 1097

Number of Holocene vents: 1

Radius of catalog (km): 1.4

Number of earthquakes: 184

Days of good data: 3351

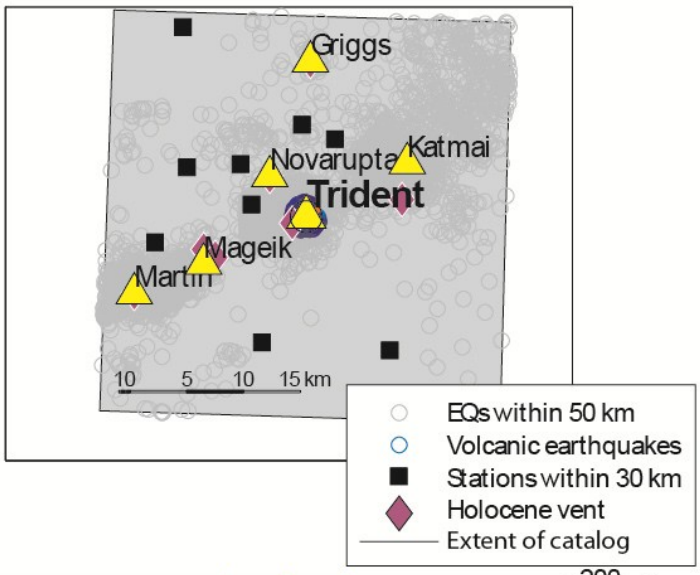

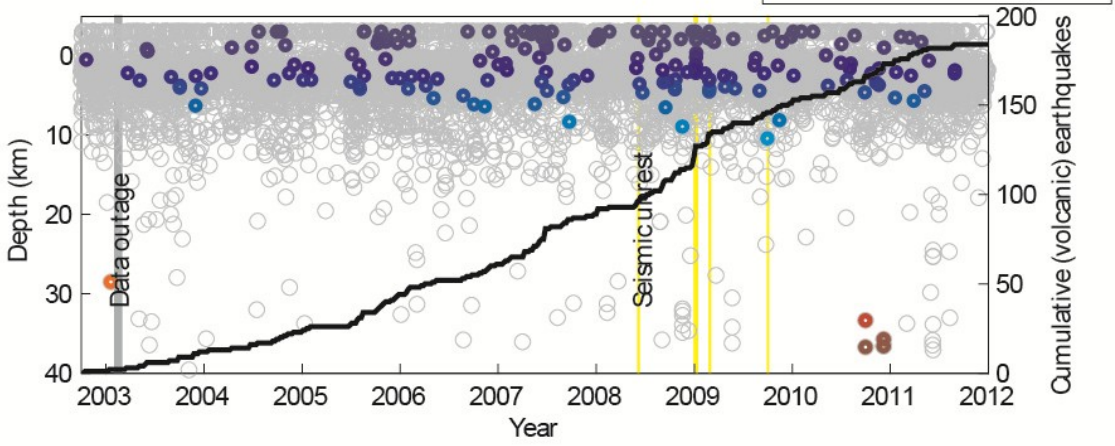

Appendix 3.A-33

Volcano: Novarupta
Latitude: 58.2654 N
Longitude: -155.1591 E
Elevation (m): 841
Number of Holocene vents: 1
Radius of catalog (km): 1
Number of earthquakes: 10
Days of good data: 3351

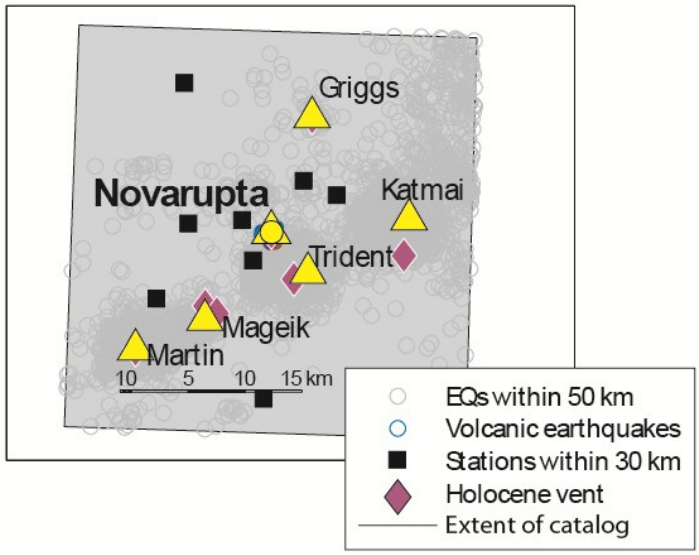

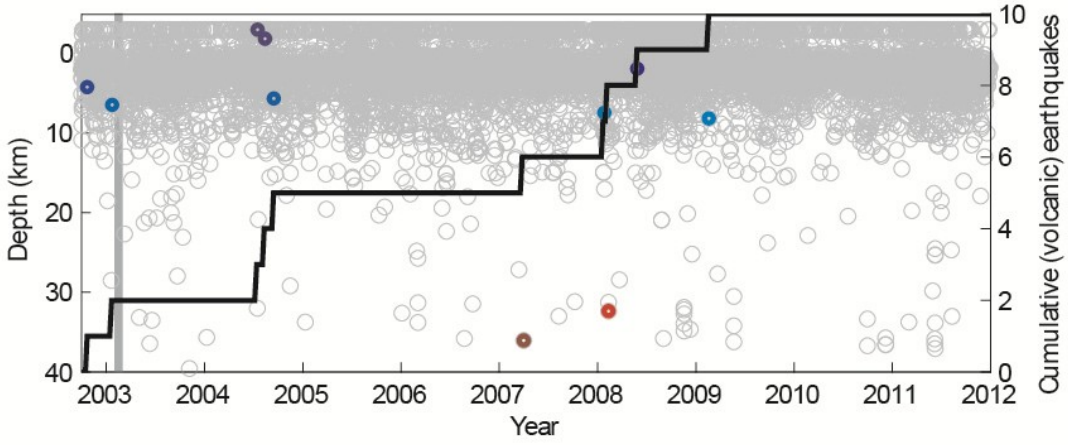

Appendix 3.A-34

Volcano: Katmai
Latitude: 58.279 N
Longitude: -154.9533 E
Elevation (m): 2047
Number of Holocene vents: 1
Radius of catalog (km): 5
Number of earthquakes: 1716
Days of good data: 3351

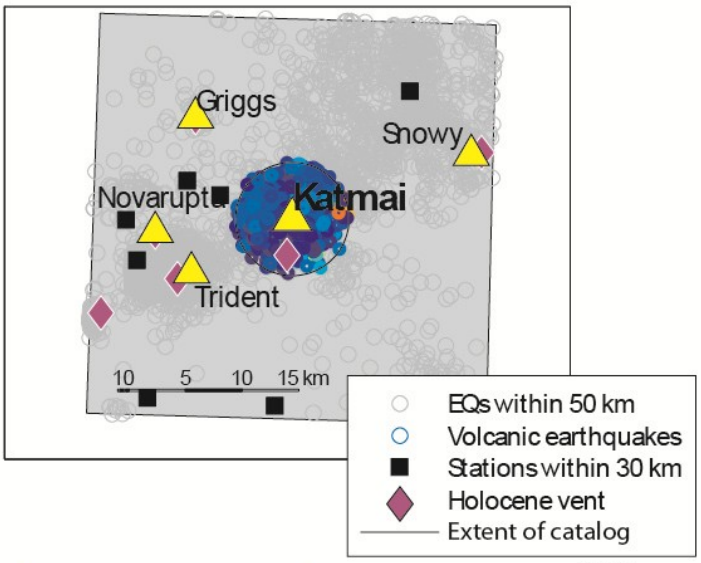

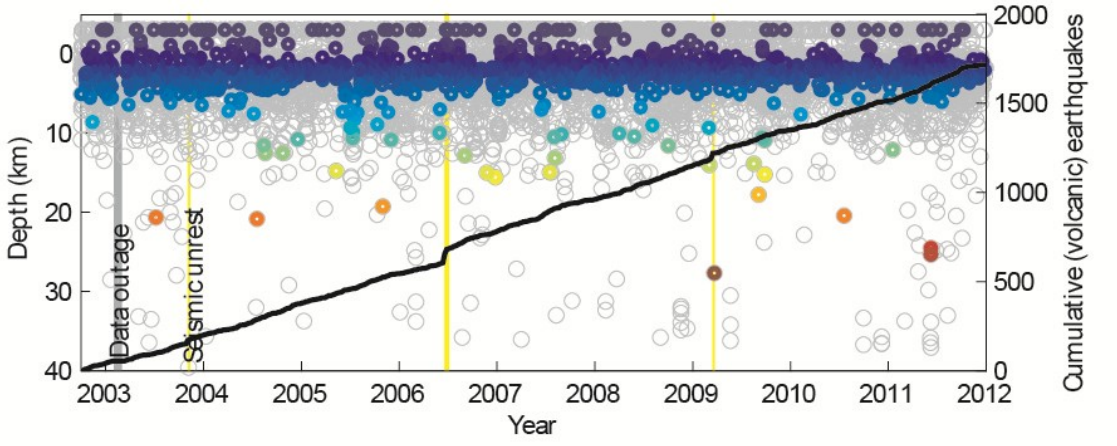

Appendix 3.A-35

Volcano: Griggs

Latitude: 58.3572 N

Longitude: -155.1037 E

Elevation (m): 2317

Number of Holocene vents: 1

Radius of catalog (km): 3

Number of earthquakes: 42

Days of good data: 3379

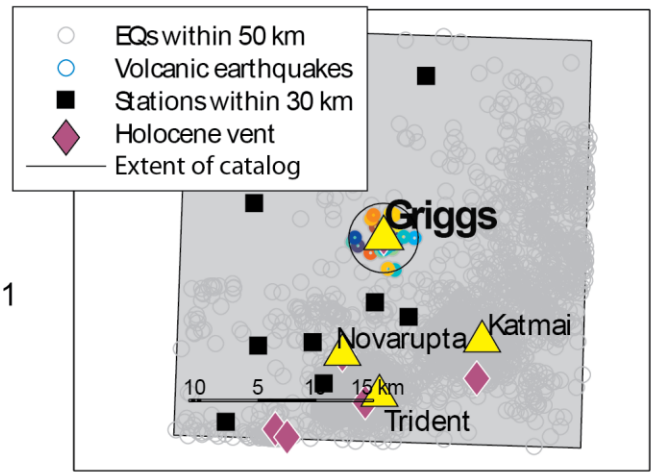

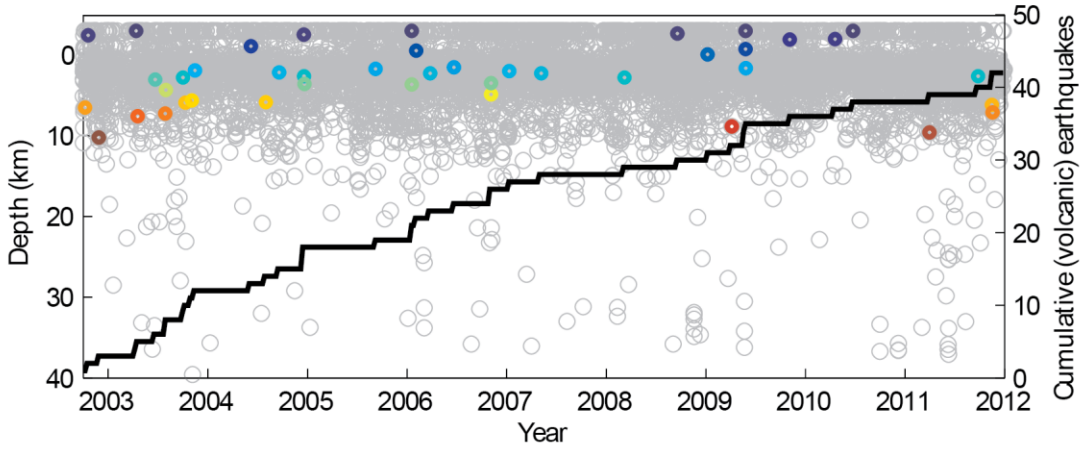

Appendix 3.A-36

Volcano: Snowy
Latitude: 58.3336 N
Longitude: -154.6859 E
Elevation (m): 2161
Number of Holocene vents: 1
Radius of catalog (km): 5
Number of earthquakes: 203
Days of good data: 2952

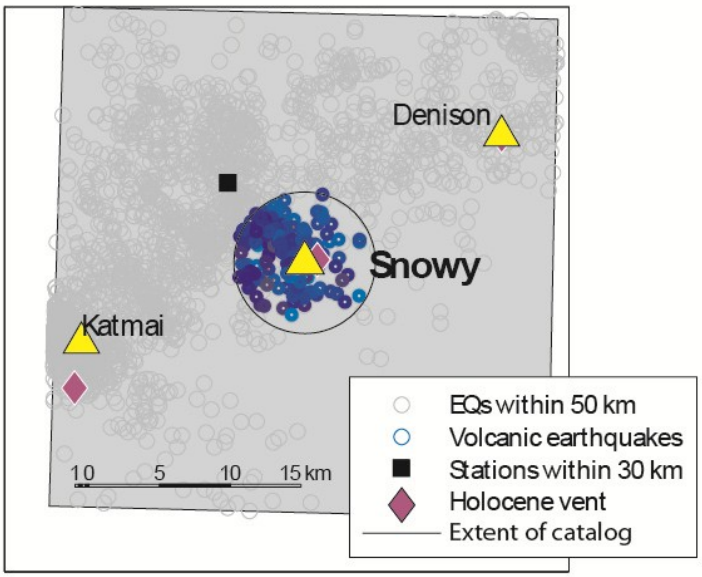

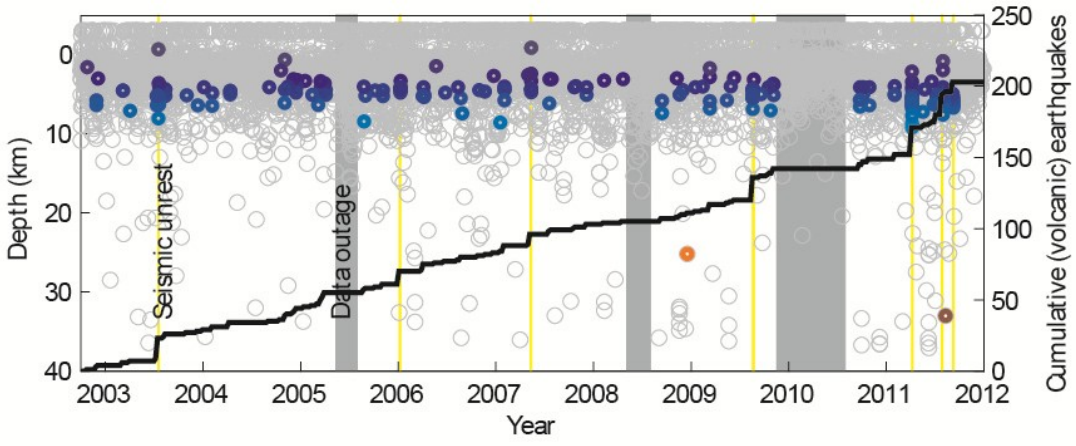

Appendix 3.A-37

Volcano: Denison

Latitude: 58.4173 N

Longitude: -154.451 E

Elevation (m): 2318

Number of Holocene vents: 1

Radius of catalog (km): 2

Number of earthquakes: 32

Days of good data: 2762

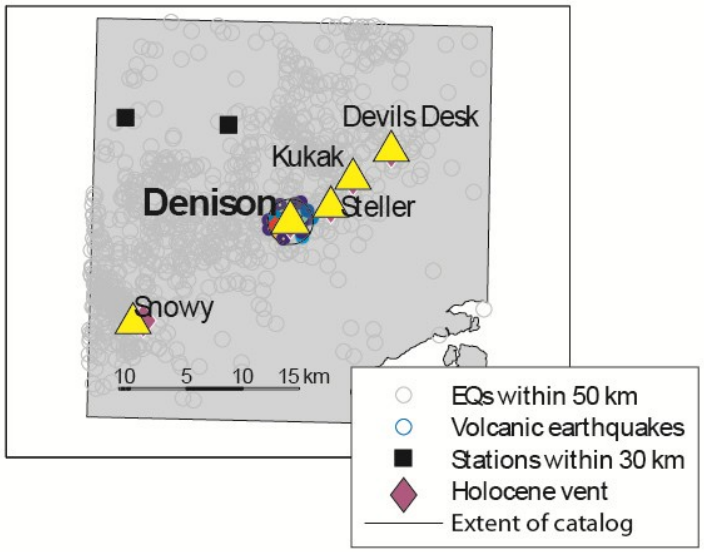

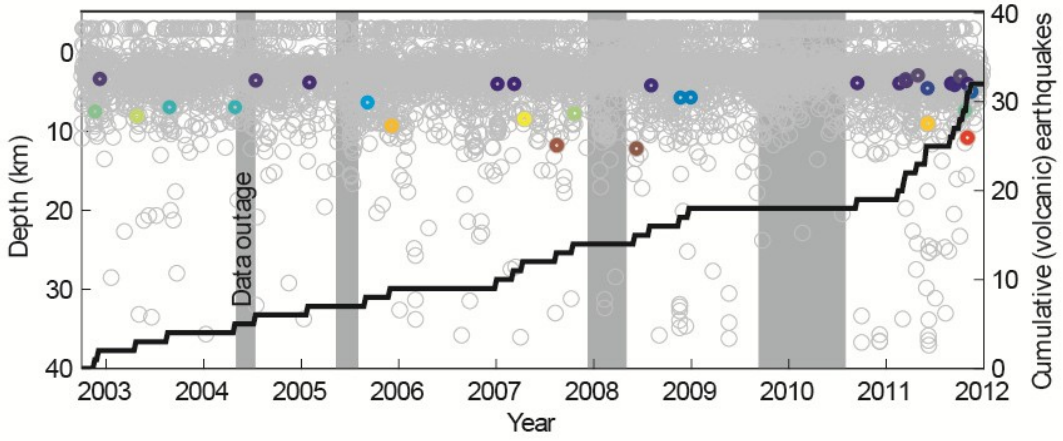

Appendix 3.A-38

Volcano: Steller
Latitude: 58.4301 N
Longitude: -154.3903 E
Elevation (m): 2272
Number of Holocene vents: 1
Radius of catalog (km): 2
Number of earthquakes: 18
Days of good data: 2762

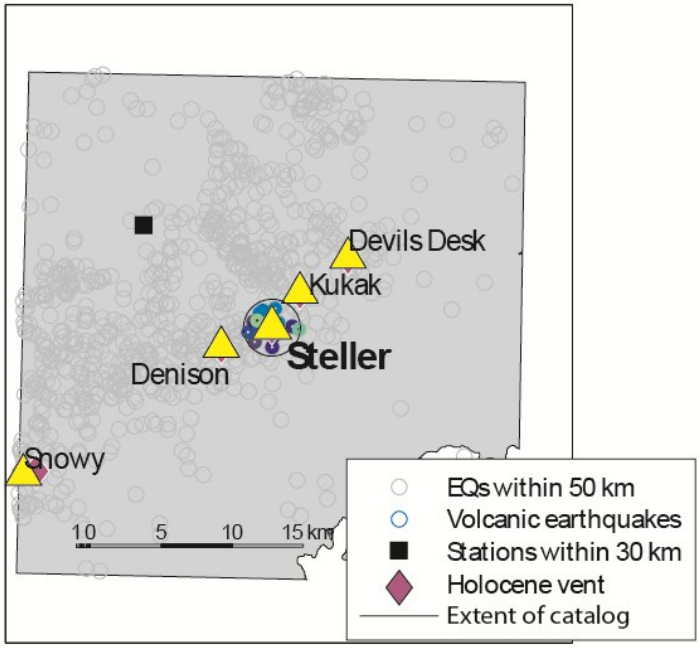

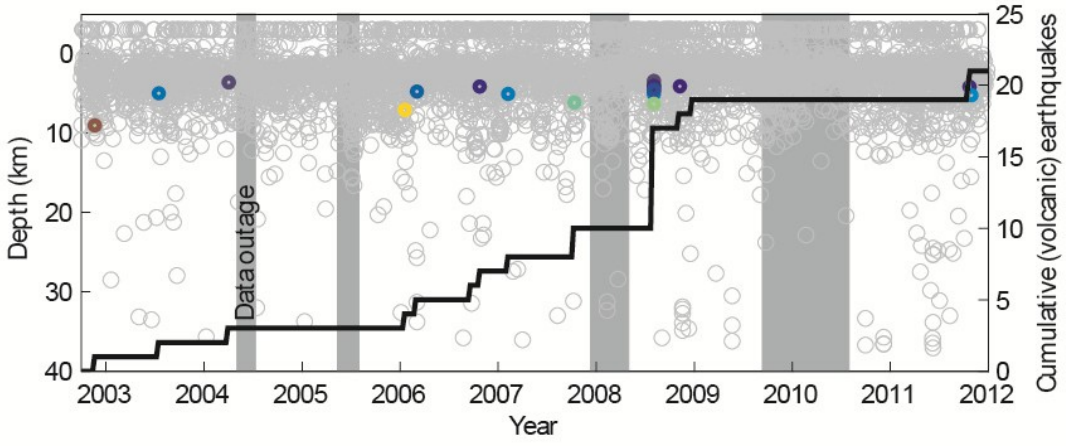

Appendix 3.A-39

Volcano: Kukak

Latitude: 58.4528 N

Longitude: -154.3573 E

Elevation (m): 1806

Number of Holocene vents: 1

Radius of catalog (km): 2

Number of earthquakes: 20

Days of good data: 2762

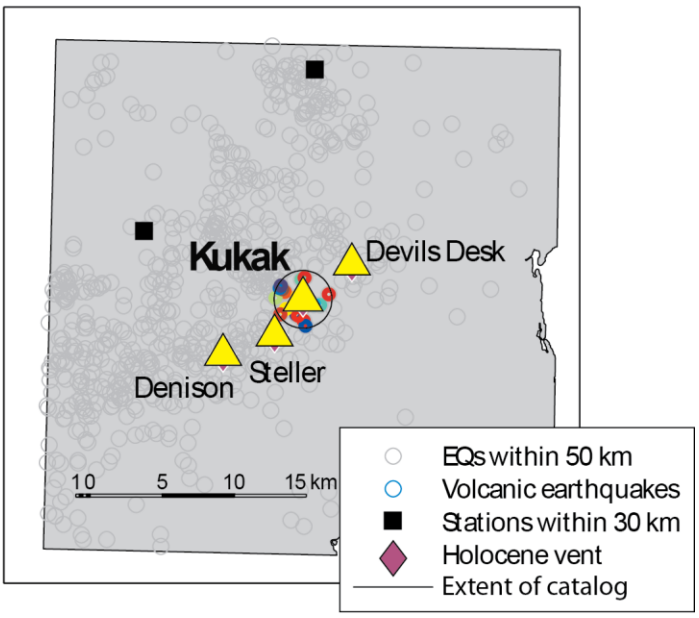

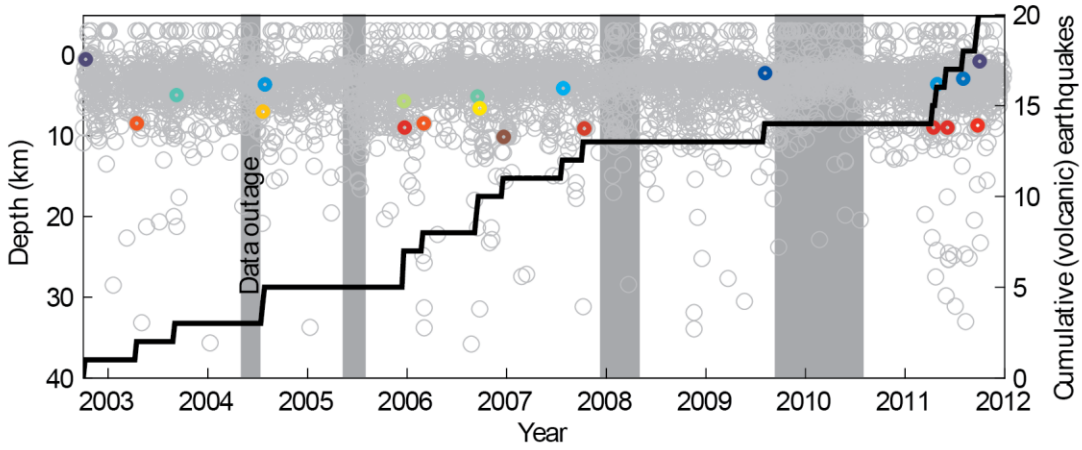

Appendix 3.A-40

Volcano: Devils Desk
Latitude: 58.4753 N
Longitude: -154.3001 E
Elevation (m): 1954
Number of Holocene vents: 1
Radius of catalog (km): 2.5
Number of earthquakes: 21
Days of good data: 2762

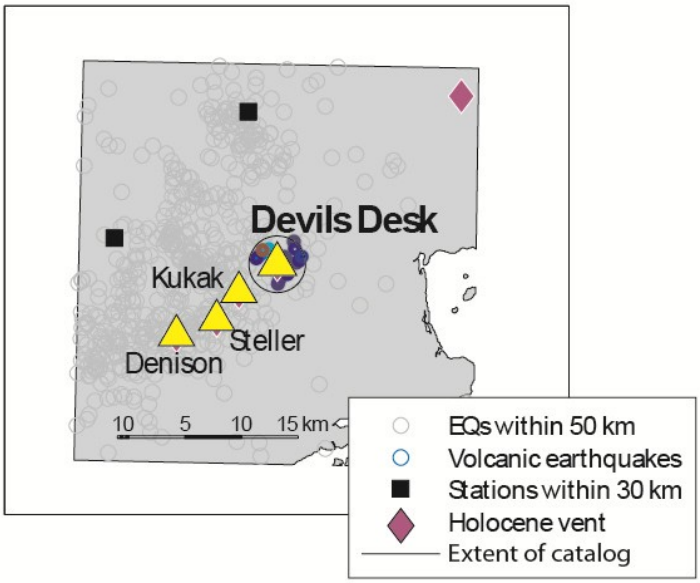

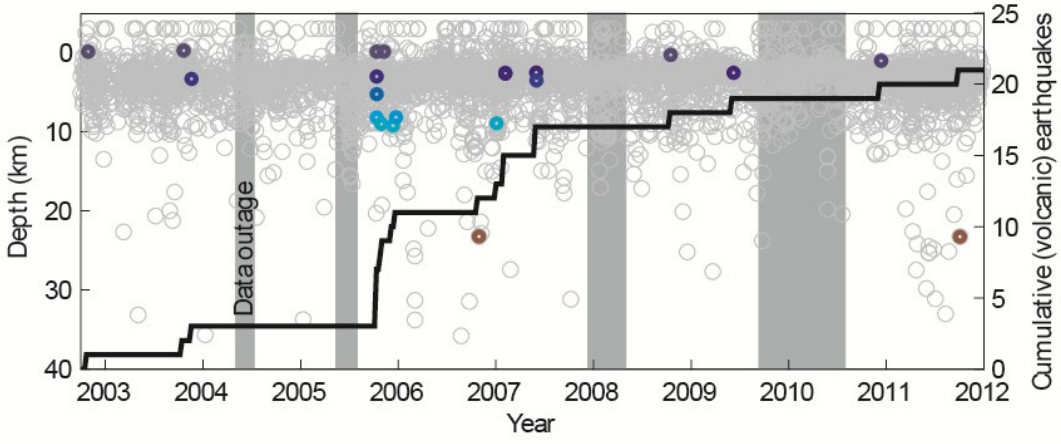

Appendix 3.A-41

Volcano: Fourpeaked
Latitude: 58.7703 N
Longitude: -153.6738 E
Elevation (m): 2104
Number of Holocene vents: 1
Radius of catalog (km): 8
Number of earthquakes: 487
Days of good data: 2608

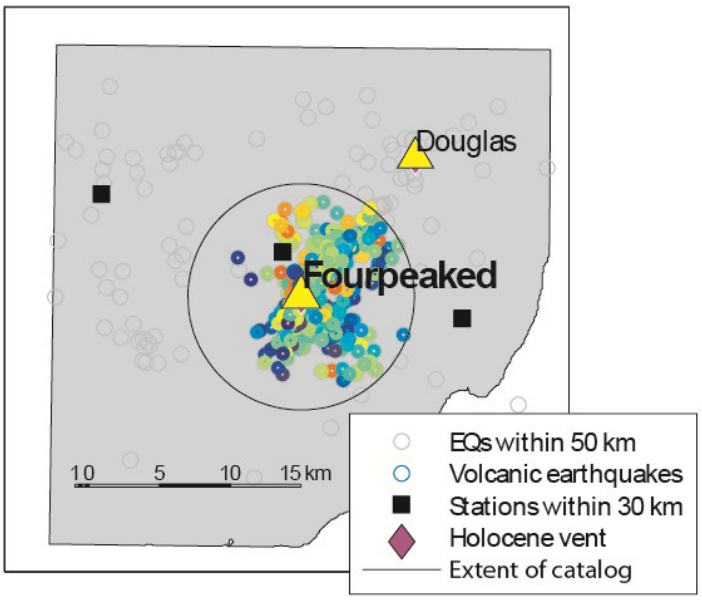

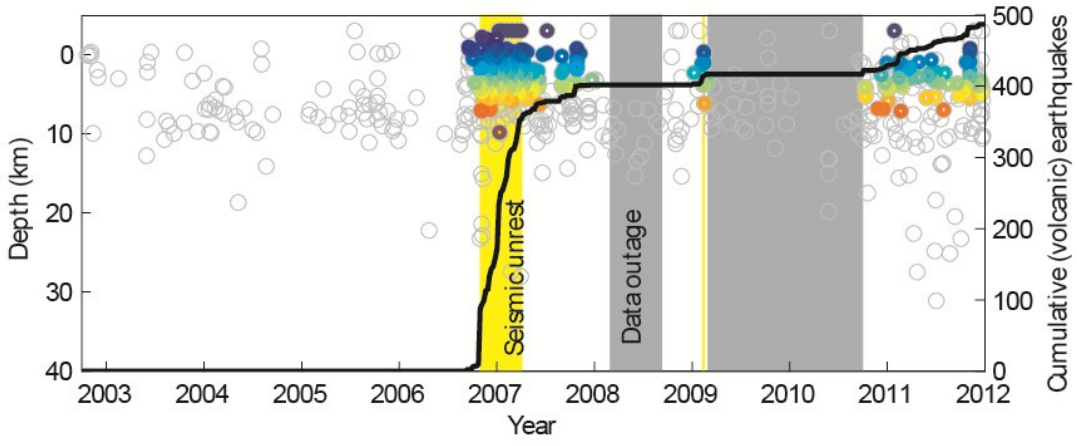

Appendix 3.A-42

Volcano: Douglas
Latitude: 58.8596 N
Longitude: -153.5351 E
Elevation (m): 2140
Number of Holocene vents: 1
Radius of catalog (km): 3
Number of earthquakes: 12
Days of good data: 2608

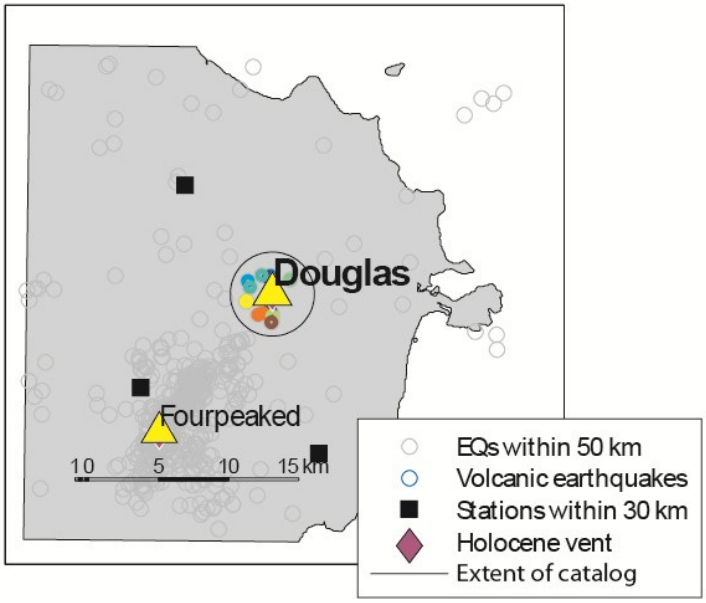

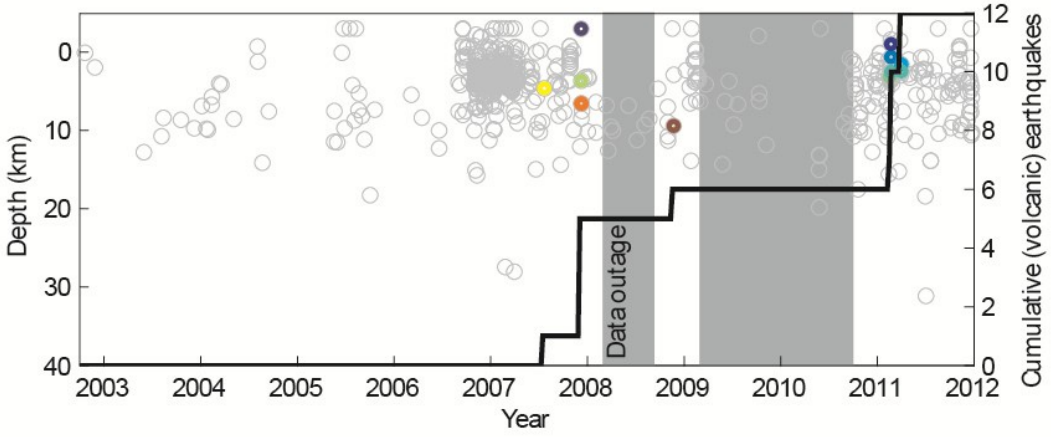

Appendix 3.A-43

Volcano: Augustine

Latitude: 59.3626 N

Longitude: -153.435 E

Elevation (m): 1260

Number of Holocene vents: 1

Radius of catalog (km): 1.5

Number of earthquakes: 3582

Days of good data: 3379

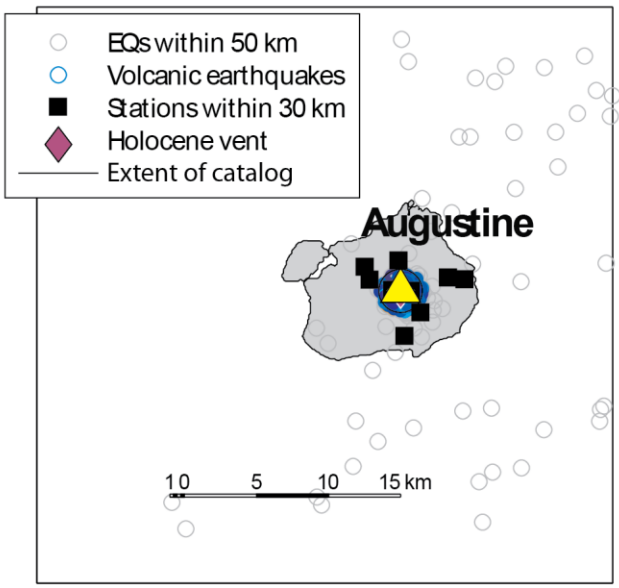

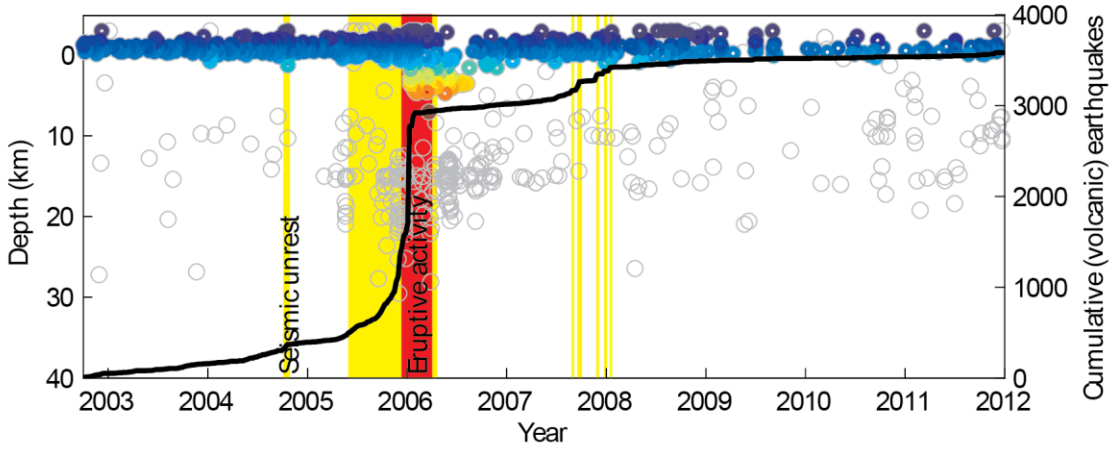

Appendix 3.A-44

Volcano: Iliamna
Latitude: 60.0319 N
Longitude: -153.0918 E
Elevation (m): 3053
Number of Holocene vents: 4
Radius of catalog (km): 7
Number of earthquakes: 3007
Days of good data: 2633

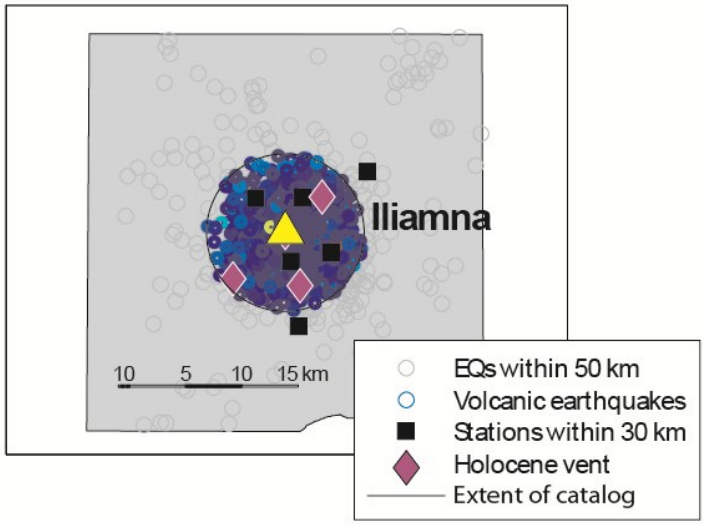

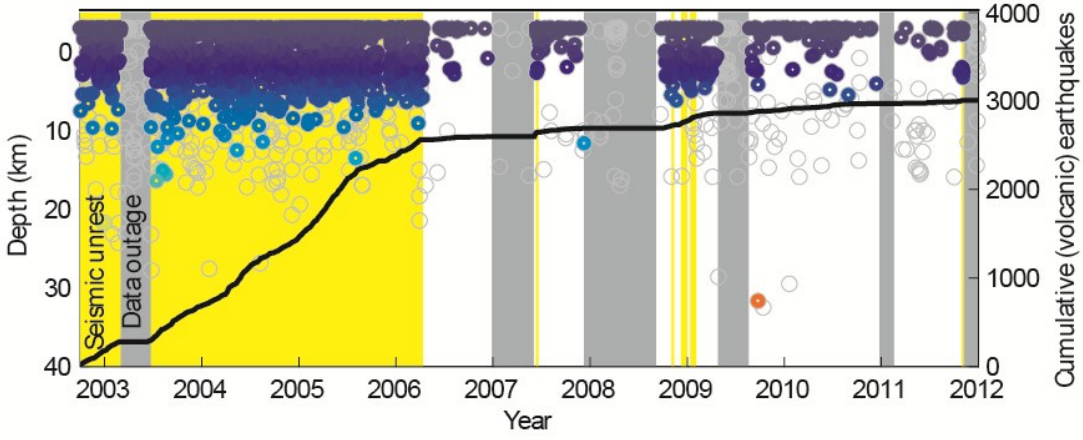

Appendix 3.A-45

Volcano: Redoubt
Latitude: 60.4852 N
Longitude: -152.7438 E
Elevation (m): 3108
Number of Holocene vents: 3
Radius of catalog (km): 8
Number of earthquakes: 4908
Days of good data: 2693

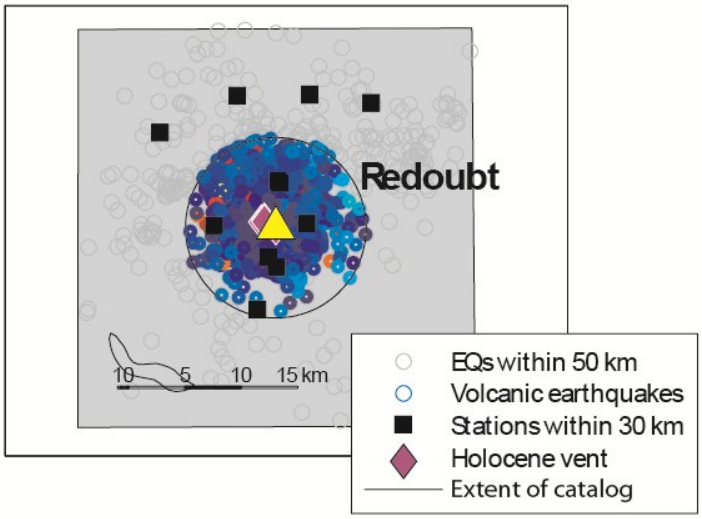

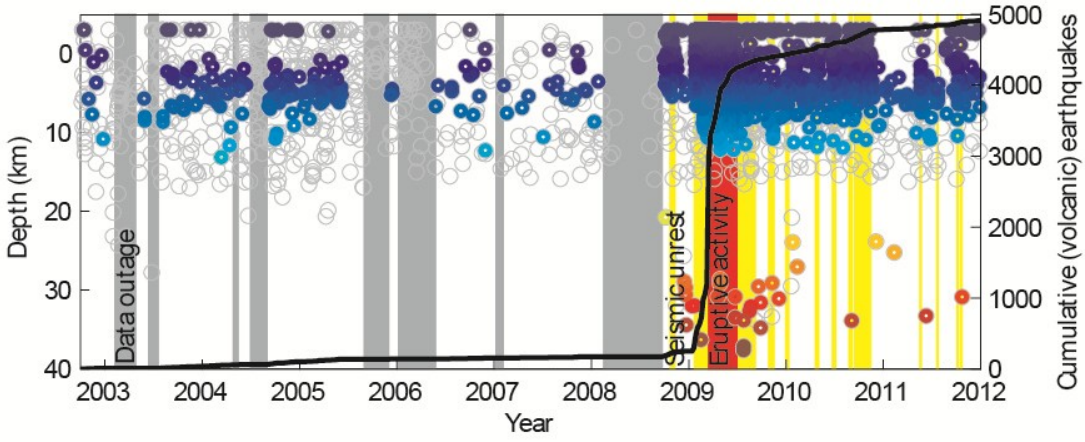

Appendix 3.A-46

Volcano: Spurr
Latitude: 61.2989 N
Longitude: -152.2539 E
Elevation (m): 3374
Number of Holocene vents: 2
Radius of catalog (km): 10
Number of earthquakes: 7249
Days of good data: 3371

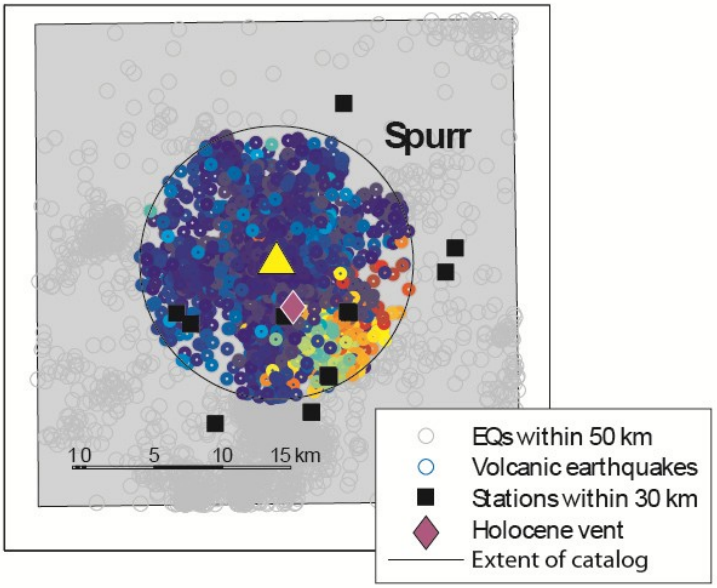

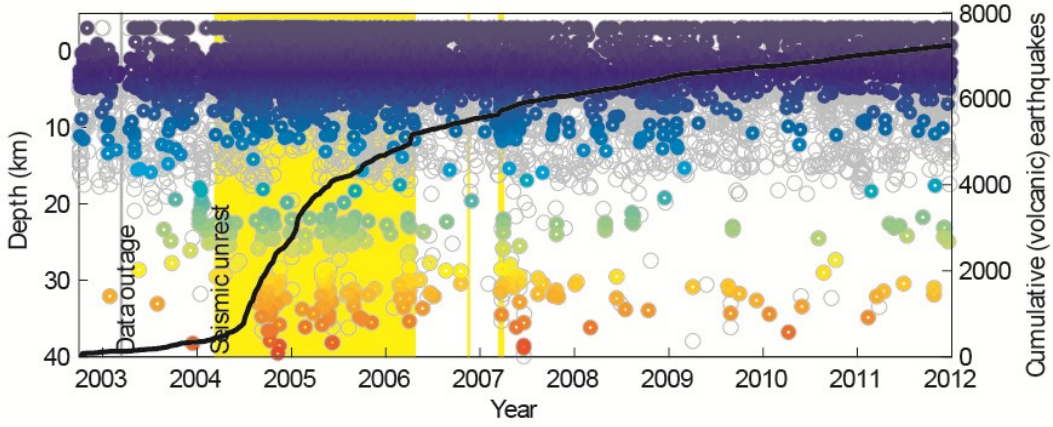

Appendix 3-B

Volcano elevation plotted as a function of the spread of seismicity, defined by a radius centred around the summit.

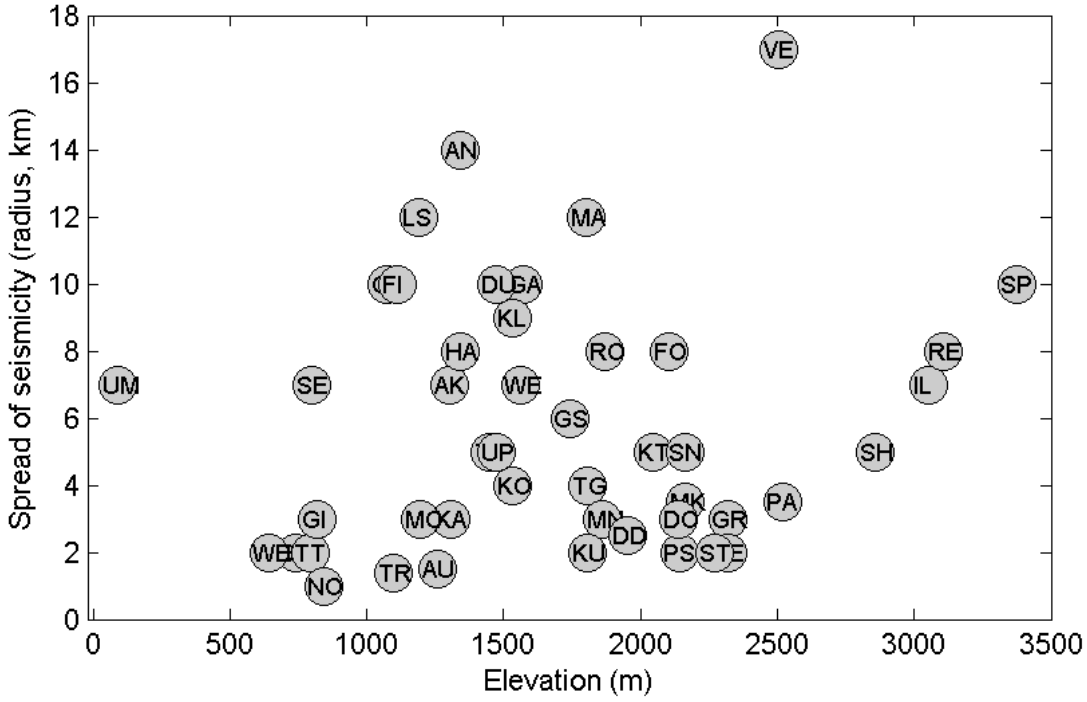

Codes: LS-Little Sitkin; SE-Semisopochnoi; GA-Gareloi; TG-Tanaga; TK-Takawangha; BO-Bobrof; KA-Kanaga; MO-Moffett; GS-Great Sitkin; KO-Korovin; KL-Kliuchef; OK-Okmok; MA-Makushin; TT-Table Top; WB-Wide Bay; AK-Akutan; GI-Gilbert; WE-Westdahl; FI-Fisher; SH-Shishaldin; RO-Roundtop; DU-Dutton; HA-Hague; PA-Pavlof; PS-Pavlof Sister; VE-Veniaminof; AN-Aniakchak; UM-Ukinrek Maars; UP-Ugashik-Peulik; MA-Martin; MK-Mageik; TR-Trident; NO-Novarupta; KT-Katmai; GR-Griggs; SN-Snowy; DE-Denison; ST-Steller; KU-Kukak; DD-Devil's Desk; FO-Fourpeaked; DO-Douglas; AU-Augustine; IL-Iliamna; RE-Redoubt; SP-Spurr.

Appendix 3-C

Spread of volcanic seismicity, defined as a radius centred on the summit, plotted as a function of median weight percent SiO2.

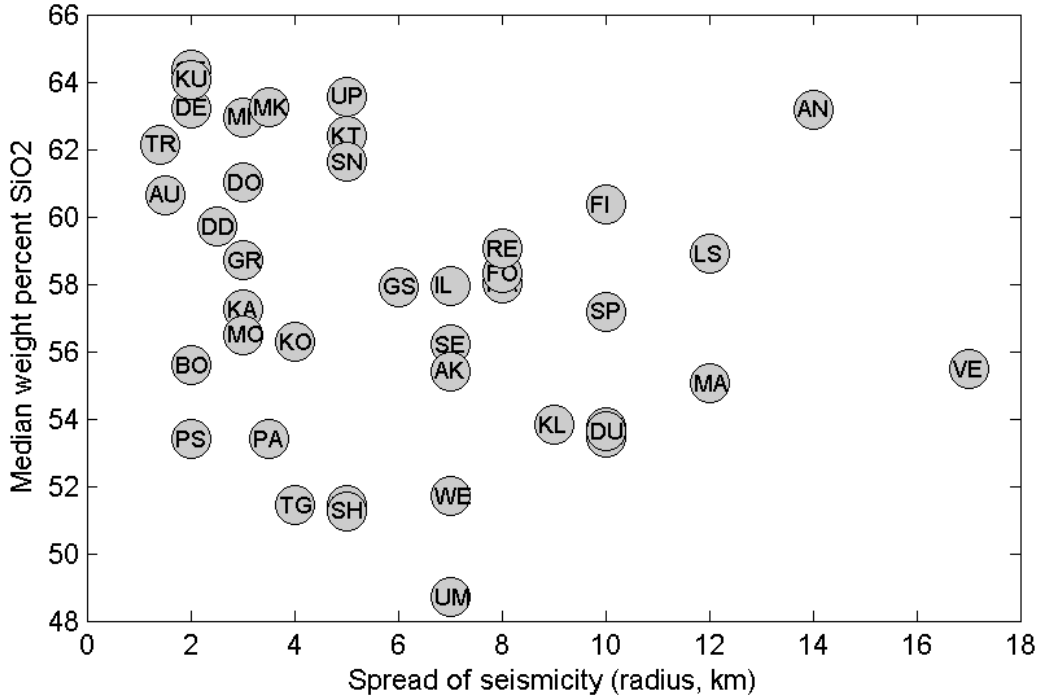

Codes: LS-Little Sitkin; SE-Semisopochnoi; GA-Gareloi; TG-Tanaga; TK-Takawangha; BO-Bobrof; KA-Kanaga; MO-Moffett; GS-Great Sitkin; KO-Korovin; KL-Kliuchef; OK-Okmok; MA-Makushin; TT-Table Top; WB-Wide Bay; AK-Akutan; GI-Gilbert; WE-Westdahl; FI-Fisher; SH-Shishaldin; RO-Roundtop; DU-Dutton; HA-Hague; PA-Pavlof; PS-Pavlof Sister; VE-Veniaminof; AN-Aniakchak; UM-Ukinrek Maars; UP-Ugashik-Peulik; MA-Martin; MK-Mageik; TR-Trident; NO-Novarupta; KT-Katmai; GR-Griggs; SN-Snowy; DE-Denison; ST-Steller; KU-Kukak; DD-Devil's Desk; FO-Fourpeaked; DO-Douglas; AU-Augustine; IL-Iliamna; RE-Redoubt; SP-Spurr.

Appendix 3-D

Available moment tensor solutions for earthquakes in the upper 30 km of the crust between 1976 and 2012.

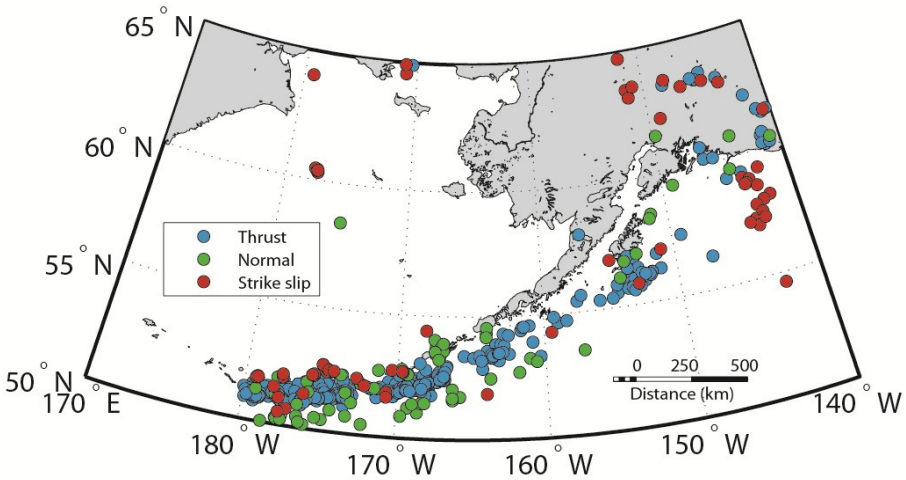

Moment tensor solutions are subset into groups as follows: thrust earthquakes have the T axis between 45-90˚and Null axis between 45-90˚; normal earthquakes have the T axis between 0-45˚ and the Null axis between 0-45˚; and strike-slip earthquakes have the T axis between 0-45˚ and the Null axis between 45-90˚ (source: www.globalcmt.org/CMTsearch.html).

Appendix 3-E

Distribution of cumulative earthquake magnitude per year of data using only events that occurred outside of volcanic unrest, within 3 km depth bins below each volcano, ordered east to west.

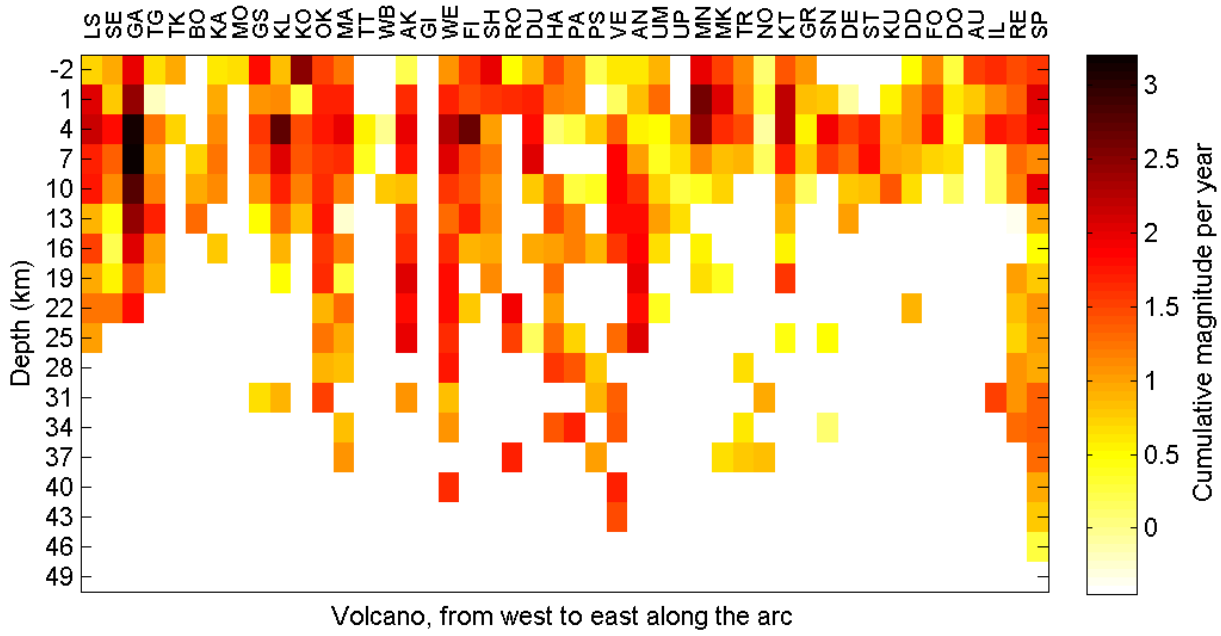

Codes: LS-Little Sitkin; SE-Semisopochnoi; GA-Gareloi; TG-Tanaga; TK-Takawangha; BO-Bobrof; KA-Kanaga; MO-Moffett; GS-Great Sitkin; KO-Korovin; KL-Kliuchef; OK-Okmok; MA-Makushin; TT-Table Top; WB-Wide Bay; AK-Akutan; GI-Gilbert; WE-Westdahl; FI-Fisher; SH-Shishaldin; RO-Roundtop; DU-Dutton; HA-Hague; PA-Pavlof; PS-Pavlof Sister; VE-Veniaminof; AN-Aniakchak; UM-Ukinrek Maars; UP-Ugashik-Peulik; MA-Martin; MK-Mageik; TR-Trident; NO-Novarupta; KT-Katmai; GR-Griggs; SN-Snowy; DE-Denison; ST-Steller; KU-Kukak; DD-Devil's Desk; FO-Fourpeaked; DO-Douglas; AU-Augustine; IL-Iliamna; RE-Redoubt; SP-Spurr.

Appendix 3-F

Distribution of cumulative earthquake magnitude per year of data using only events with magnitudes greater than 1.4 within 3 km depth bins below each volcano, ordered east to west.

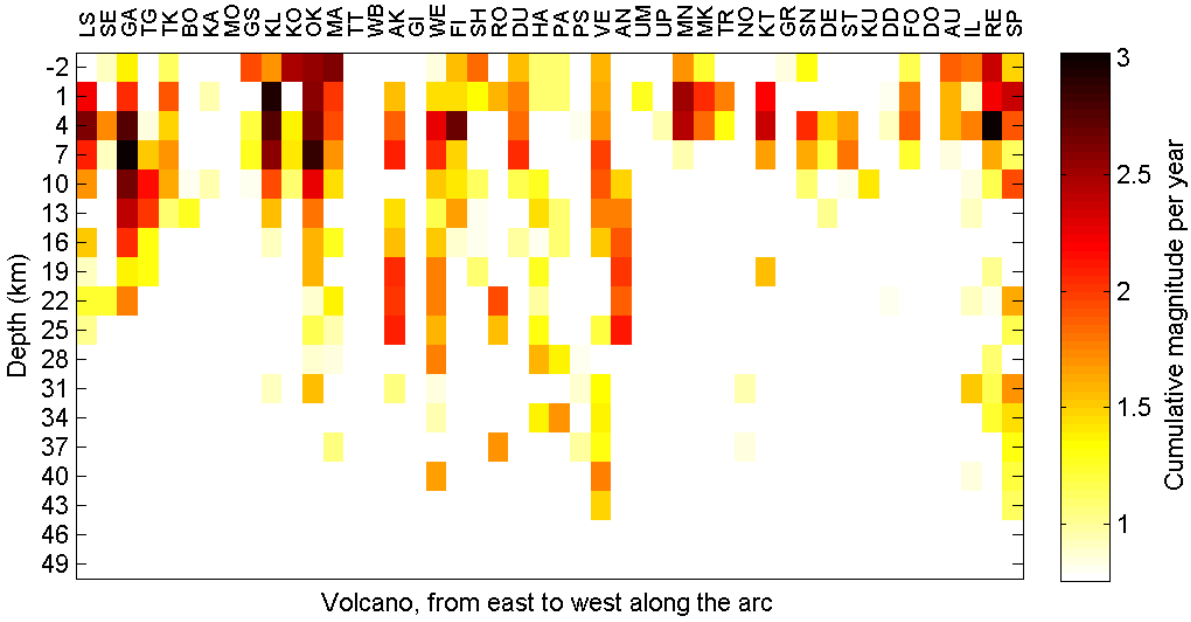

Codes: LS-Little Sitkin; SE-Semisopochnoi; GA-Gareloi; TG-Tanaga; TK-Takawangha; BO-Bobrof; KA-Kanaga; MO-Moffett; GS-Great Sitkin; KO-Korovin; KL-Kliuchef; OK-Okmok; MA-Makushin; TT-Table Top; WB-Wide Bay; AK-Akutan; GI-Gilbert; WE-Westdahl; FI-Fisher; SH-Shishaldin; RO-Roundtop; DU-Dutton; HA-Hague; PA-Pavlof; PS-Pavlof Sister; VE-Veniaminof; AN-Aniakchak; UM-Ukinrek Maars; UP-Ugashik-Peulik; MA-Martin; MK-Mageik; TR-Trident; NO-Novarupta; KT-Katmai; GR-Griggs; SN-Snowy; DE-Denison; ST-Steller; KU-Kukak; DD-Devil's Desk; FO-Fourpeaked; DO-Douglas; AU-Augustine; IL-Iliamna; RE-Redoubt; SP-Spurr.

Conclusion

Motivated by the need to improve our ability to monitor volcanoes, my goal for this thesis was to advance our understanding of how volcanic processes generate volcano-seismic signals. I used seismic data recorded over a 10 year period across the Aleutian arc volcanoes to search for trends and characteristic signals and related them to volcanic processes. I examined the short-lived eruption seismicity that is limited to only the few weeks during which a volcano is active, the seismicity that occurs in the months following an eruption, and the long-term volcano seismicity that occurs in the years in which volcanoes are dormant.

To study eruptive volcanic seismicity, I examined the rich seismic dataset that was recorded during the 2009 eruption of Redoubt Volcano. I was able show that the progression of magma through conduit system at Redoubt could be readily tracked by the seismicity. Many of my interpretations benefited greatly from the numerous other datasets collected during the eruption. Rarely was there volcanic activity that did not manifest itself in some way seismically, however, serving as a reminder that seismic observations are one of the most powerful methods with which to monitor active volcanoes.

I next studied the seismicity that occurred in the year following the end of the eruptive activity at Redoubt Volcano. During this period there were a number of unexplained bursts of shallow seismicity that did not culminate in eruptive activity despite closely mirroring seismic signals that had preceded explosions less than a year prior. I was able to show that these episodes of shallow seismicity were in fact related to volcanic processes much deeper in the volcanic edifice, by demonstrating that earthquakes that were related to magmatic activity during the eruption were also present during the renewed shallow unrest. These results show that magmatic processes can continue for many months after eruptions end, suggesting that volcanoes can stay active for much longer than previously thought.

In the final chapter I characterize volcanic earthquakes on a much broader scale by analyzing nearly 10 years of continuous seismic data across 46 volcanoes in the Aleutian arc in order to search for regional-scale trends in volcano seismicity. I found that volcanic earthquakes below 20 km depth are much more common in the central region of the arc than they are in the eastern and western regions. When I compared these results to trends in volcano geochemistry, I found that the transition from shallow to deeper volcanic earthquakes between the eastern and central regions of the arc coincides with a drop in the median weight percent SiO_2 of the volcanic systems. To explain these trends, I hypothesize that the regional tectonics control the ascent of magma through the crust. I note the locations of the Amlia fracture zone and the Becharof Lakes fault zone—two features that have been previously identified in other studies as major stress boundaries (e.g. Ryan et al., 2012; Decker et al., 2008)—that coincide with the transition in volcanic earthquake depths, and use these as evidence to show that the central portion of the arc has a different stress regime than those regions to the east and west. In my model the increase in deep volcanic earthquakes in the central region of the arc is a manifestation of increased magmatic flux through the crust, which is further evidenced by the location of the largest and most active volcanic centers in the arc. These results suggest that arc dynamics may have a greater influence over volcanoes than had previously been considered, and once again emphasize how volcanic seismicity provides a unique window through which we can investigate how volcanic systems work.

It is my hope that my research will not only contribute to a better understanding of processes which underlie arc volcanism, but that it will also contribute to the volcano monitoring mission in Alaska.

References

Chouet, B.A., 1988. Resonance of a fluid-driven crack; radiation properties and implications for the source of long-period events and harmonic tramor: Journal of Geophysical Research 93, 4375-4400.

Chouet, B.A., Matoza, R.S., 2013. A multi-decadal view of seismic methods for detecting precursors of magma movement and eruption. Journal of Volcanology and Geothermal Research, 252, 108-175, doi: 10.1016/j.jvolgeores.2012.11.013.

Decker, P.L., Reifenstuhl, R.R., and Gillis, R.J., 2008, Structural linkage of major tectonic elements, Ugashik Lakes - Becharof Lake region, northeastern Alaska Peninsula (presentation): DNR Spring Technical Review Meeting, Anchorage, Alaska, March 26-27, 2008: Alaska Division of Geological & Geophysical Surveys, 18 p.

DeRoin, N., McNutt, S.R., 2012. Rockfalls at Augustine Volcano, Alaska: The influence of eruption precursors and seasonal factors on occurrence patterns 1997–2009: Journal of Geophysical Research, 211-212, 61-65, doi: 10.1016/j.jvolgeores.2011.11.003.

Hotovec, A., Prejean, S., Vidale, J., Gomberg, J., 2012. Strongly Gliding Harmonic Tremor During the 2009 Eruption of Redoubt Volcano. Journal of Volcanology and Geothermal Research, doi:10.1016/j.jvolgeores.2012.01.001.

Iverson, R.M., Dzurisin, D., Gardner, C.A.,Gerlach, T.M., LaHusen, R.G., Lisowski, M., Major, J.J., Malone, S.D., Messerich, J.A., Moran, S.C., Pallister, J.S., Qamar, A.I., Schilling, S.P., Vallance, J.W., 2006. Dynamics of seismogenic volcanic extrusion at Mount St. Helens in 2004-05: Nature 444 (7118), 439-443, doi: 10.1038/nature05322.

Omori, F., 1912. The eruptions and earthquakes of the Asama-yama: Bulletin of the Imperial Earthquake Investigation Committee 6, 1-147.

Ryan, H.F., Amy E. Draut, Katie Keranen, and David W. Scholl, 2012, Influence of the Amlia fracture zone on the evolution of the Aleutian Terrace forearc basin, central Aleutian subduction zone, *Geosphere*; v. 8; no. 6; p. 1254–1273; doi:10.1130/GES00815.1.

Zobin, V.M., 2012. Introduction to volcanic seismology. Elsevier, Amsterdam.